

3-24-2016

Electro-Mechanical Characterization of Carbon Nanotube Sheets in Simulated Space Environments: The Dawn of “Carbon Spacecraft”

Jacob W. Singleton

Follow this and additional works at: <https://scholar.afit.edu/etd>



Part of the [Aerospace Engineering Commons](#)

Recommended Citation

Singleton, Jacob W., "Electro-Mechanical Characterization of Carbon Nanotube Sheets in Simulated Space Environments: The Dawn of “Carbon Spacecraft”" (2016). *Theses and Dissertations*. 450.
<https://scholar.afit.edu/etd/450>

This Thesis is brought to you for free and open access by the Student Graduate Works at AFIT Scholar. It has been accepted for inclusion in Theses and Dissertations by an authorized administrator of AFIT Scholar. For more information, please contact richard.mansfield@afit.edu.



**ELECTRO-MECHANICAL CHARACTERIZATION OF CARBON NANOTUBE
SHEETS IN SIMULATED SPACE ENVIRONMENTS: THE DAWN OF
“CARBON SPACECRAFT”**

THESIS

Jacob W. Singleton, Second Lieutenant, USAF

AFIT-ENY-MS-16-M-240

**DEPARTMENT OF THE AIR FORCE
AIR UNIVERSITY**

AIR FORCE INSTITUTE OF TECHNOLOGY

Wright-Patterson Air Force Base, Ohio

DISTRIBUTION STATEMENT A. APPROVED FOR PUBLIC RELEASE;
DISTRIBUTION UNLIMITED.

The views expressed in this thesis are those of the author and do not reflect the official policy or position of the United States Air Force, Department of Defense, or the United States Government. This material is declared a work of the United States Government and is not subject to copyright protection in the United States.

AFIT-ENY-MS-16-M-240

ELECTRO-MECHANICAL CHARACTERIZATION OF CARBON NANOTUBE
SHEETS IN SIMULATED SPACE ENVIRONMENTS: THE DAWN OF
“CARBON SPACECRAFT”

THESIS

Presented to the Faculty

Department of Aeronautics and Astronautics

Graduate School of Engineering and Management

Air Force Institute of Technology

Air University

Air Education and Training Command

In Partial Fulfillment of the Requirements for the
Degree of Master of Science in Astronautical Engineering

Jacob W. Singleton, BS

Second Lieutenant, USAF

March 2016

DISTRIBUTION STATEMENT A. APPROVED FOR PUBLIC RELEASE;
DISTRIBUTION UNLIMITED.

AFIT-ENY-MS-16-M-240

ELECTRO-MECHANICAL CHARACTERIZATION OF CARBON NANOTUBE
SHEETS IN SIMULATED SPACE ENVIRONMENTS: THE DAWN OF
“CARBON SPACECRAFT”

Jacob W. Singleton, BS
Second Lieutenant, USAF

Committee Membership:

Shankar Mall, PhD
Chair

Heath E. Misak, PhD
Member

Maj Ryan P. O’Hara
Member

Abstract

CNT based materials are exciting candidates for spacecraft by virtue of their unprecedented specific mechanical and electrical properties. Analysis performed in this thesis identifies 14 diverse types of CNT-sheets with distinct variables, and discovers the mechanisms and phenomena controlling macroscopic properties. The specimen variables include treatment (acid treatment vs. non-acid), polymer coatings (polystyrene and thermoplastic polyurethane), production method (enhanced production (EP) vs. standard production), and combinations. Mechanical testing includes tensile-tests and the investigation of surface morphology with scanning electron microscopy and energy-dispersive x-ray spectroscopy. Physical properties testing include electromagnetic interference (EMI) shielding effectiveness (SE) and electrical conductivity. This research also examines the resilience of CNT-sheets to atomic oxygen and thermal fatigue in space.

EP CNT-sheets, while cost effective have decreased mechanical and electrical properties as a result of large compositions of catalysts and impurities. Acid treatment increases both mechanical and electrical properties. The acid treated sheets are better consolidated and have reduced impurities which lead to the superior properties. This investigation found that mechanical strength and EMI SE are unaffected by atomic oxygen and thermal fatigue. Young's modulus increases in both environments while strain decreases. Electrical conductivity decreases from atomic oxygen for both specimens as a result of reduced conductive area. Thermal fatigue diminishes conductivity in the acid treated sheets. Mechanisms and analysis developed in this study are instrumental for improving and developing applications requiring the electro-

AFIT-ENY-MS-16-M-240

mechanical properties of CNT-sheets. This research takes a crucial step forward in realizing the full theoretical performance of CNT-sheets and illuminates the dawn of “carbon spacecraft”.

AFIT-ENY-MS-16-M-240

To my children and remarkable wife

Acknowledgments

I want to thank my advisor Dr. Shankar Mall for his cheerful disposition that made a thesis more conquerable. His guidance helped me to explore and understand more deeply. I am grateful for Dr. Heath Misak for engaging with my research daily and always being available for tackling issues and discussing results. His mentorship was critical through each step of completing such a large task and he frequently went above and beyond in helping me be successful. I thank Jamie Smith and the lab technicians at the Air Force Institute of Technology who offered support during testing. The assistance of Ben Wilson and Scott Apt at the Materials and Manufacturing Directorate, AFRL helped me run EMI shielding tests and acquire exceptional high resolution images with the FEG-SEM. I thank my incredible wife for supporting me through each day and sacrificing through each hour to support our family in the greater and more challenging work within our home. My young daughters have come to believe that the uniform I wear each day means that I am going to school. I acknowledge the men and women who wear the same uniform each day in defending our freedoms and who make the ultimate sacrifice. Finally, I acknowledge Jesus Christ who gathered twelve baskets left over after feeding five thousand from a small offering of bread and fish. Through a similar miracle, He took the little time that I gave to him and blessed it. He then provided more than enough time for me to complete all of my work, to bless my family, and to be filled.

Jacob W. Singleton

Table of Contents

	Page
Abstract.....	iv
Acknowledgments.....	vii
Table of Contents.....	viii
List of Figures.....	xi
List of Tables.....	xvi
List of Equations.....	xvii
List of Abbreviations and Symbols.....	1
I. Introduction.....	5
1.1 Space Vehicles.....	6
1.2 Carbon Nanotubes.....	8
1.3 Problem Statement.....	10
1.4 Research Objectives.....	11
1.5 Summary.....	12
II. Literature Review.....	14
Chapter Overview.....	14
2.1 Space Vehicles.....	14
2.3 Space Environment.....	16
2.3.1 <i>Thermal Fatigue</i>	17
2.3.2 <i>Atomic Oxygen</i>	19
2.3.3 <i>Electromagnetic Interference</i>	22
2.1 Carbon Nanotubes.....	23
2.1.1 <i>Mechanical Properties</i>	27
2.1.2 <i>Electrical Properties</i>	28
2.2 Manufacturing Parameters for Improved Properties and Production.....	31
2.2.1 <i>Chemical Treatment</i>	31
2.2.2 <i>Polymer Coatings</i>	33
2.2.3 <i>Production Rate</i>	33
2.4 Relevant Research.....	34
III. Methodology.....	38
3.1 Introduction to Methodology.....	38

3.2 Test Specimens and Preparation	38
3.2.1 <i>Apparent Thickness</i>	41
3.3 Tensile Test Equipment and Method	42
3.4 EMI Shielding Test Equipment and Method	43
3.5 Electrical Conductivity Test Equipment and Method.....	47
3.6 SEM and EDX Equipment	50
3.7 Space Environments Exposure Facilities	51
3.7.1 <i>Atomic Oxygen Equipment and Method</i>	51
3.7.2 <i>Thermal Fatigue Equipment and Method</i>	53
3.8 Test Plan Summary.....	55
3.9 Assumptions and Limitations	57
 IV. Analysis and Results.....	 58
4.1 Chapter Overview	58
4.2 Apparent Properties.....	59
4.1 CNT-Sheet Baseline Mechanical Properties	61
4.1.1 <i>Specimen Failure and CNT Alignment</i>	64
4.2.1 <i>Volumetric Density</i>	72
4.2.2 <i>Areal Density</i>	75
4.2.3 <i>Specific Properties</i>	77
4.2.4 <i>Overview of Manufacturing Parameters</i>	79
4.2.5 <i>Polymer Coated Specimens</i>	84
4.2 CNT-Sheet Baseline Electrical Properties	88
4.2.1 <i>Volumetric Density</i>	90
4.2.2 <i>Areal Density</i>	91
4.2.3 <i>Apparent Thickness</i>	92
4.2.4 <i>Overview of Manufacturing Parameters</i>	94
4.3 Effects from Space Environments.....	98
4.3.1 <i>Atomic Oxygen Results</i>	100
4.3.2 <i>Thermal Fatigue Results</i>	107
 V. Conclusions and Recommendations	 112
5.1 Chapter Overview	112
5.2 Conclusions of Research.....	112
5.3 Significance of Research.....	119
5.4 Recommendations for Action	120
5.5 Recommendations for Future Research	120
 Appendix A. Images of CNT-sheet Specimen Failure	 123
 Appendix B. Matlab Script for Line Extraction and Hough Transform.....	 127
 Appendix C. Other Applications of Carbon Nanotube Materials.....	 128

Bibliography	129
Vita.....	135

List of Figures

	Page
Figure 1. CNT composite struts supporting the rocket engine motor on the Juno spacecraft [4]	7
Figure 2. Single Wall Carbon Nanotube (SWNT) [7]	9
Figure 3. 1996 photo of X-33 VentureStar: Lockheed Martin proposed spacecraft [23].	15
Figure 4. Percentage of space vehicle failures vs. ETTI.....	16
Figure 5. Thermal regimes by altitude [29]	18
Figure 6. Composition regimes by altitude [29]	19
Figure 7. Chiral vector and CNT structure	24
Figure 8. Different types of CNT [41]	25
Figure 9. Band structure for nanotubes [56]: SWNT armchair metallic nanotube (a, d), SWNT (15,0) zigzag metallic nanotube (b, e), and SWNT (16,0) zigzag semiconducting nanotube(c, f).....	29
Figure 10. CNT-yarn (a) fracture in CNT bundles after thermal fatigue (b) delamination (lower arrow) and crack formation (upper arrow) from kink band formation in thermal fatigued CNT-yarn.....	34
Figure 11. CNT yarn after atomic oxygen exposure: (a) surface damage before tensile test and (b) surface damage seen after tensile failure.....	35
Figure 12. Preparation of support on Juno spacecraft [4] with outer layer CNT-sheet	36
Figure 13. (a) Schematic of CNT-sheet manufacturing process and (b) enhanced production	39
Figure 14. Summary of specimen variables.....	40

Figure 15. MTS Tytron 250 tensile test machine	42
Figure 16. Tensile test specimens: (a) prepared specimen and (b) necking after strain ...	43
Figure 17. Agilent PNA Microwave Network Analyzer test setup	44
Figure 18. EMI shielding effectiveness across frequency range	45
Figure 19. EMI shielding test specimen	46
Figure 20. Four wire electrical resistance measurement technique	48
Figure 21. Four wire test set up	48
Figure 22. Electrical gauge measured by Zeiss optical microscope for (a) 1cm gauge length used for baseline properties and (b) 2mm gauge length used for exposed specimens.....	49
Figure 23. Imaging instrumentation (a) Zeiss optical microscope and (b) FEI Quanta 450 SEM EDX.....	50
Figure 24. Atomic oxygen testbed diagram.....	52
Figure 25. Atomic oxygen prepared specimens.....	52
Figure 26. FTS ThermoJet ES for precision temperature cycles	53
Figure 27. Three temperature cycles for thermal fatigue environment	54
Figure 28. Test Matrix	56
Figure 29. Areal density vs. thickness	60
Figure 30. (a) Stress-strain curves for manufacturing parameters and (b) strength by specimen type	62
Figure 31. Bar charts showing (a) Young's modulus and (b) failure strain by specimen type	64

Figure 32. Illustration of CNT bundles in sheets after stretching. Randomly oriented and tangled CNT bundles before strain (a) and straightened, packed form after tensile strain 65

Figure 33. (a) Specimen, (b) Necking specimen before failure, (c) Specimen failure, and (d) acid treated EP CNT-sheet after tensile failure..... 66

Figure 34. Illustration of typical stress-strain curves for CNT-sheets (a) and images of necking after failure for (b) acid treated specimen 5, (c) standard reference specimen 1, and (d) enhanced production polymer coated specimen 14..... 68

Figure 35. Matlab line extraction before strain with SEM morphology and line vectors 70

Figure 36. Hough line transform before strain..... 70

Figure 37. Matlab line extraction after strain with SEM morphology and line vectors ... 71

Figure 38. Hough line transform after strain 71

Figure 39. (a) Strength and (b) Young’s modulus vs. volumetric density..... 73

Figure 40. Strain to failure vs. volumetric density..... 74

Figure 41. (a) Apparent strength and (b) apparent modulus vs areal density 76

Figure 42. Failure strain vs. areal density 76

Figure 43. Specific strength vs. specific modulus 79

Figure 44. Surface morphology of untreated specimen 1 at (a) 10kx magnification and (b) 50kx 81

Figure 45. Surface morphology of acid treated specimen 6 at (a) 10k magnification and (b) 50kx..... 81

Figure 46. SEM images of enhanced production specimen 3 at 10kx magnification..... 82

Figure 47. SEM image of EP CNT sheet at 50kx magnification and (b) internal layer at 25kx	82
Figure 48. Internal layers in CNT thickness comparing (a) EP CNT-sheet and (b) Standard production specimen.....	84
Figure 49. Tensile stress-strain curve for polymer coated CNT-sheet specimens.....	86
Figure 50. Surface morphology of PSb coated specimen 10 at 20kx magnification	87
Figure 51. Surface morphology of TPU coated specimen 11 at 20kx magnification.....	87
Figure 52. Conductivity and EMI shielding by manufacturing parameter type	89
Figure 53. Electrical properties vs. density: (a) conductivity and (b) EMI SE.....	90
Figure 54. Electrical properties vs. areal density: (a) conductivity and (b) EMI SE.....	91
Figure 55. Electrical properties vs. thickness: (a) conductivity and (b) EMI SE	92
Figure 56. Electrical properties per unit thickness: (a) Conductivity and (b) EMI SE.....	94
Figure 57. Surface morphology at 20kx magnification for untreated specimen 1.....	95
Figure 58. Surface morphology for at 20kx magnification for acid treated specimen 6 ..	96
Figure 59. Surface morphology for at 20kx magnification for enhanced production specimen 4	96
Figure 60. Surface morphology for at 20kx magnification for PSb coated specimen 10.	97
Figure 61. Effects of atomic oxygen on (a) specific strength, and (b) specific stiffness	101
Figure 62. Effects of atomic oxygen on (a) failure strain, and (b) areal density	101
Figure 63. Effects of atomic oxygen on (a) conductivity and (b) EMI shielding.....	102
Figure 64. Surface morphology and EDX of CNT-sheets for specimen 1 before exposure	103
Figure 65. Surface morphology and EDX of CNT-sheets for specimen 1 after ATOX..	103

Figure 66. Surface morphology and EDX of CNT-sheets for specimen 6 before exposure	104
Figure 67. Surface morphology and EDX of CNT-sheets for specimen 6 after ATOX	104
Figure 68. Exposed catalyst material after ATOX.....	106
Figure 69. Effects of thermal fatigue on (a) specific strength, and (b) specific stiffness	108
Figure 70. Effects of thermal fatigue on (a) failure strain, and (b) areal density.....	108
Figure 71. Effects of thermal fatigue on (a) conductivity and (b) EMI shielding	109
Figure 72. Surface morphology of CNT-sheets after thermal fatigue for specimen 1 ...	110
Figure 73. Surface morphology of CNT-sheets after thermal fatigue for specimen 6 ...	110

List of Tables

	Page
Table 1. Properties of some spacecraft materials.....	9
Table 2. Investigative Questions and Methodology	12
Table 3. Reported mechanical properties of CNT-sheets	27
Table 4. Details of CNT-sheets.....	41
Table 5. Specific properties of steel and aluminum.....	77
Table 6. Details of polymer coated CNT-sheets, types E-F	85
Table 7. Details of CNT sheets for space environment exposure.....	99
Table 8. Specific strength and stiffness, strain, apparent conductivity and EMI shielding for space environment exposure	100
Table 9. Atomic weight composition of CNT-sheets before and after atomic oxygen ..	105
Table 10. Apparent tensile strength, modulus and failure strain of CNT-sheets baseline properties	113
Table 11. Apparent tensile strength, modulus, and failure strain for polymer coated CNT- sheets.....	113
Table 12. Apparent conductivity and EMI shielding effectiveness of CNT-sheets	114
Table 13. T-test results assuming unequal variances for property changes in CNT-sheets	116
Table 14. Summary of space environment effects on CNT-sheets.....	117

List of Equations

	Page
Equation 1. Photo dissociation of diatomic oxygen into atomic oxygen.....	20
Equation 2. Wave equation.....	20
Equation 3. Required photo dissociation energy	21
Equation 4. Chiral vector	23
Equation 5. Chiral angle	24
Equation 6. Carbon nanotube circumference.....	25
Equation 7. Carbon nanotube diameter.....	25
Equation 8. Nitric acid reaction with CNT-yarn.....	32
Equation 9. EMI shielding effectiveness	45
Equation 10. Orbital period according to Kepler’s third law.....	54
Equation 11. Number of simulated thermal cycles.....	54
Equation 12. Apparent Stress.....	61
Equation 13. Strain.....	61
Equation 14. Young’s modulus.....	63
Equation 15. Volumetric density	72
Equation 16. Areal density.....	75
Equation 17. Specific strength	78
Equation 18. Specific modulus	78
Equation 19. Resistivity	88
Equation 20. Conductivity	88

List of Abbreviations and Symbols

\$/kg	cost per kilogram
μm	micron or micro meter
Å	Angstrom
AACVD	Aerosol Assisted Chemical Vapor Deposition
AACCVD	Alcohol Catalytic Chemical Vapor Deposition
AFIT	Air Force Institute of Technology
AFB	Air Force Base
AFRL	Air Force Research Laboratory
Al	Aluminum
At%	Atomic Percent
atm	1 atmosphere
atoms/cm ³	atoms per cubic centimeter
atoms/m ²	atoms per square meter
ATOX	Atomic Oxygen
AWG	American Wire Gauge
°C	Degrees Celsius
°C/min	degrees Celsius per minute
C	Carbon
CFRP	Carbon Fiber Reinforced Polymer
CNT	Carbon Nanotube
cm	centimeter
cm ³ O-atom ⁻¹	cubic centimeter per atomic oxygen atom

Co	Cobalt
COO ⁻	Carboxylate ion
COOH	Carboxyl function group
Cu	Copper
CVD	Chemical Vapor Deposition
CCVD	Hybrid Laser Assisted Thermal CVD
CS ₂	Carbon Disulfide
dB	decibels
DoD	Department of Defense
EDX	Energy Dispersive X-ray Spectroscopy
EMI	Electromagnetic Interference
EP	Enhance Production
eV	electron volt
Fe	Iron
FEG	Field Emission Gun
g/cm ³	grams per cubic centimeter
g/m ²	grams per square meter
GPa	Giga Pascal
Gr/Ep	Graphite Epoxy
H ⁺	Hydrogen ion
H ₂ O	Water molecule
He	Helium

HiPCO	High Pressure Carbon Monoxide
HNO ₃	Nitric acid
HSS	High Strength Steel
Hz	Hertz
In	inch
ISR	Intelligence Surveillance and Reconnaissance
ISS	International Space Station
K	Kelvin
km	kilometer
km/s	kilometer per second
LDEF	Long Duration Exposure Facility
LEO	Low Earth Orbit
L/min	Liters per minute
mΩ	milli-ohms
MPa	Mega Pascal
MTS	Microforce Testing System
MWNT	Multi-walled Nanotube
N ₂	Nitrogen
Ni	Nickel
NO ₂	Nitrogen dioxide
nm	nanometer
NTI	Nanocomp Technologies, Inc.
O	Atomic Oxygen

O ₂	Diatomic Oxygen
O ₃	Ozone
OH	Hydroxyl function group
OM	Optical Microscope
PNA	Performance Network Analyzer
PNT	Position Navigation and Timing
PSb	Polystyrene
S/cm	Siemens per square meter
SEM	Scanning Electron Microscope
SSTO	Single-Stage-to-Orbit
STS	Space Transportation System
SWNT	Single wall Nanotube
TPU	Thermoplastic Polyurethane
US	United States
USA	United States of America
UV	Ultraviolet
WPAFB	Wright Patterson Air Force Base
wt %	weight percent

I. Introduction

On a military base in the continental United States, an airman remotely operates an unmanned aircraft over 7,000 miles away and is able to provide current intelligence and alert local allies of an impending attack. Battle operators and planners who were once required to work in theater can now leverage capabilities to apply precision effects globally. This is only one capability facilitated by space born systems. Material science and engineering has been at the forefront of key advances since the first introduction of technology in space. The United States military has great interest in what the next steps will be in these advanced space systems. Carbon Nanotubes (CNTs) attract a focused effort to take advantage of military superiority they offer for the Department of Defense (DoD). This is due to their impressive mechanical and physical properties that surpass that of current technology. While exhibiting superior mechanical performance, CNTs also excite the DoD in multi-purposed structures because they also have desirable electrical and thermal properties. The convincing application of CNTs in next generation space structures is finally spotlighted by its low density. Innovative technology has been the floor upon which the United States stands with superiority in military power. Regardless of category or domain, all technology finds building blocks in the science of materials. As the world ventures further into space, materials must be lightweight and structurally strong to survive launch conditions. Once in space these materials need to be durable in the harsh space environments found in orbit. In the last half century, the exploitation of advanced materials have led to new vision in the capabilities of space vehicles however the potential benefits found in the unbounded field of space are still constrained by

material technology. Carbon nanotubes, first reported in 1991, are the world's strongest materials with expansive properties that enable the future of spacecraft. The material foundation must be verified for any technology demonstration and the durability of these materials in the requisite environment must be validated.

1.1 Space Vehicles

Airpower is defined as “the ability to project military power or influence through the control and exploitation of air, space, and cyberspace to achieve strategic, operational, or tactical objectives” [1]. The first volume of Air Force Doctrine states that space systems provide many enabling capabilities to support airpower. In 2011, General James E. Cartwright, Vice Chairman, Joint Chiefs of Staff stated “Space power is a critical enabler to national security and it is where the US has competitive edge” [2]. The same spacecraft employed to observe hostile territory is also used to debilitate adversaries, removing their ability to hide their military activity. Space vehicles, hundreds to even thousands of kilometers away and traveling at rates of kilometers per second, provide intelligence, surveillance and reconnaissance, command and control, and global communication, in a global domain denied to both land and sea assets. In the Joint Publication on Space Operations, contributions of space assets also provide “global communications; positioning, navigation, and timing (PNT); services; environmental monitoring; space-based intelligence, surveillance, and reconnaissance (ISR); and warning services to combatant commanders (CCDRs), services, and agencies” [3]. As the warfighter's ultimate high ground, space is no longer an adventure or a race, but a “prerequisite for all other military operations” [1].

Launched in 2011, the Juno spacecraft will arrive at the planet Jupiter in July 2016 with the first ever CNT-based composites in its structure. The inclusion of CNTs simplified production and reduced weight demonstrating improved rigidity and EMI/ESD shielding and meeting all system requirements [4]. The Juno spacecraft is shown in Figure 1.

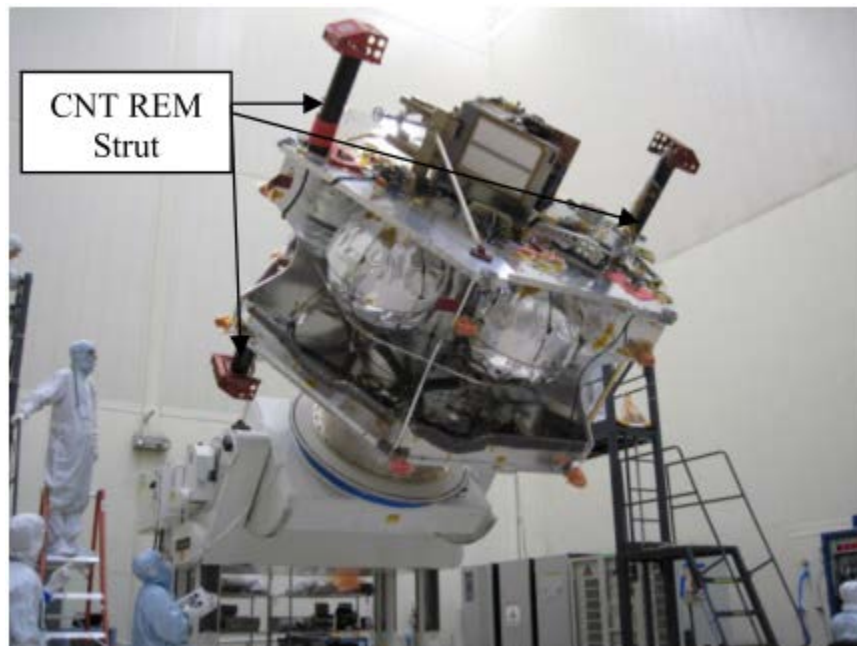


Figure 1. CNT composite struts supporting the rocket engine motor on the Juno spacecraft [4]

Because CNTs are extremely lightweight, their properties can be leveraged in most space structures and in electrical applications. The majority of mass in most satellites lies in the structure and the significant amounts of heavy copper used for electrical components. Mechanical and electrical properties are therefore the most important considerations for the greatest impacts on weight reductions for space systems.

A report prepared by Ivan Bekey from the Advanced Technology Division at National Systems Group reviews the expected effects of carbon nanotubes on the weight and potential cost for spacecraft and launch vehicles in the near and far terms [5]. Results from this report demonstrated the benefit of introducing CNTs to satellites and launch vehicles. The improvements provided by the CNT-based materials and its introduction to the Juno spacecraft assert the dawn of carbon spacecraft.

1.2 Carbon Nanotubes

What does the world's strongest and stiffest material look like? Is it a metallic structure like steel or aluminum or is it found among more recent materials like high performance composites? Take the impressive properties defined by the honeycomb lattice structure of doubly valently atomic bonded carbon molecules found in a planar sheet of graphene and roll it into a cylindrical tube. In this nanostructure, a material unlike any other is found. With diameters typically around 1-2 nm [6], a carbon nanotube was discovered. Carbon nanotube strengths are 200 times greater than steel, 5 times more electrically conductive than copper, and are half the density of aluminum which is the "Gold Standard" used in space. Properties of some materials used in spacecraft are shown in Table 1 with comparisons to current state CNT-yarns and the potential properties found in a pure single wall carbon nanotube (SWNT). Early stage estimations like those in Bekey's report do not come without many guiding assumptions. One of the largest assumptions is the expected development of current CNT bulk material properties.

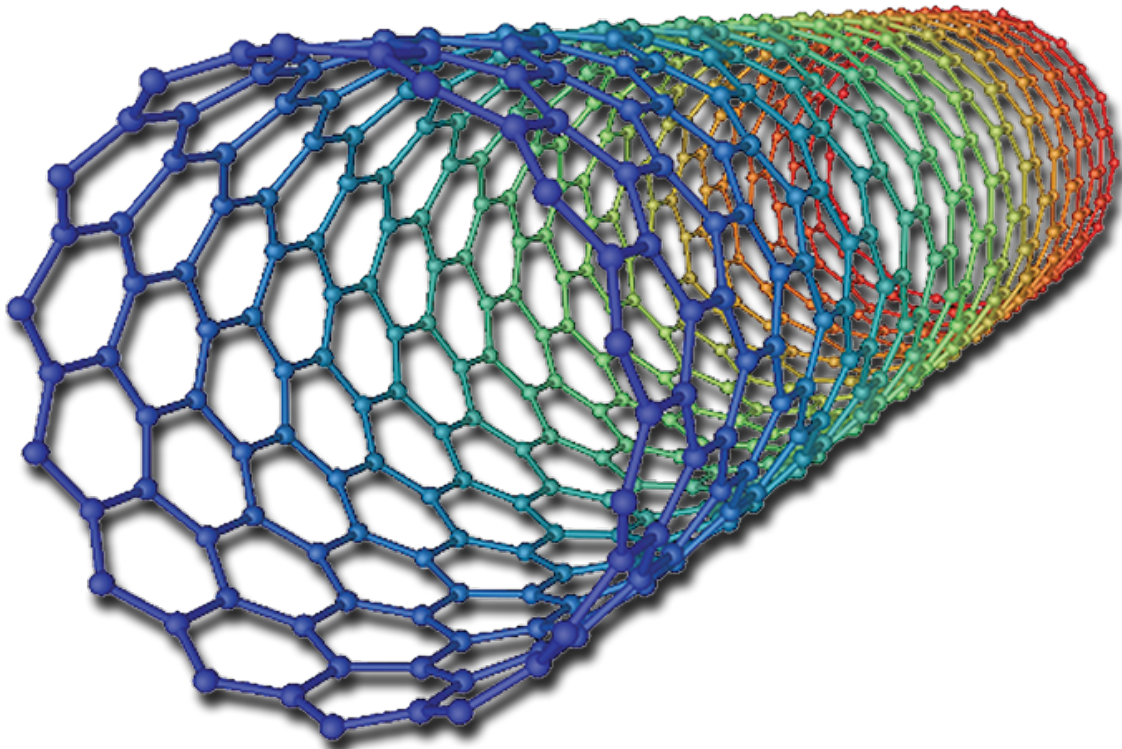


Figure 2. Single Wall Carbon Nanotube (SWNT) [7]

Table 1. Properties of current spacecraft materials

	Young's Modulus (GPa)	Tensile Strength (GPa)	Strain at Failure	Density (g/cm ³)	Conductivity (S/cm)	Specific strength (Al = 1)	Specific conductivity (Cu = 1)
Al Alloy	70	.51	8 %	2.7	3.77x10 ⁵	1	2
HSS	220	1.4	0.7 %	7.8	1.68x10 ⁴	1	0.03
Copper	130	.21	0.6%	8.96	6.00x10 ⁵	0.1	1
Kevlar	120	3	2.5 %	1.4	NA	12	0
Spectra	113	3.3	2.9 %	.97	NA	19	0
CFRP	300	4	1 %	1.5	150	15	0.001
CNT	55	1.1	2 %	1.24	3000	5	.04
Yarn							
Potential SWNT	1000	30	1%	1.24	10x10 ⁷	>128	>1200

Information collected from [8][9][10][11][12][13][14][15][16]

Individual CNTs have fantastic properties; however when they are converted to bulk products such as sheets, yarns, etc., their properties does not show similar performance.

Therefore, it is of great importance to fully understand the mechanical and physical

properties of these CNT products. Previous work in characterizing the electro/mechanical properties of CNT materials for DoD applications have largely been focused on these yarns [17], referenced in Table 1, and other nanocomposites that incorporate CNTs [18][19]. With the advancement of manufacturing, it is now possible to look more closely at the performance of CNT-sheets and their application to space systems.

1.3 Problem Statement

A present challenge that limits the full introduction of CNTs into spacecraft is that the holistic properties observed in bulk CNT materials remain low, unlike an individual CNT. Research seeking to characterize the performance of these exciting materials continues to chase the rapidly changing products and the varying methods being used to improve their performance.

Recent manufacturing parameters for improving CNT-sheet properties includes functionalization and purification with acid treatments [20], and polymer intercalation for enhanced load transfer [21]. The effects of different production rates, acid treatments, and polymer coatings are still not well understood. The resultant effects of surface modification of the CNTs from functionalization is just one question reported with need of further investigation [22]. Varying manufacturing methods also create different properties in the final materials and need to be better understood. Descriptions of CNT-sheets with different production methods are not available and their resulting material properties have not been reported. Effects from physical parameters such as density and thickness are not available to understand trends in the bulk CNT materials where properties vary widely. The synergistic effect of acid treatments and polymer coatings

with enhanced production are also in need of investigation. This is necessary research in order to determine optimization of properties for use in structural applications and those requiring electrical conductivity and shielding from electromagnetic interference (EMI). Further, little evaluation of the effects of the space environments on CNT-sheets is available. This study addresses some of these important issues.

1.4 Research Objectives

This research investigates the electro/mechanical properties of CNT-sheets manufactured with different areal densities, acid treatments, production rates, and polymer coatings. The effects of these manufacturing parameters are discussed with experimentally based conclusions made regarding trends in tensile behavior, electrical properties, and an investigation of morphology and microstructure. After achieving an in-depth understanding of the CNT-sheet properties, this research will highlight their performance in some of the unique conditions of the space environment.

Three investigative questions are summarized in Table 2 along with the associated methodology used to answer each of them. The first question investigates the mechanical properties of different CNT-sheets by considering the relationship with tensile behavior and microstructural parameters found from a scanning electron microscopy (SEM). The second objective investigates the electrical properties through a four point resistivity test and EMI shielding test. Finally the thermal and atomic oxygen conditions of low-earth orbit are simulated. Post exposure effects on the CNT materials are studied with the same methodology from objectives 1 and 2 for comparison to the baseline material properties.

Table 2. Investigative Questions and Methodology

Investigative Question	Methodology
1. What are the baseline mechanical properties of CNT sheets and what are the manufacturing parameters that create those properties?	1.1 Tensile behavior under monatomic loading 1.2 Scanning Electron Microscopy
2. What are the baseline electrical properties of CNT sheets and what are the manufacturing parameters that create those properties?	2.1 Four point electrical impedance test 2.2 EMI shielding with network analyzer 2.3 Scanning Electron Microscopy
3. What are the resulting effects of two space environments; thermal fatigue and atomic oxygen exposure, on electro-mechanical properties?	3.1 Hyper-thermal atomic oxygen exposure 3.2 Thermal cycling 3.3 Scanning Electron Microscopy 3.4 Energy Dispersive X-ray Spectroscopy 3.5 Tensile behavior under monatomic loading 3.6 Four point electrical impedance test 3.7 EMI Shielding with network analyzer

1.5 Summary

The results from the present study will be a critical piece for the DoD in introducing CNT materials into space. Carbon Nanotubes have long been seen as the “Holy Grail” for next generation advanced materials. As an emerging technology, its primitive beginnings have caused it to be less efficient in desired properties. New manufacturing methods to optimize bulk CNT-sheets properties are currently being developed. The first generation of material scientists and engineers experienced with these materials is emerging. Steps are currently being taken towards more flight experiments utilizing these novel CNT based products in space. The current state of these CNT materials and how their properties perform in the harsh environment of space must first be investigated. Utilizing the facilities at the Air Force Institute of Technology

partnering with the facilities at the Air Force Research Laboratory and Montana State University, these materials are rigorously tested in the prelaunch and space environments to answer these critical questions.

Will the Air Force bridge the material gap to make the Single-Stage-to-Orbit (SSTO) launch vehicle possible? Will the DoD's next generation satellites incorporate CNT harnessing for light weight electrical power? What about Radiation/EMI shielding for advanced electronics, next generation batteries and solar panels, or ultra-large deployable structures for the most advanced capabilities seen in space communications and surveillance? The dawn of the carbon spacecraft is illuminated with the results of this thesis work at the Air Force Institute of Technology.

II. Literature Review

Chapter Overview

The content of this chapter reviews the previous work that supports this project and develops the need for CNT materials in space systems. In a metallurgical assessment of requirements for spacecraft materials, it was recognized in the early days of space exploration that conventional metals do not have high enough specific properties, and most spacecraft technology will continue to be replaced by lighter and more complex substitutes [23]. Exploring the current state and understanding of CNT materials will demonstrate the value of experimental research in answering the investigative questions laid out in Table 2 of chapter 1.

2.1 Space Vehicles

No application better epitomizes the revolutionary impacts of CNT structures in space than the single-stage-to-orbit (SSTO) launch vehicle which has historically been impossible. Far-term weight reductions estimated with the potential specific properties of SWNTs warrant a look at the SSTO. SSTO concepts were a hot topic with researchers and large budget projects in the 1980-1990s which ended with canceled programs due to a lack in technology readiness. A successful SSTO vehicle requires a mass fraction of less than 10% which means its mass at launch has to be over 90% propellant [24]. This would require an 18% decrease in the launch vehicle weight or a 7% increase in specific impulse for engine efficiency based off of technology current in the last decade [25]. Kuczera et al. further emphasized lightweight materials as 1 of 3 enabling technologies for reusable space transport, requiring strong lightweight materials resilient to hot

temperatures reaching up to 1800 K beyond the capabilities of metallic structures like titanium [26]. The consequence of CNT applications in spacecraft and launch vehicles is revolutionary for future space systems.

For a satellite, the spacecraft bus is defined as all of the components that provide the functionality of the payload. This generally includes systems like structure and thermal management, propulsion, attitude determination and control, power, command and data handling, and telemetry and tracking. Because of the widespread properties of CNTs, each subsystem of the satellite bus is impacted in weight savings and functionality. These are just a few projected outcomes for using CNTs in space systems. Changes in the development of spacecraft that require mission assurance for greater than ten years have made it necessary to confirm the reliability of materials in the harsh space environment [23].



Figure 3. 1996 photo of X-33 VentureStar: Lockheed Martin proposed spacecraft [27]

2.3 Space Environment

Volume 1 of Air Force Doctrine outlines that among the different domains of the USAF, “Air, Space, and Cyberspace are separate domains requiring exploitation of different sets of physical laws to operate in, but are linked by the effects they can produce together” [1]. The important effects of superiority in each of these domains have been established and it is important to understand the unique physical laws found in space. Another study performed by The Aerospace Corporation clearly showed the importance of testing with a relationship between failures and the thoroughness of testing performed for 454 U.S. satellites. Figure 3 shows the percent of vehicle failures versus the Environmental Test Thoroughness Index (ETTI) [28]. Less than 10% of spacecraft that fully satisfied the DoD standard practices, outlined in the MIL-STD 1540d [29], suffered failure. On the other hand, more than 60% failed when only half the recommended testing was completed. Clearly, environmental testing on space technology is a critical requirement for successful operations.

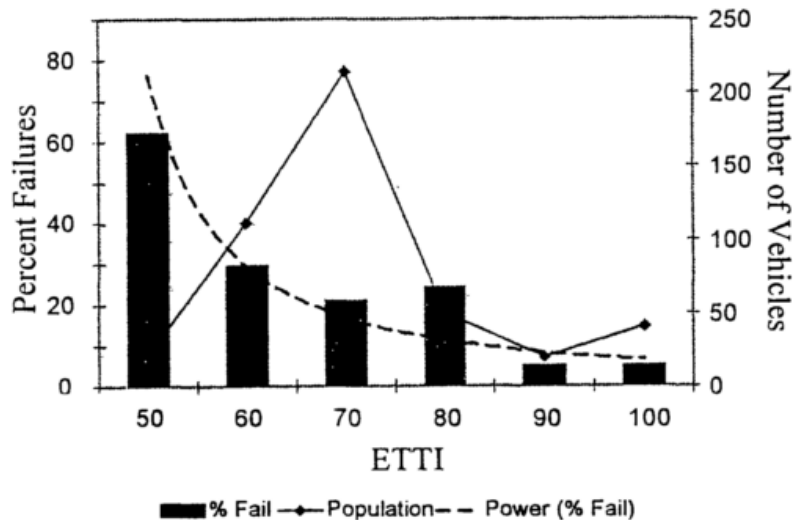


Figure 4. Percentage of space vehicle failures vs. ETTI

Simply put, the unique environment of space needs to be understood and how it affects CNT materials before being able to operate in it. Without this foundation, the space domain falls. Historically this has happened because of the degeneration of materials in the harsh conditions of space and is still today one of the limitations to our space vehicles. According to the joint publication on space operations the space environment “is a significant limiting factor influencing every aspect of a satellite’s size, weight, and power affecting the performance and life-span of any operational spacecraft” [3]. The environment in LEO consists mainly of atomic oxygen (ATOX), UV radiation, ionizing radiation, high vacuum, plasma, temperature cycles, micrometeoroids, and other debris [30]. These various “phenomena in space can affect communications, navigation accuracy, sensor performance, and even cause electronic failure” [3]. Among the most serious causes of degradation effects are ATOX and thermal fatigue. These can be better understood by looking at thermal and composition models of the upper atmosphere where spacecraft orbit.

2.3.1 Thermal Fatigue.

Low earth orbit (LEO) includes altitudes ranging between approximately 160km upwards to 3000 km with most LEO satellites under 1000km [31]. The thermal regime associated with this important range of altitudes starts in the thermosphere which increases from approximately 200 K to a maximum of 700-1900 K in the altitude range of 85 km to 600 km [32]. The temperatures reached are affected by the solar cycle as seen in Figure 5. These extreme temperatures reached in orbit do not burn up vehicles immediately because the density of the atmosphere is drastically reduced. A more meaningful representation of temperature comes from the kinetic temperature which

refers to the average kinetic energy of particles. While the temperature is high it would not feel hot unless the particle density was higher allowing more energy to be absorbed from the sun. Reflect on the difference in heat one experiences by putting their hand in 200°C air in an oven versus submerging it into water at the same temperature. The less intense experience found in the air would be exaggerated further as one went higher in the atmosphere where it approaches a vacuum and high energy gaseous particles are less common.

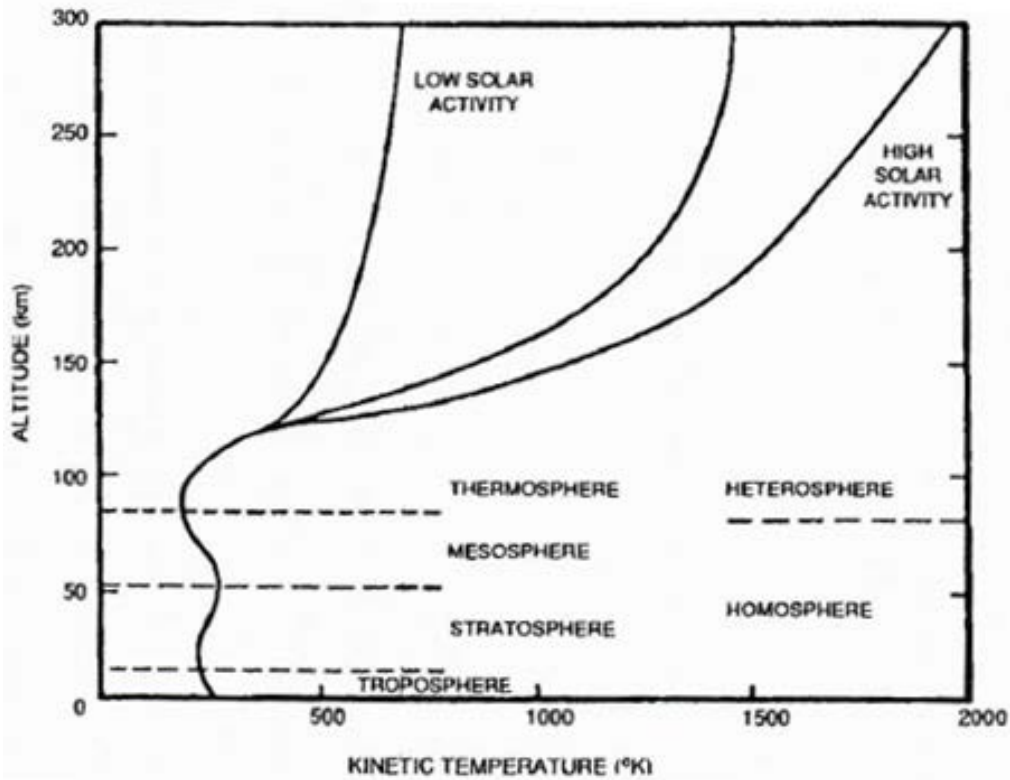


Figure 5. Thermal regimes by altitude [33]

Spacecraft in LEO still cycle between extreme temperatures because the structures move at rates required for orbit around 7.8 km/s. Satellite surface materials can

reach severe temperatures from -150 to +150°C [34]. For practical applications of internal components, a design range is recommended from -70 to 60°C [31].

2.3.2 Atomic Oxygen

Important information about another serious hazard for LEO spacecraft is found by looking at the chemical composition regimes at the same altitudes. While the lower atmosphere is predominantly nitrogen (N_2) and diatomic oxygen (O_2), LEO altitudes above approximately 200km are dominated by atomic oxygen (O) as seen in Figure 6. The thermosphere is dominated by atomic oxygen until approximately 750 km where it is then dominated by helium [33].

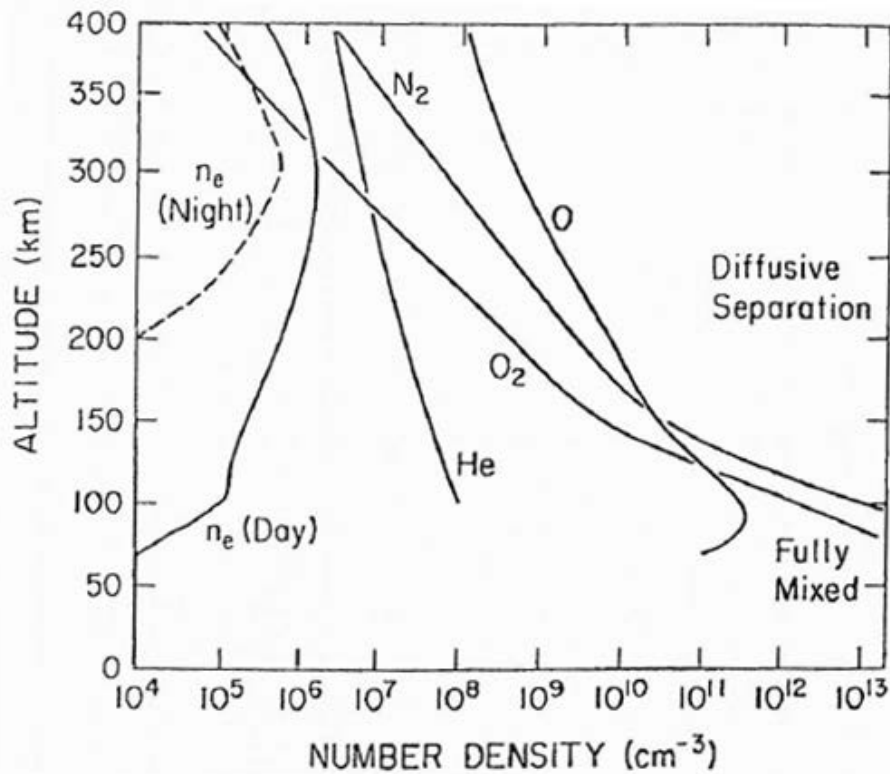


Figure 6. Composition regimes by altitude [33]

The rich atomic oxygen environment comes from the photo dissociation of molecular oxygen by UV radiation and is a hazard to many materials [30]. Atomic oxygen remains in this form at higher altitudes where molecules are sparser and are less likely to interact and form ozone (O₃). Ultraviolet radiation from the sun must be below 190 nm to photo chemically dissociate diatomic oxygen [32]. This change is shown in Equation 1 where the required energy is the photon frequency multiplied by Planck's constant. The frequency is related to wavelength by the wave equation in Equation 2 and can then finally be used in Equation 3 to determine the required photo dissociation energy. This shows solar radiation energies of greater than 6.5eV in the atmosphere causing the formation of atomic oxygen.



Where:

O₂ = diatomic oxygen

h = Planck's constant (6.626 x 10⁻³⁴ J·s)

ν = photon frequency

O = atomic oxygen

KE = resulting kinetic energy

$$c = \lambda \times \nu \quad (2)$$

Where:

c = speed of light (3.00 x 10⁸ m/s)

λ = wavelength

ν = frequency

$$E = hv = \frac{hc}{\lambda} = 6.5 \text{ eV} \quad (3)$$

Where:

E = required photo dissociation energy

1eV = 1.60218×10^{-19} J

ATOX was reported from measurements on shuttle missions STS-8 and 41-G to react with materials including organic films, advanced composites, and metalized surfaces [35]. This can cause degradation in spacecraft materials and components including sensor payloads. Atomic oxygen has shown to be a cause of erosion, corrosion, and oxidation of many materials. For this reason, literature has requested that more coatings with good atomic oxygen durability be developed [23]. Kapton is an example of a film material commonly used in space for insulation and seals. Atomic oxygen effects in LEO are evaluated by Leger et al. who reported kapton eroding at a rate of $2.8 \mu\text{m}$ for every 10^{24} atoms/ m^2 of atomic oxygen fluence [36]. At this rate a kapton film used for supporting solar cells with a designed thickness of $25.4 \mu\text{m}$ could be completely eroded in less than two years. Because space vehicle lifetimes can be designed for 15-30 years, understanding the effects of ATOX on materials is essential. New materials with less reactivity and degradation to ATOX would be a hot topic. The use of advanced composites for space hardware has increased with carbon fiber reinforced polymer (CFRP) composites being desirable for lightweight structural properties. A variety of these materials have also been shown to have ATOX interactions resulting in surface

degradation, erosion, and changes in surface morphology [37]. Grossman et al. describes that exposure of composite materials in this environment can result in degrading effects to include chemical, electrical, thermal, optical and mechanical property changes, and surface erosion [30].

The LEO altitude consists of approximately 80% ATOX and ~20% nitrogen molecules [30]. ATOX is found in densities of $\sim 10^6$ - 10^9 atoms/cm³ ranging through solar cycles [30][38]. All the time ATOX is impacting orbiting space vehicles at rates of 7-8km/s for altitudes around 300 km. This orbital velocity leads to ATOX flux of approximately 10^{12} - 10^{15} atoms/cm²s which hits the spacecraft surface with a kinetic energy of about 5eV [39]. The effects of ATOX on different materials have been an important topic of investigation since its observed effects during the space shuttle missions. More than 1000 materials have been evaluated on space shuttle missions (STS-6, STS-8, STS-17, STS-32, STS-41, STS-46) and on satellite platforms [30]. Among these materials, organic polymers were found to degrade in space because of their reactions with ATOX [38]. Shin et al. reports ATOX erosion leading to dimensional changes, mass loss, and degradation to mechanical properties [34]. A study looking at organic composites flown on the long duration exposure facility (LDEF) showed that the most detrimental effect of the space environment was in material loss from ATOX erosion [34]. This comprehensive material testing in space was conducted before the existence of CNTs in bulk material forms.

2.3.3 Electromagnetic Interference

Effects of radiation from the sun can cause changes to a material's mechanical and electrical properties and introduces electromagnetic interference that can disrupt

spacecraft operations [18]. This ionizing radiation found in space can cause both short term and long term affects in electrical circuits including data loss and permanent damage [32]. Material surfaces can build up electrical charges from charged particles in the space plasma. This build-up can lead to undesirable signals and discharges on the surface which create electromechanical interference (EMI). One way to prevent EMI is through shielding [40].

2.1 Carbon Nanotubes

The first reported discovery of the carbon nanotube was in 1991 by Iijima [41] which accelerated the research of what would become the most actively investigated structure in the last century [42]. From just the years 2000 to 2007, the number of papers published annually increased steadily from under 1000 to over 5000 [43]. Single wall nanotubes (SWNTs) are defined with a single layer structure having a typical diameter of 1.4 nm [6]. Carbon nanotube structures can be modeled and defined by a chiral vector in Equation 4 [44]. Chirality refers to the CNT structure existing in different forms.

$$C = na_1 + ma_2 \quad (4)$$

Where:

n, m = integers representing CNT chirality

a₁,a₂ = unit vectors

Different CNT structures can be formed by conceptually folding the graphene sheet in Figure 7. In the case where SWNT (0,0) is joined with SWNT (3,3), the

circumference is parallel to the unit vector a_1 and is classified as a zigzag nanotube with $(n,0)$. The chiral angle for this class is 0° from Equation 5 [6].

$$\theta = \sin^{-1} \left[\frac{m\sqrt{3}}{2n+m} \right] \quad (5)$$

Where:
 $n, m =$ integers representing CNT chirality

By joining the SWNT $(2, 2)$ to SWNT $(0, 0)$, a different class is produced called armchair nanotubes represented by (n, n) and where the chiral angle is 30° . The final group are called chiral nanotubes with chiral angles $0^\circ < \theta < 30^\circ$. An example for a chiral nanotube formed from the graphene sheet in Figure 7 is found by matching SWNT $(3,1)$ with SWNT $(0,0)$ which would have a chiral angle of 20.27° .

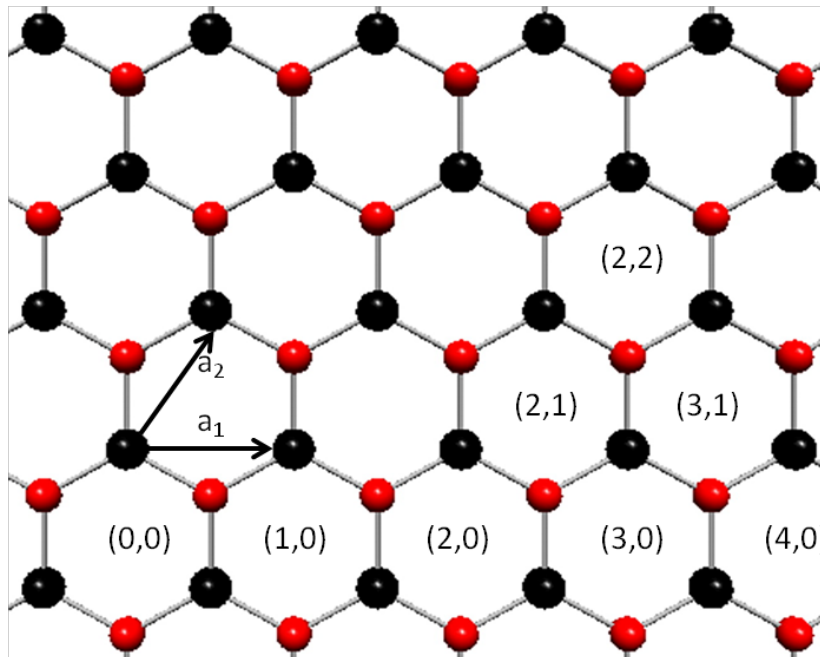


Figure 7. Chiral vector and CNT structure

The magnitude of the CNT circumference and diameter are represented in Equation 6 and Equation 7 respectively [6].

$$C_h = a(n^2 + m^2 + nm)^{1/2} \quad (6)$$

$$d_t = \frac{C_h}{\pi} = \frac{a(n^2 + m^2 + nm)^{1/2}}{\pi} \quad (7)$$

Where:

a = length of the unit vector equal to 2.46 Å

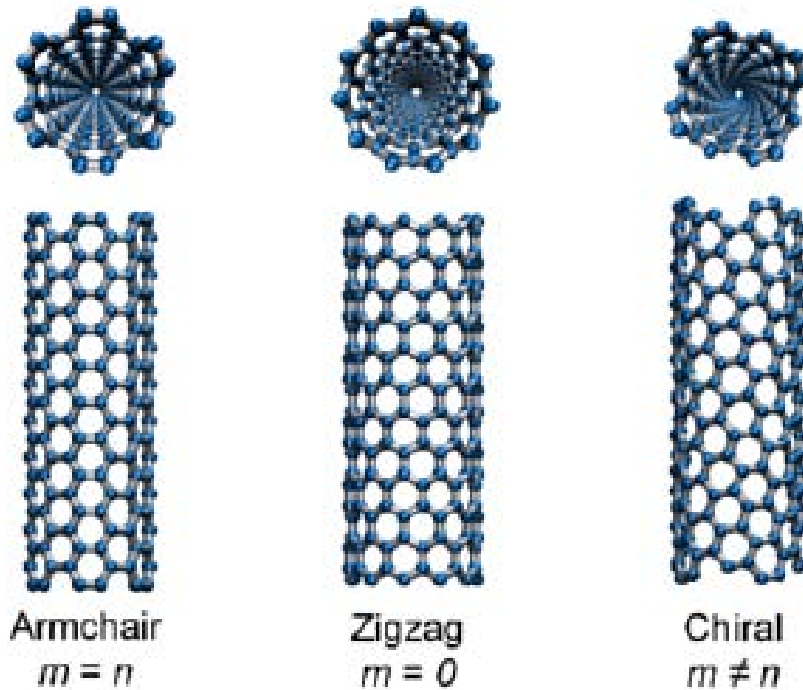


Figure 8. Different types of CNT [45]

Successful synthesis methods have been developed which include arc discharge, laser ablation, and chemical vapor deposition [42]. Each of these has varying forms along with pros and cons for their use. Arc-discharge is a process attributed to the first success in mass production of CNTs [42]. Laser ablation is less useful for large scale production, but was pioneering as a method for fullerene production. It supported the discovery of the use of metal catalysts used to produce SWNTs with laser ablation that would be used in future methods of producing CNTs [42]. Chemical vapor deposition has been the method of more extensive research in literature and includes various forms including traditional thermochemical CVD, plasma enhanced CVD, aerosol assisted (AA-CVD), high pressure decomposition of CO gas (HiPCO), alcohol catalytic (AACVD), and a hybrid laser assisted thermal CVD (LCVD) [42]. In each of these CVD methods, carbon saturates onto a catalyst which is then precipitated from one point in the form of a carbon nanotube. The HiPCO method uniquely forms the catalyst by the decomposition of a metal containing compound and has improved synthesis by being able to produce larger quantities of high-quality SWNTs [46]. One historic problem with this method has been the larger catalyst content typically found around 14 wt% [43].

Individual nanotubes have a tendency to group together as bundles, sometimes called ropes, which becomes the building block to larger bulk CNT products. Two macro-scale CNT products include yarns[47] and sheets [48] which can be produced by drawing mechanically interconnected CNTs from a vertically aligned CNT forest or drawn and deposited from a CNT aerogel. CNT-sheets, first produced in 1998 at Rice University, were produced out of a purification process in a film where small bundles of tubes were interconnected like the fibers in a sheet of paper [43]. Because of this

appearance, they received the name “buckypaper” [49]. Although their conception was unintended, a new nano-structured material made with CNTs was formed with interesting properties.

2.1.1 Mechanical Properties

Carbon Nanotubes (CNTs) have extraordinary mechanical properties with a SWNT theoretically achieving strengths and Young’s Moduli of approximately 30 and 1000 GPa respectively and less than 5.3% strain at failure [13]. Bulk mechanical properties achieved in macroscopic applications, however, persist in falling below their potential as the world’s most advanced material. SWNT properties are shown with several measured properties of CNT-sheets in Table 3.

SWNT “buckypaper” are built in a similar manner to paper by filtration of SWNTs in water before being densified [49]. These introductory products yield low properties with groups of SWNT fibrous networks only being bonded with weak van der Waals networks at contact joints [50]. Coleman et al. reports strength and modulus of an example pristine sheet as 6.29 MPa and 2.3 GPa respectively [21]. Tensile tests performed on a 14µm thick sheet reported strengths on the order of 10-20 MPa [43].

Table 3. Reported mechanical properties of CNT-sheets

Properties	SWNT	Sheets
Strength	30 GPa [13]	6.29 [21] 10-20 MPa [43]
Modulus	1000 GPa [13]	2.3 GPa [21]
Strain to failure	5.3% [13]	Not Available

Chemical vapor deposition (CVD) was a method developed capable of producing high quality SWNT and MWNT CNT forests on substrates grown as vertically aligned

forests [51][52]. Large improvements in mechanical properties have also come from the improvement of the CNT drawing process [53][54]. The HiPCO method has also improved manufacturing rates and cost by spraying a $\text{Fe}(\text{CO})_5$ catalyst into a reactor operating at temperatures around 1050°C and held at 30 atm [55]. The impressive strengths of these free-standing CNT-sheets from newer methods is expected to come from the mechanically interconnected fibers [48].

Because these CNT synthesis methods grow CNTs over metal catalysts such as Ni, Fe, and Co, metal impurities remain as residue contained within the carbon layers in the sheets [56] and may decrease the integrity of bulk mechanical properties [57]. Other impurities besides encapsulated metals include amorphous carbon fullerenes, and other carbon nanoparticles, which have been removed by different methods of purification including acid treatment [56]. The process of purification is discussed in a later section as a method for improving bulk mechanical and electrical properties.

2.1.2 Electrical Properties

Carbon nanotubes (CNTs) display impressive electrical properties in their nano-scale form. In addition to exceptional physical properties, their mechanical performance makes them a unique and exciting solution to advanced multi-purposed structures that are electrically conductive. Single-walled nanotubes (SWNTs) can be semi-conducting, and have the ability to transport electrons over long lengths with little interruption resulting in higher conductivity than copper [55][58]. Focused efforts across the Department of Defense (DoD) and industry are looking for solutions in maintaining these physical properties with bulk CNT products.

One of the unique properties of CNTs is that depending on their structure they can be metallic like copper or semiconducting. A third of zigzag and chiral tubes are metallic, where $n-m=3p$ with p being an integer [6]. Along with these, and the armchair structure, all multi-wall nanotubes (MWNTs) are metallic and have electrically conductive properties. This electronic structure in a SWNT is further understood in the energy dispersion of graphene where there is overlap between the π orbitals with a band structure built by a small boundary with limited number of states around the atomic circumference dimensions [43]. Whether or not a nanotube is metallic or semiconducting is determined by if the energy bands (Figure 9a, b, c) in the 1D dispersion or band structure (shown by the dotted lines) cross through the corner of the hexagon.

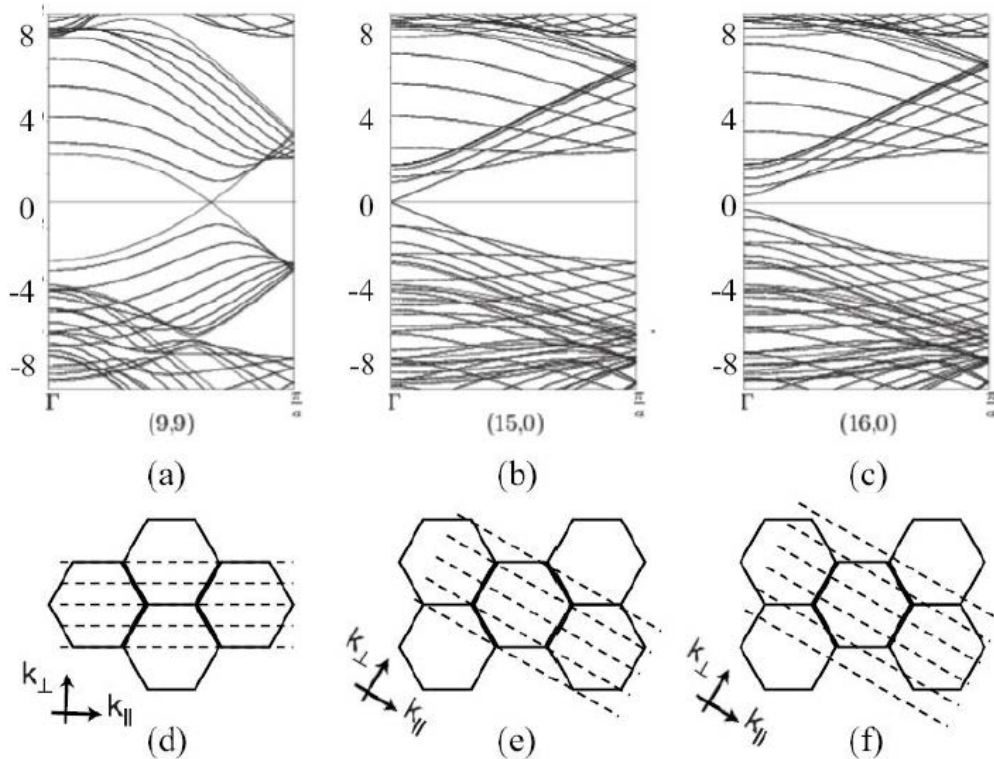


Figure 9. Band structure for nanotubes [59]: SWNT armchair metallic nanotube (a, d), SWNT (15,0) zigzag metallic nanotube (b, e), and SWNT (16,0) zigzag semiconducting nanotube(c, f)

This is the point where the conduction and the valence band of the graphene lattice touch and electrons can transport. For the case of the SWNT (9,9) armchair tube, two energy bounds cross demonstrating its metallic nature. For the SWNT(15,0) case the energy bands cross but in the SNWT(16,0) case it becomes semi-conductive where a band gap is found between the quantization lines shown and the point of valence band connection [59].

CNT sheets demonstrate the bulk scale manufacturability of thin, non-woven fabric-like products being produced with large areal dimensions. CNT-sheets are manufactured in a way where CNTs are dispersed in random orientations in a fibrous network [50]. Mechanical bonding and interlocking between CNT bundles on the micro scale are also important for the electrical properties as electricity looks for paths through the directionally conductive nanotubes. Newer synthesis methods incorporate the growth of high-quality single-wall and multi-wall CNT forests on substrates with chemical vapor deposition (CVD) as a possibility to produce low cost CNTs [51][52]. More order is found in CVD grown nanotubes and electrostatic force microscopy has verified long, mean free paths in these semiconducting nanotubes [55]. The impressive properties of free-standing CNT-sheets produced from CVD methods, including HiPCO that have more interfibril mechanical coupling, provide a path to improved electrical properties. A report demonstrated the production of self-supporting films that are densified into strong sheets from an electronically conducting aerogel. Zhang et al. explains here that electronic properties may be contributed to lateral forking of the CNT fibril groups that interconnect to the forked ends of other fibril groups [48]. In order to improve electrical

performance of fabricated CNT devices the nanotubes must also be cleaned from residual catalysts [55].

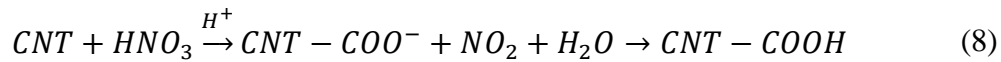
The ability of a material to shield electromagnetic interference (EMI) is another important physical property related to electrical parameters. In 2012, Hunt studied the EMI shielding capabilities of S-glass composites created with MWNTs [18]. Misak et al. has investigated the electrical properties of CNT yarns with analysis on the method of acid treatment to achieve different physical properties [17][20]. Research is needed to understand these properties in CNT-sheets along with the manufacturing parameters that create them.

2.2 Manufacturing Parameters for Improved Properties and Production

2.2.1 Chemical Treatment

A challenge to reaching the potential properties of CNTs is due to the lack of purity in the bulk products presented by carbonaceous or metallic impurities from residual catalysts. Carbonaceous impurities including amorphous carbon, fullerenes, carbon nanoparticles, and metal encapsulating graphitic polyhedrons have been observed in CNT products produced by different methods [56]. Hou et al. reports that fullerenes can be easily removed in some organic solvents. Amorphous carbon is also reported to be removed under gentle oxidization. Metal impurities can be dissolved in acids but can be difficult to remove completely when they become encapsulated inside of layers. Purification methods include gas and liquid phase oxidation, physical methods, polymer extraction, acid treatments and CS₂ extraction [56].

Acid treatment and functionalization with triethylenetetramine also creates covalently and ionically bonded amine functional groups on the CNT sidewalls [22]. Misak et al. used ATR spectroscopy to verify the presence of carboxyl and hydroxyl groups (e.g., COOH, COO⁻, OH, etc.) in CNT yarns treated with nitric acid. The reaction with nitric acid to form carboxyl groups on the CNT yarns is shown in Equation 8.



Where:

CNT = carbon nanotube

HNO₃ = Nitric acid

H⁺ = hydrogen ion

COO⁻ = carboxylate ion

NO₂ = nitrogen dioxide

H₂O = water

COOH = carboxyl function group

Niu et al. reported in 1996 that treating CNTs with nitric acid removed 90% of catalyst residue and found that it helped break down aggregated CNTs in preparation of sheets [60]. The reduction of CNT agglomeration and surface modification from acid treatments was demonstrated for improved CNT bulk mechanical properties [22][61]. The dispersion from these processes has been instrumental in the improvement of nano composites by improving the bonding of CNTs with the composite matrix [62].

The additions of function groups also create structural defects on the CNTs reducing its overall potential strength. Frankland et al. expects that functionalization of less than 1% will improve interactions without decreasing the CNTs strength significantly [63]. Work performed in 2009 focused on efficiently using acidic oxidation

while minimizing damage to the nanotubes resulting in a finding that low concentration nitric acid was the most effective [64].

2.2.2 Polymer Coatings

Another challenge to CNTs in review of investigated manufacturing parameters is the length of manufactured CNTs. While longer CNTs have been produced with lengths of greater than 1 mm [65], purification with nitric acid result in shorter CNTs [55]. In 2012, Wang et al. reported higher electrical conductivities in bulk products using longer CNTs [65]. With challenges in producing longer CNTs, polymer intercalation into the CNT sheets has been researched and reported in 2003 and 2006 by Coleman et al. to improve bulk mechanical properties by load transmission between nanotubes [21] [66]. Spitalsky et al. reviewed the current state of polymers used with filler CNTs in 2009 reporting on a large range of these nanocomposite electrical properties [67]. Spitalsky's report presented enhanced electrical conductivity in nanocomposites with MWNT fillers. With a large range of polymers and combinations of CNTs, this study investigates high CNT weight percent sheets with polystyrene (PSb) and thermoplastic polyurethane (TPU).

2.2.3 Production Rate

Manufacturing processes are under continual investigation to make bulk CNT products available for application. CNT-sheets have recently been manufactured with an enhanced production rate (EP) that is not well understood. This enhanced production rate is expected to be a high value method for producing more CNTs in less time. This study investigates EP CNT-sheets as a manufacturing parameter affecting mechanical and

electrical properties. In addition, this study looks at the synergistic effects of polymer intercalation and acid treatment with EP CNT-sheets.

2.4 Relevant Research

Thermal environment testing to simulate thermal fatigue in low earth orbit (LEO) for other material studies has been performed by cycling between temperatures of -70 to 100°C at rates anywhere between 3-5°C/min [34] [68] [69]. Thermal fatigue was performed on CNT-yarns with smaller temperature ranges of -50 to +70°C with an accelerated rate of 55°C/min to achieve 5000 cycles [70]. Misak et al. reported no effects in tensile strength but an 18% decrease in electrical conductivity due to yarn buckling and fractures shown in Figure 10.

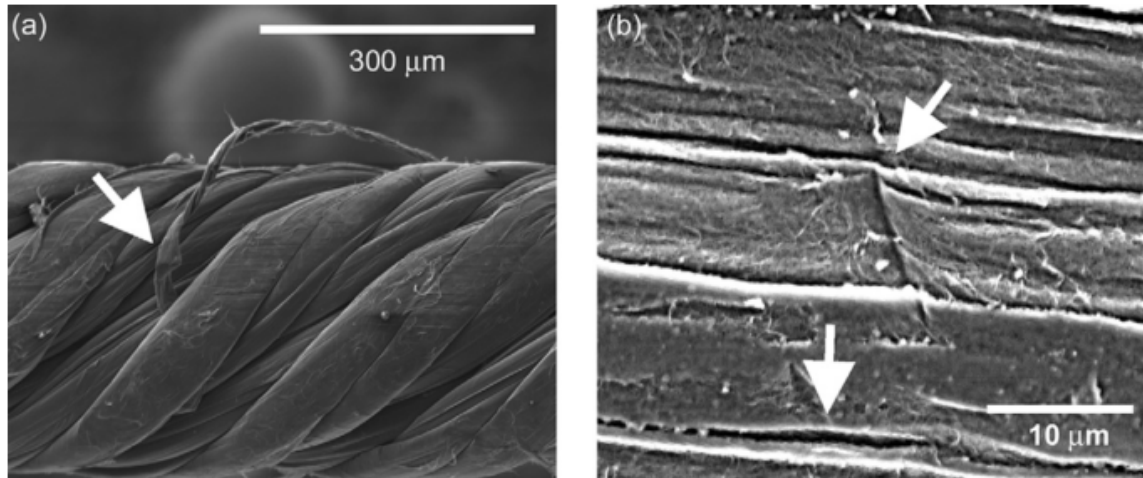


Figure 10. CNT-yarn (a) fracture in CNT bundles after thermal fatigue (b) delamination (lower arrow) and crack formation (upper arrow) from kink band formation in thermal fatigued CNT-yarn

Multi-wall nanotubes (MWNT) are used as reinforcements to carbon fiber reinforced plastics and tin-ply composites as solutions to improved resistance to LEO space environments [68]. Moon et al. demonstrated that incorporating MWNTs into

composites increased baseline tensile strength and improved resistance to the LEO environment including atomic oxygen (ATOX) and thermal fatigue. Results showed the composites with MWNTs most notably less reactive to ATOX and more resilient to ATOX in orbit [68]. Han et al. reported a slight reduction in tensile strength and stiffness by 3.27% and 3.99% respectively for Gr/Ep composites exposed to LEO simulated ATOX as well as surface erosion and mass loss [69]. Hypothermal atomic oxygen effects have also been studied on CNT yarns under a nominal fluence of 2×10^{20} atoms/m² in order to simulate LEO conditions. Misak et al. reports an erosion rate of 2.64×10^{-25} cm³/atom, which is comparable to highly ordered pyrolytic graphite [70]. No tensile strength was lost and a minor decrease of conductivity was found (2.5%). Surface defects were found under scanning electron microscopy after ATOX exposure in Figure 11. Defects like these would restrict electron movement and cause the minor reduction in conductivity.

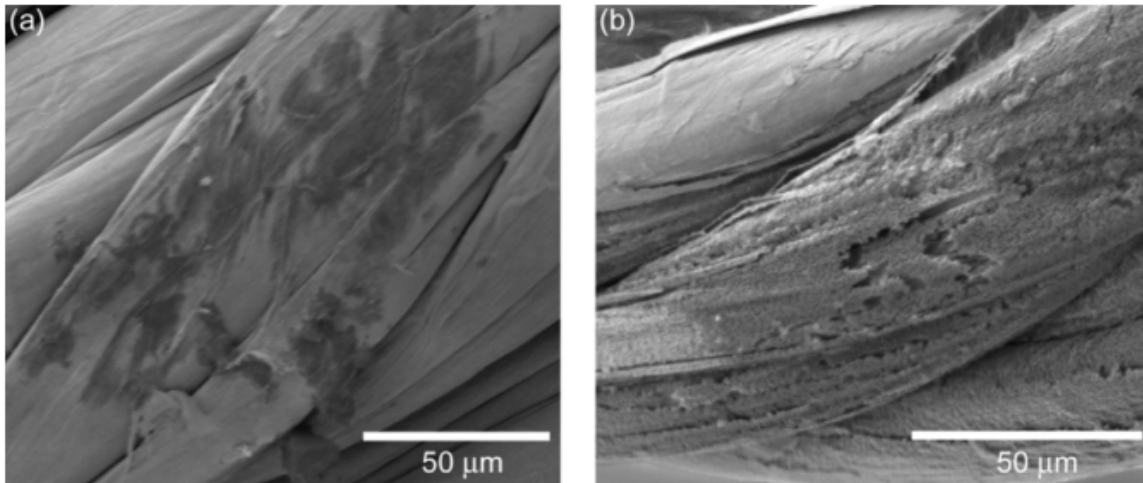


Figure 11. CNT yarn after atomic oxygen exposure: (a) surface damage before tensile test and (b) surface damage seen after tensile failure

EMI shielding effectiveness was evaluated by Captain Peter Hunt at AFIT in 2012 on composites formed with carbon nanofibers and MWNTs under fatigue. He discovered that composites with CNTs had better EMI shielding which performance was dependent on the concentration of CNTs [18]. CNT based composites were concluded to be promising materials for shielding against EMI in space structures. In 2013, engineers at Lockheed Martin presented work including the incorporation of CNT sheets into the outer layer of CNT-based composites for use on the Juno spacecraft [4]. EMI shielding effectiveness was tested over the range of 20 MHz to 18 GHz. Success was found in using a CNT-sheet as the outermost ply of a composite layup, improving the surface conductivity of the composite and improving shielding effectiveness. Flight ready components are used on the Juno spacecraft and open the door to CNT-based composite materials on other future spacecraft. Figure 12 shows the use of a CNT-sheet wrapped as the outer ply of a composite layup for ESD on the rocket engine motor support struts fabricated for Juno.



Figure 12. Preparation of support on Juno spacecraft [4] with outer layer CNT-sheet

2.5 Summary

CNTs carry the most impressive material properties known and current research is exploiting their properties for the coming of the most advanced architecture of spacecraft technology the world has seen. A review of literature has presented a background to the current state of CNT material science and engineering. The current technology limitation is that bulk CNT products have reduced properties compared to individual CNTs. This current technology limitation prevents the use of CNTs in every subsystem of a satellite or launch vehicle. The collective community is faced with the challenge of improving the bulk material properties to that of the theoretical possibilities. Investigations have grown in number with highlighted interest in manufacturing methods, acid treatment, and polymer coatings. These manufacturing parameters under review are all possible ways to improve the mechanical and electrical properties of CNT-sheets which are less understood throughout industry and academia. Further research is needed to understand the parameters that create the holistic properties in the CNT-sheets and how these manufacturing parameters interact. Exploring and understanding the factors that affect these bulk properties will allow their improvement. The exhaustive testing which has been previously performed on other materials in the space environment has not yet been performed on CNT-sheets. The investigative questions introduced in the introduction need to be answered and are the objective of the methodology presented in the next chapter. Answers to each of these questions will bring engineers one step closer to the successful use of CNT-sheets in orbit and are the goals of this thesis.

III. Methodology

3.1 Introduction to Methodology

The content of this chapter details the preparation of test specimens and the test procedures used. Extensive testing was performed with facilities and equipment located at AFIT, the AFRL Materials and Manufacturing lab at WPAFB, OH, and through support facilities at Montana State University. Testing procedures and simulated space environments conducted at AFIT included tensile testing, SEM imaging, electrical conductivity, and thermal fatigue. EMI shielding performance was evaluated with facilities at AFRL. An SEM was also used at AFRL with a field emission gun (FEG) for additional high resolution images. Samples were sent to Montana State University for exposure to hyperthermal atomic oxygen bombardment.

3.2 Test Specimens and Preparation

The CNT-sheets investigated in this study were manufactured by Nanocomp Technologies, Inc. (NTI), Concord, New Hampshire, USA. CNT-sheets used are composed of synthetic nano fibers deposited onto a translating drum into a non-woven textile form mat [71] shown schematically in Figure 13a. CNTs are grown from iron catalysts that are present on the CNT-sheet as contaminants if not post treated. Nitric acid treatment is utilized to dissolve/reduce iron catalysts. NTI also uses an enhanced production method by depositing larger amounts of CNTs at faster rates to increase the production quantity thereby reducing costs of CNT-sheets. Specimens from these sheets are referred to as enhanced production (EP) in this study. Individual single layer CNT networks can be as thin as 50 nanometers [48], and are therefore layered to form thicker

sheets for bulk/macro applications. EP CNT-sheets, i.e. sheets manufactured by enhanced production, have generally less number of layers with thicker dimensions seen in Figure 13b. This is one way to increase production yield with reduced complexity and requiring fewer high temperature furnaces and reactors. Details of the manufacturing and acid treatment parameters are not available due to their proprietary nature. The content of the results discussion will therefore focus on the investigation of known manufacturing parameters present in different samples and characterize their observed mechanical and electrical performance to better understand each of them.

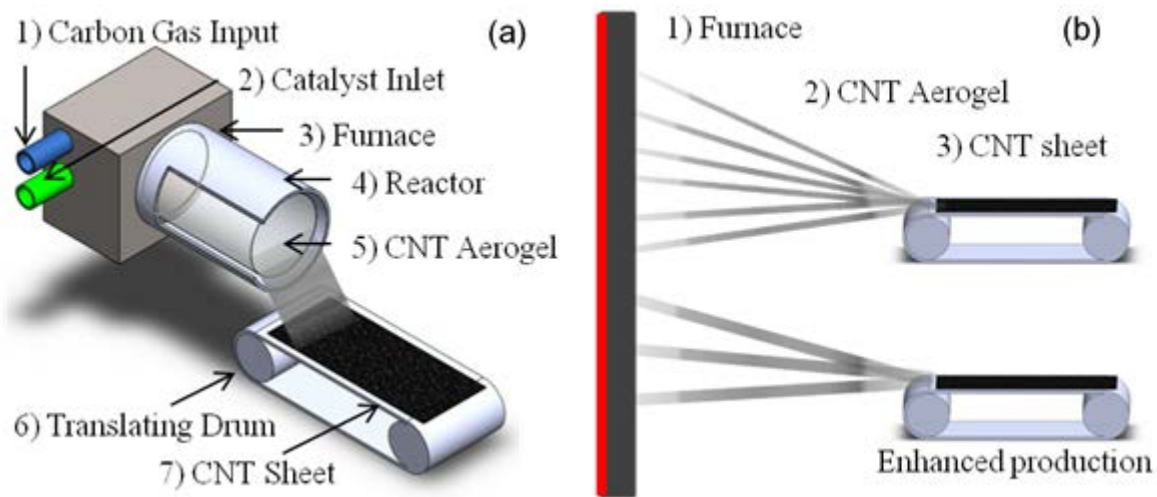


Figure 13. (a) Schematic of CNT-sheet manufacturing process and (b) enhanced production

There are 14 unique CNT-sheets investigated in this study with different variables involving production rate, acid treatment, and polymer coatings. These 14 sheets in Table 4 are categorized into six groups based on similarities among them. Specimens are numbered 1-14 and are further identified with a letter and shape shown in Figure 14. These identifiers help distinguish the variables in the presented data and discussion. Type

A is the first classification which includes the reference material with the standard production rate and no acid treatment or polymer coating. The second category, type B, is enhanced production (EP) CNT-sheets. Types, C and D, are respectively non-EP and EP while both being treated with nitric acid. The last two types, E and F, are also respectively non-EP and EP while both being coated with different polymers. Each sheet from each type varies by thickness and areal density. Each specimen type will be represented by a symbol shown in Figure 14 that will be used in subsequent figures.







	Standard Production	Enhanced Production
Not Treated	A Specimen 1 	B Specimen 2 Specimen 3 Specimen 4 
Acid Treated	C Specimen 5 Specimen 6 Specimen 9 	D Specimen 7 Specimen 8 
Polymer Coating	E Specimen 10 Specimen 11 	F Specimen 12 Specimen 13 Specimen 14 

Figure 14. Summary of specimen variables

3.2.1 Apparent Thickness

Determining properties like strength, stiffness, and conductivity requires the cross sectional area for CNT-sheets. Thicknesses ranged anywhere between 15 and 60 μm in this study. Determining these small dimensions is difficult because of the nanoscale voids among CNTs, residual catalyst impurities encapsulated between layers, and possible factors found in the packing details of CNTs in the production process [17]. The thickness across each sheet also can vary moderately. Using a material thickness gauge with a resolution of 2 μm , the thickness was measured at several locations across the surface of each specimen. The measurements for thickness were averaged with an associated standard deviation. For unknown variables related to packing factor of CNT's, voids, and impurities, properties that depend on thickness will be referred to as "apparent" property in the text..

Table 4. Details of CNT-sheets

Identifier Group – specimen	Thickness* (μm)	Volumetric Density* (g/cm^3)	Areal Density (g/m^2)	EP	Acid Treated	Polymer Coating
A - 1	39.11 \pm 2.77	0.38 \pm 0.02	15.08 \pm 0.10			
B - 2	25.77 \pm 7.31	0.46 \pm 0.11	11.28 \pm 0.31	X		
B - 3	45.00 \pm 5.54	0.46 \pm 0.03	20.74 \pm 1.32	X		
B - 4	25.11 \pm 4.34	0.50 \pm 0.05	12.35 \pm 0.84	X		
C - 5	19.20 \pm 2.43	0.52 \pm 0.06	9.98 \pm 0.10		X	
C - 6	23.44 \pm 1.83	0.49 \pm 0.04	11.43 \pm 1.50		X	
C - 9	51.67 \pm 4.67	0.31 \pm 0.02	15.92 \pm 1.32		X	
D - 7	18.23 \pm 0.52	0.58 \pm 0.12	10.53 \pm 2.51	X	X	
D - 8	23.11 \pm 0.77	0.40 \pm 0.04	9.24 \pm 0.74	X	X	
E - 10	40.22 \pm 6.47	0.59 \pm 0.10	23.45 \pm 1.14			X
E - 11	59.67 \pm 2.03	0.28 \pm 0.00	16.96 \pm 0.50			X
F - 12	50.33 \pm 4.36	0.47 \pm 0.03	23.53 \pm 1.30	X		X
F - 13	30.62 \pm 7.23	0.49 \pm 0.06	14.80 \pm 1.63	X		X
F - 14	32.82 \pm 8.00	0.45 \pm 0.12	14.21 \pm 1.19	X		X

*Apparent property.

3.3 Tensile Test Equipment and Method

The CNT sheets were tested until they fractured under monotonic tensile loading condition using a MTS Tytron 250 bench-type test machine with a 50 N load cell shown in Figure 15. Each specimen was prepared with an approximate width and gauge length of 12.5 and 40 mm respectively.

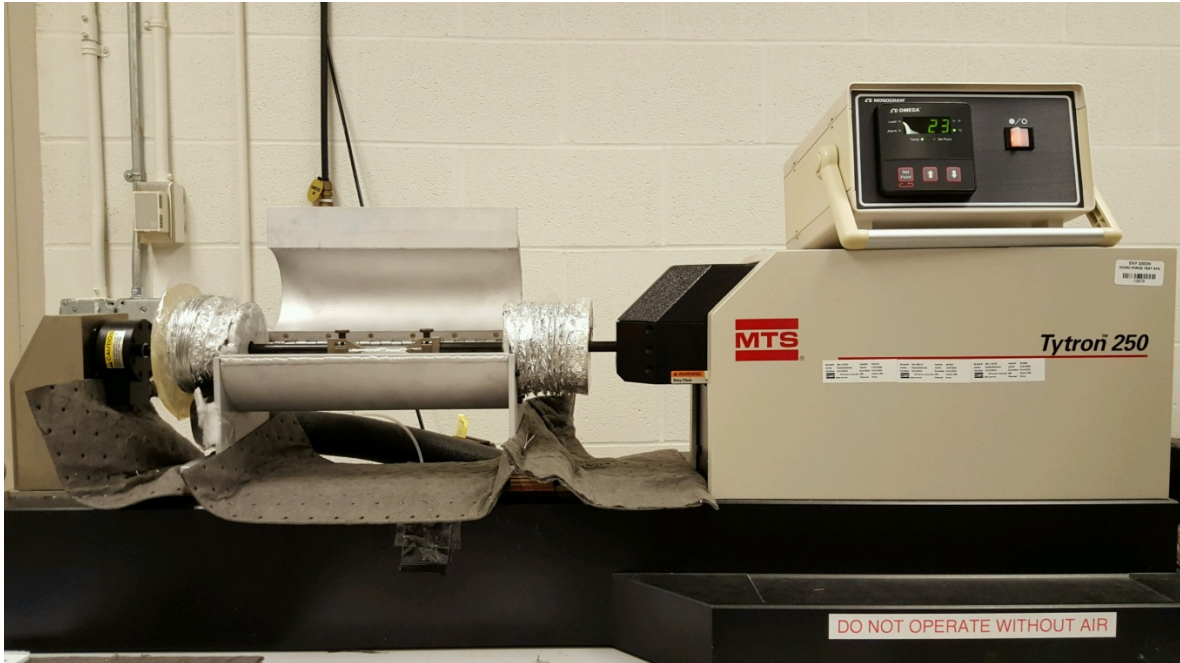


Figure 15. MTS Tytron 250 tensile test machine

CNT sheet specimens were glued between two thin pieces of fiberglass with epoxy resin to protect ends from premature failure at the grips. A test specimen before tension is shown in Figure 16a. The specimens were tested under displacement controlled mode and pulled at a strain rate of 2 mm/min. Straight samples were used instead of dog bone specimens. Large amounts of strain were observed. This created the necking seen in Figure 16b.

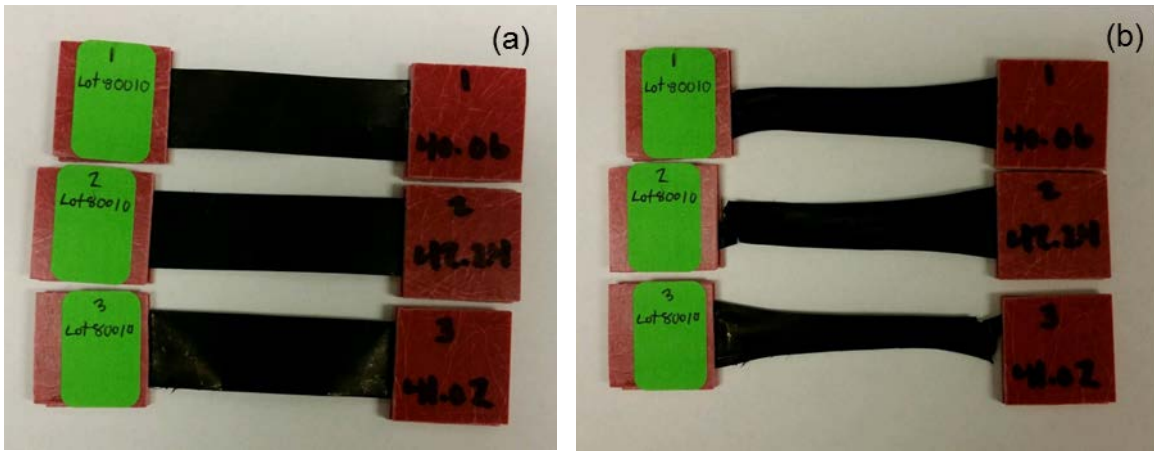


Figure 16. Tensile test specimens: (a) prepared specimen and (b) necking after strain

This necking led to tearing failure at locations away from the center point. . Conventional studies required failure to occur in the center of the sample for valid mechanical analysis. However, the purpose of this study is for practical use and understanding the mechanisms involved in failure, thus data is collected for near grip failures and center failures. Failures at the grips were not included in the analysis. Tensile strength data gathered from these tests are accurate representations of the sheet properties with no pre-conditioned alignment. Detailed discussion on the mechanical properties and alignment of CNT-sheets is provided in the analysis and results chapter.

3.4 EMI Shielding Test Equipment and Method

EMI tests were performed at the AFRL Materials and Manufacturing Directorate's characterization lab. To evaluate the material effectiveness of EMI shielding, a range of signals at different frequencies were produced and sent through the sample with an Agilent PNA Microwave Network Analyzer shown in Figure 17.

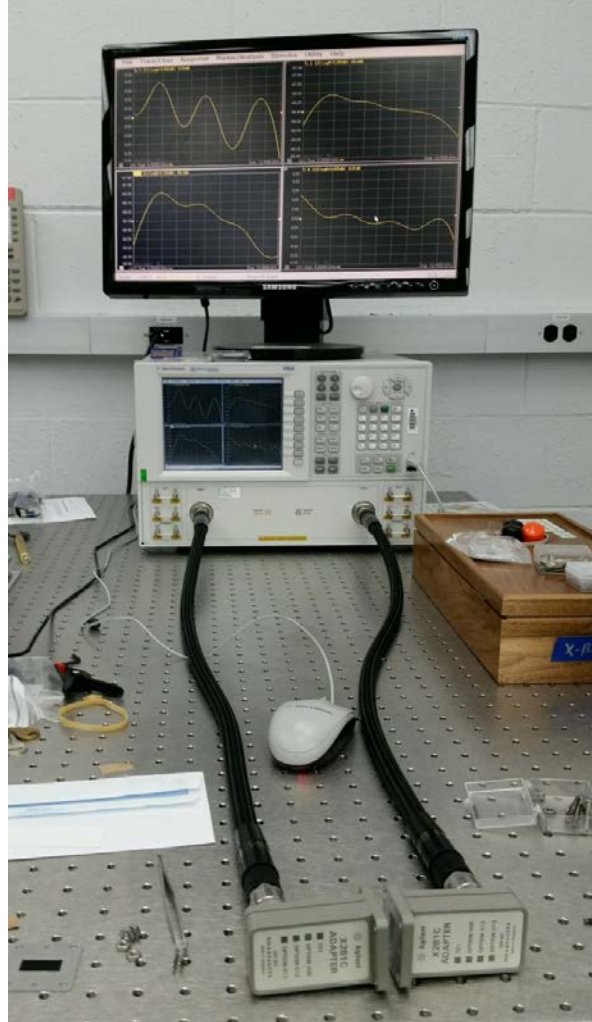


Figure 17. Agilent PNA Microwave Network Analyzer test setup

The ranges of tested frequencies were 8.2 to 12.4 GHz (X-band) and signals were sent in both directions through the material to verify directional consistency in shielding properties. The system incorporates a transmission measurement with signals represented as S_{ab} , the first subscript being the PNA port number where the signal output is measured. The second subscript b is the PNA port number where the signal is applied. Data acquired included S_{12} and S_{21} for transmission signals as well as S_{11} and S_{22} for reflectance. Output measurements are provided in decibels (dB) for each step in the

frequency range and three representative curves are shown in Figure 18 for different specimen types.

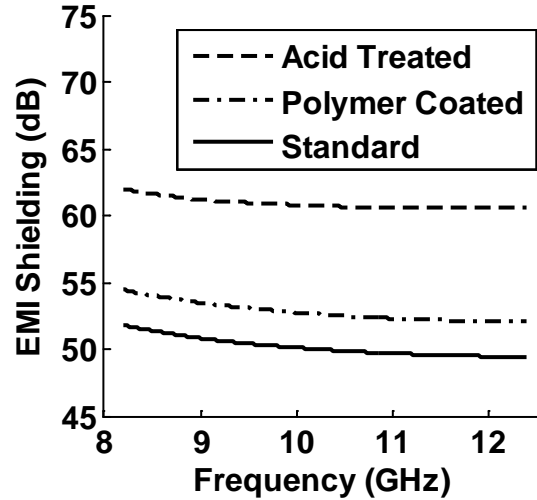


Figure 18. EMI shielding effectiveness across frequency range

The EMI shielding effectiveness (SE) relationship in decibels determined from the PNA is shown in Equation 9 [18]. They are also converted to their reciprocal positive value to be consistent with common representations of EMI SE.

$$SE(dB) = 10\text{Log}_{10} \frac{P_{in}}{P_{out}} \quad (9)$$

Where:

SE = EMI shielding effectiveness (dB)

P_{in} = the measured output frequency power into port 2

P_{out} = the measured frequency power transmitted from port 1

Each specimen was placed between two machined aluminum plates that exposed a portion of the CNT-sheet where the frequencies would be sent through. The plated

specimen was then inserted in-between the adaptors at the end of each cable extending from the PNA ports. A prepared sample is shown in Figure 19.

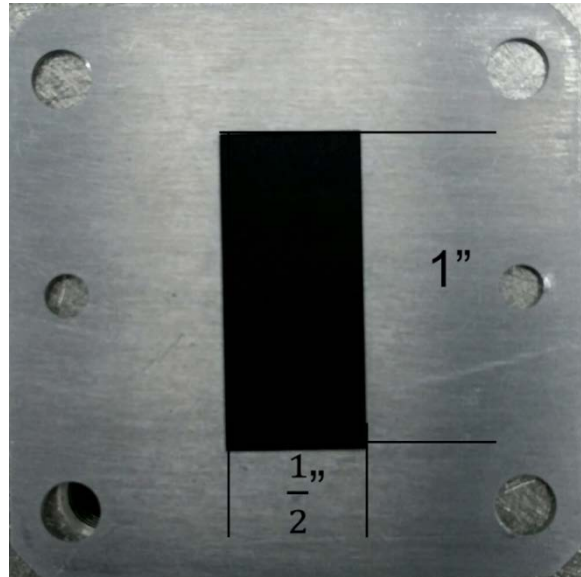


Figure 19. EMI shielding test specimen

Each time the network analyzer was set up to retrieve EMI shielding data, a calibration was performed. The X-band calibration kit, #30 X11644A, was used for the wavelength range being analyzed. First a “short” calibration was performed with a solid aluminum block inserted between the leads. Second, a “line” calibration was performed with a thick aluminum block with a hole that allows the signals to pass through. Finally, a “through” calibration consisted of the 2 plates that house the material with no specimen in it.

The results in chapter 4 present average values and standard deviations from each specimen for a sample size of three. Because exposed samples were limited, a single specimen was tested after simulated space environments. This was also true for

conductivity where measurements were taken across the surfaces of one exposed specimen. The results for EMI SE after exposure used the same spread for standard deviation as the baseline results. This is an important assumption that suggests the exposure environment and its effects were consistent across the specimens. These considerations are used in a T-test for the results section to discuss the level of confidence by which changes in properties occur due to the space environments.

3.5 Electrical Conductivity Test Equipment and Method

A four wire resistance test is an accurate measuring technique for conductivity. In a four wire technique there are four connection points along the length of the sample. Two of the leads provided current electrodes and the other two measure voltage. The separation of current and voltage electrodes eliminates the increased resistance from the leads and their contact. The inside voltage electrodes are only “listening in” to measure the resistance in ohms across the electrical gauge length between its nodes. A schematic of the four wire technique is shown in Figure 20.

This measurement technique is more important where the resistance of the specimen is low comparable to what is provided by the copper in the leads. While CNT-sheet conductivity performance is lower than that of copper, the resistance is low enough for a four wire technique to be required to achieve accurate data.

A standard four wire procedure generally connects the wire leads directly to the specimen with some type of clamp/interface. To avoid compromising the structural integrity of the CNT fabrics that are found with thicknesses between 15 and 60 μm , the bed is set up uniquely for these materials. The four wire leads were extended with flat

copper tape onto an acrylic plate. The CNT specimen is laid across the top of the copper tape and underneath a top acrylic plate that allows the sample to be seen during the measurements. It is important to see that there are no creases in the fabric and that the specimen lay flat and straight as seen with the test set up in Figure 21.

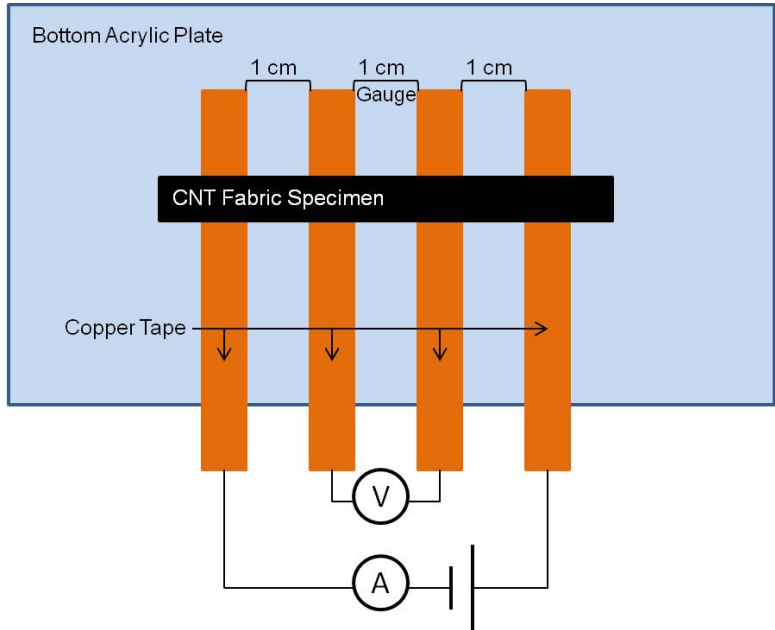


Figure 20. Four wire electrical resistance measurement technique

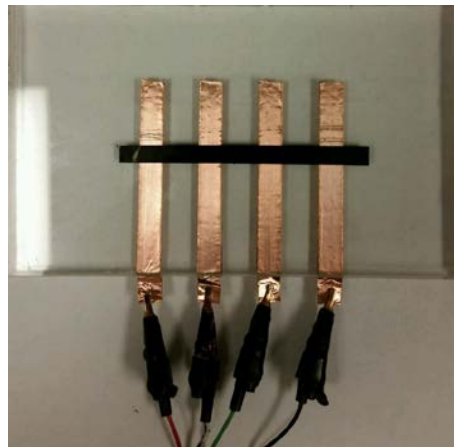


Figure 21. Four wire test set up

Each of the copper tape lines are placed with edges 1cm apart with the center separation of most interest as the electrical gauge length. An optical microscope was used to verify an accurate gauge length for calculations in Figure 22.

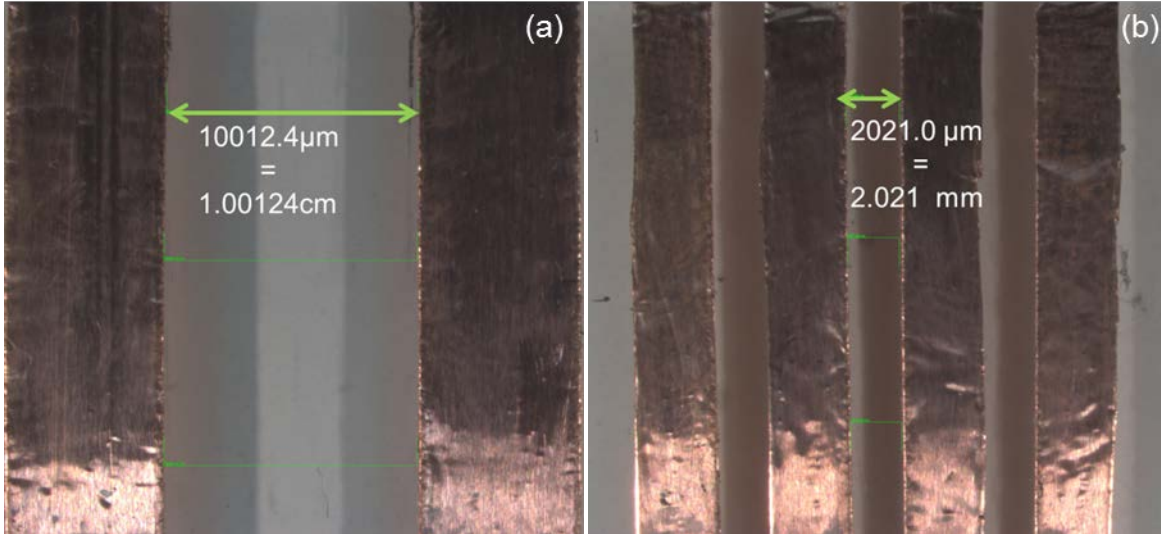


Figure 22. Electrical gauge measured by Zeiss optical microscope for (a) 1cm gauge length used for baseline properties and (b) 2mm gauge length used for exposed specimens

Calibration included measuring resistance values across 26 AWG copper wire and the copper tape with the test set up. In both cases, values were consistent to within .5 mΩ which is less than .1% error considered in the resistance measured in the CNT specimens documented in chapter 4. Specimens exposed under space environments were smaller and required a scaled version of the test in Figure 22b. A gauge length of 2mm was used and also verified with optical microscopy. Consistency was verified as the results of these tests were comparable with the un-exposed samples on the 1cm test bed. Resistance was measured on a single specimen from the same area for both the 1cm and 2mm gauge lengths and results were consistent.

3.6 SEM and EDX Equipment

The Zeiss OM shown in Figure 23a with AxioVision 40 v4.8.1.0 software located at AFIT was used for optical microscope images. An FEM Quanta 450 located at AFIT in Figure 23b used for SEM image collection along with features for energy dispersive x-ray spectroscopy (EDX) for elemental analysis of the CNT-sheets. The FEI Sirion FEG digital electron scanning microscope located at AFRL was also used for high resolution SEM image collection.

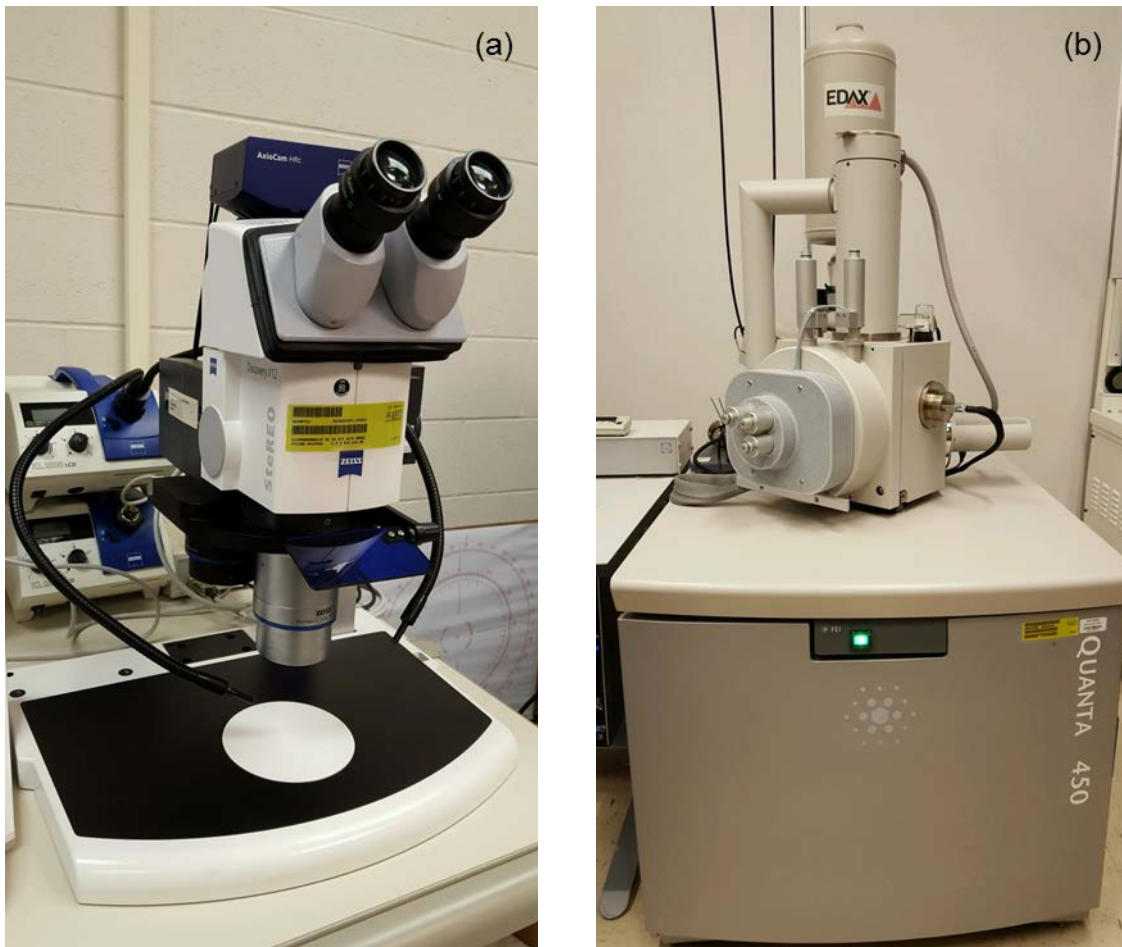


Figure 23. Imaging instrumentation (a) Zeiss optical microscope and (b) FEI Quanta 450 SEM EDX

3.7 Space Environments Exposure Facilities

3.7.1 Atomic Oxygen Equipment and Method

Two CNT-sheet specimens were sent to Montana State University to undergo hyperthermal atomic oxygen exposure for a simulated 3 month period in LEO. Exposure parameters included a directed beam containing O and O₂ in an O/O₂ mole ratio of 3 or greater with normal incidence exposure on the plate. The specimens remained at room temperature during exposure in an oil-free vacuum chamber with a base pressure <10⁻⁶ Torr. The directed beam pulsed at 2 Hz with an approximate oxygen atom flux of 2 x 10¹⁵ atoms cm⁻² pulse⁻¹. The flux is determined by parameters including altitude, orbital inclination, solar activity, and time of day generally yielding a nominal range of 10¹⁴-10¹⁵ atoms/cm²s [30]. O-atom fluence was nominal at 2.00 x 10²⁰ atoms/cm², which was based on the erosion depth of a kapton H sample that had an erosion yield of 3.00 x 10⁻²⁴ cm³ O-atom⁻¹. O-atom translational energy was nominal at 5eV with full width at half of the maximum energy with ~1.5eV energy distribution. Finally, the O₂ translational energy was nominally 8.8eV; full width at half maximum in energy distribution ~3.0 eV.

CNT-sheet specimens from type A and B were used to have a baseline CNT-sheet and an acid treated sheet. The variable of interest was the nitric acid treatment of specimen 6 from type C. The two specimens were prepared on a 3 x 3" aluminum test bed that used mounted strips of fiberglass to elevate the suspended sheets from the aluminum and hold the materials in place. This is shown in the diagram represented in Figure 24. Copper tape was used to hold down the free ends extending from the fiberglass plates. This improved the ability to safely ship the packaged test specimen and

also facilitated electrical conduction to the aluminum plate when the samples were imaged in the SEM.

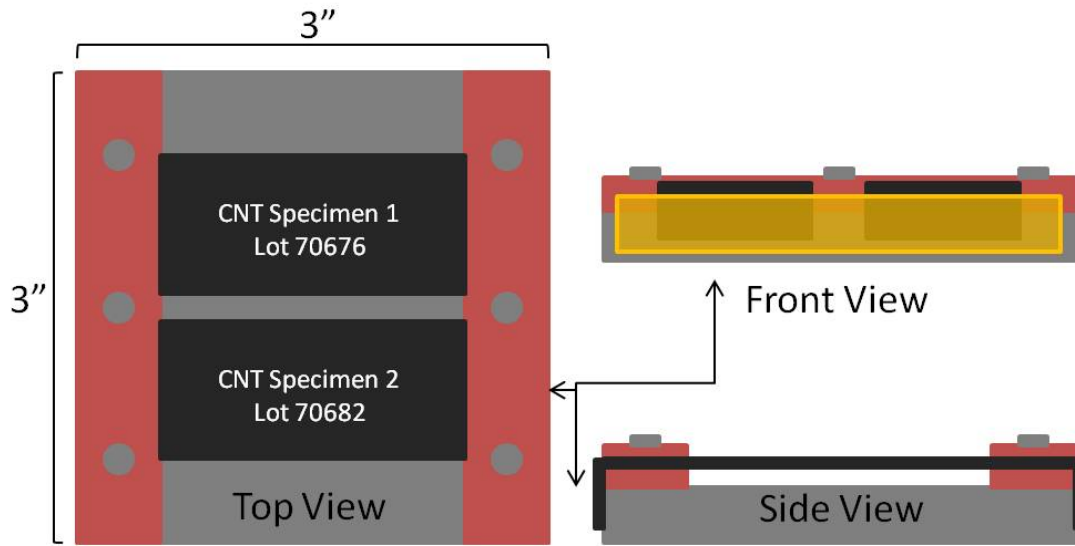


Figure 24. Atomic oxygen testbed diagram

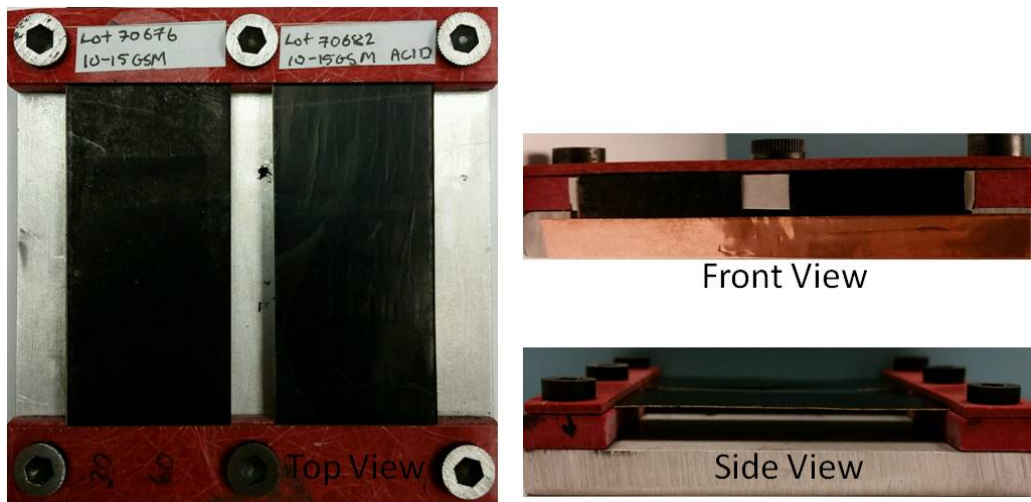


Figure 25. Atomic oxygen prepared specimens

3.7.2 Thermal Fatigue Equipment and Method

Temperature cycling was provided by a FTS ThermoJet ES in Figure 26 exposing the CNT-sheets specimens to thermal conditions found in LEO. Specimens were prepared in the same form and exposed in the same apparatus shown in Figure 25.



Figure 26. FTS ThermoJet ES for precision temperature cycles

A cycle was performed between the range of -60 and 120°C at an average rate of $18^{\circ}\text{C}/\text{min}$ with an air flow rate of $9\text{ L}/\text{min}$ in a standard room-temperature laboratory atmosphere. Consistent with ATOX exposure, thermal fatigue was performed to simulate temperature cycles seen in LEO for 3 months in orbit. Assuming an approximate circular orbit altitude of 400 km , an orbital period is calculated according to Kepler's third law in Equation 10 as approximately 90 minutes.

$$T = 2\pi \sqrt{\frac{a^3}{\mu}} = 92.6 \text{ min} \quad (10)$$

Where:

a = the orbit's semi major axis or radius for circular orbit
 μ = the earth's gravitational parameter ($3.986 \times 10^{14} \text{ m}^3\text{s}^{-2}$)

The number of thermal cycles simulated was calculated in Equation 11 as 1440 orbits for a consideration of 3 months to be consistent with atomic oxygen exposure.

Three of the thermal cycles are shown in Figure 27.

$$N(3mo) = \left(\frac{90 \text{ min}}{1 \text{ orbit}} \cdot \frac{1 \text{ day}}{1440 \text{ min}} \cdot \frac{1}{90 \text{ days}} \right)^{-1} \quad (11)$$

Where:

N = the number of orbit cycles in a 3 month period

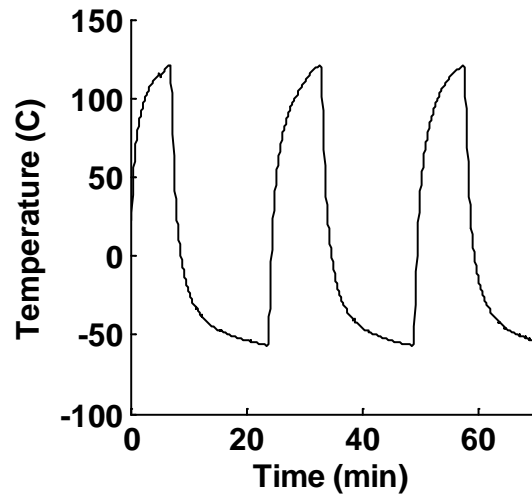


Figure 27. Three temperature cycles for thermal fatigue environment

3.8 Test Plan Summary

The tests described in this chapter have been conducted to meet each of the investigative questions outlined in the introduction. Specimens tested included 14 distinct CNT-sheets that are categorized into 6 types that include several different variables of interest. Baseline electro/mechanical properties are measured in the first phase of research including SEM imagery of their surface morphology and microstructure. Also in the first phase, atomic oxygen exposure was conducted requiring samples to be shipped early on in the testing process. The second phase of testing focused on space environment exposure. Thermal cycling took approximately 1 month for all 1440 cycles to be completed. Baseline physical properties were completed during this time with electrical conduction tests being performed on all 14 specimens. Finally, a third phase revisited the same investigative procedures used to evaluate baseline properties. This time, tests were performed on only two specimen groups to evaluate the effects of the space environments on untreated and acid treated CNT-sheets. A test matrix is represented in Figure 28 that summarizes the flow of each testing phase with a timeline and shows how each phase relates to the others. The described test plan allows the characterization of all 14 types of CNT-sheets and each manufacturing parameter under investigation. It also allows a clear comparison of two specimen groups for before and after exposure to see the effects of the space environments on CNT-sheets. Following this matrix each of the investigative questions are answered and discussed in the next chapter.

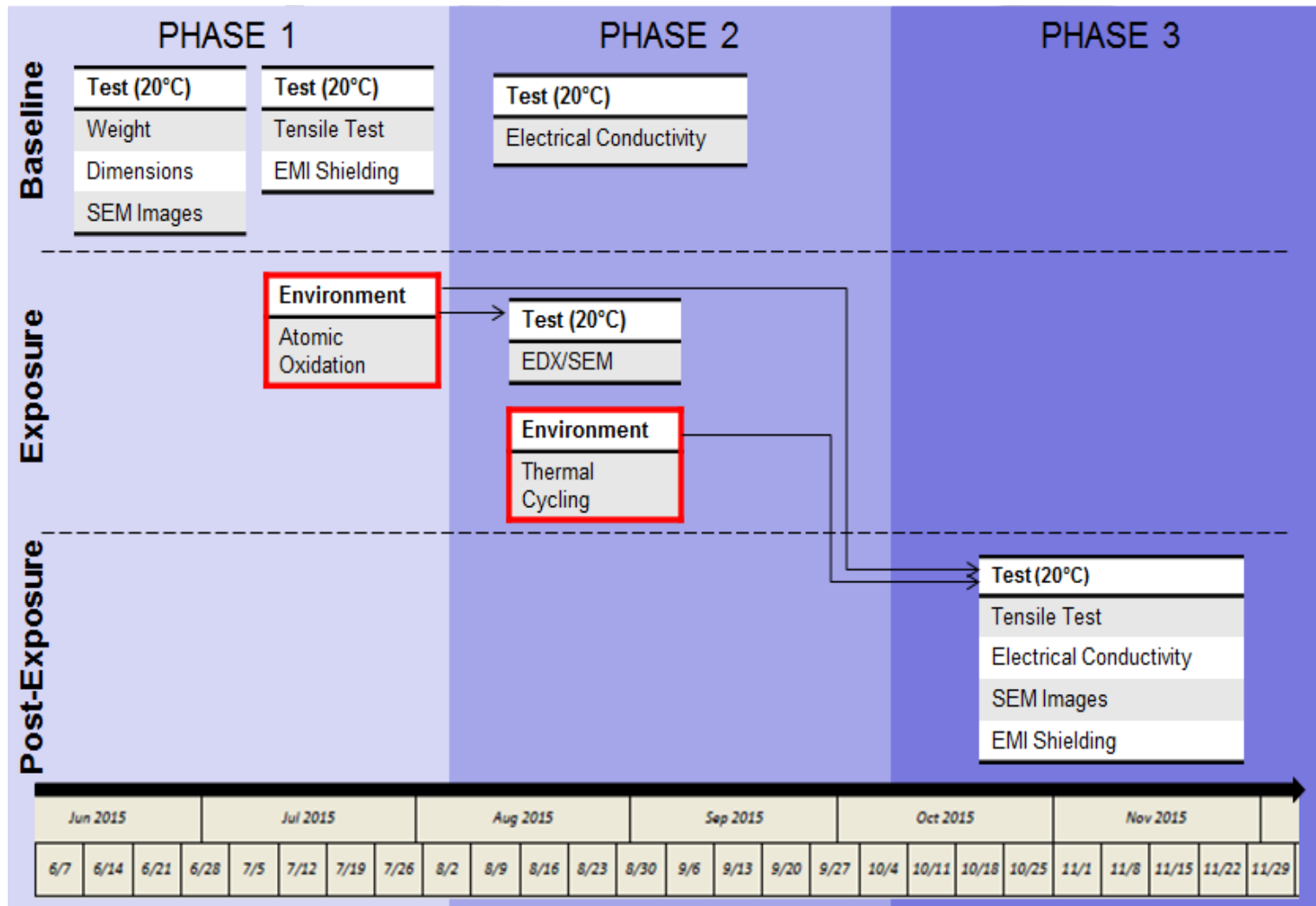


Figure 28. Test Matrix

3.9 Assumptions and Limitations

It is important to outline some of the assumptions and limitations in this research. The first is that the environments simulated are not an exhaustive list of the hazards in space but include two of the most strenuous on space vehicle materials. The environments are simulated because of the rare accessibility of space for testing real affects in orbit.

Operation requirements for DoD space vehicle systems include functioning lifetimes of (15+) years. This is an important requirement due to the expense of launch and the critical need to always have resilient systems and capabilities in space. It is an unpractical demand to simulate space environments in real-time over the course of 15 years or even 1 year in the case of a thesis timeline. For this reason, simulated space environments are accelerated with intensity to match the acceptable conditions of what a spacecraft will see over the observed time frame. In this study, a time of 3 months in LEO was simulated for thermal fatigue and atomic oxygen. The results can then be propagated forward to anticipate long term effects.

The cost and availability of CNT-sheets limited the amount of materials to test. For all baseline mechanical and electrical tests, 3 valid data points were acquired. Materials exposed to space environments were limited to a small sample of 4 specimens for each type. Three specimens were used for tensile tests and the fourth was used for conductivity and EMI SE.

IV. Analysis and Results

4.1 Chapter Overview

This chapter covers the results and analysis for each of the tests performed in this research. First, 8 of the 14 specimens from specimen types A-D are tensile tested to quantify apparent strength, stiffness, and amount of strain at failure. Trends are reviewed in each of these properties with volumetric density, areal density, and thickness. The effects of production rate and acid treatment are also reviewed in these trends with their effects on properties. Investigation of how morphology and microstructure relates to the measured properties is performed with scattering electron microscopy (SEM). Analysis of alignment that happens in the CNT-sheets under tensile loading is also performed. Finally, these same mechanical properties are analyzed separately for the polymer coated specimens due to unique behavior caused by the amount of polymer content.

Baseline electrical properties are then measured for all 14 specimens in the 6 different types. Electrical conductivity and EMI shielding effectiveness is presented and their trends related to volumetric density, areal density, and thickness. The physical parameters observed under SEM are also used here to explain the influence of important manufacturing parameters affecting electrical properties.

The last analysis looks at the mechanical and electrical properties of standard production CNT-sheets, specimen 1 and 6, after exposure to atomic oxygen and thermal fatigue. The manufacturing parameter highlighted here is the acid treatment of specimen 6 from type B. Specific strength, stiffness, and the amount of strain at failure are reviewed for exposed specimens with comparisons of the baseline properties previously tested. Elemental analysis is performed with energy dispersive x-ray spectroscopy for

both specimens before and after atomic oxygen to investigate the erosion of CNTs and the addition of oxygen into the CNT-sheets. SEM is used to observe changes in surface morphology for both the atomic oxygen and thermal fatigue specimens and support the analysis of changes found in material properties.

All of these analyses will help to answer each of the investigative questions posed at the beginning of this study and provide knowledge needed by scientists and engineers to successfully use CNT-sheets in space.

4.2 Apparent Properties

Thickness is an important parameter that distinguishes CNT-sheets from other bulk/macro CNT materials like yarn. It is included into calculations of strength, modulus of elasticity, and electrical conductivity in addition to being a possible factor in EMI shielding effectiveness. It is a difficult measurement for two reasons. One reason is that it is difficult to observe voids in the material and packing parameters that vary between production parameters and the effects of acid treatment. In addition to this, thickness is not a controlled manufacturing parameter like areal density when they are produced which leads to varying thickness across specimens. Other difficulties found during measurements were differences in how spongy each sheet was and the resolution of the thickness measurement device. As mentioned in the chapter 3, properties using the thickness measurement are referred to as “apparent.” In the study of CNT-yarns, tenacity was used as the representation of strength, which is strength per linear density. It removes uncertainties found in the cross sectional area. A comparable representation for sheets would be strength divided by areal density or specific properties. For this study, apparent

properties are used to present volumetric strength, modulus of elasticity, and conductivity to be consistent with results presented for similar materials in literature. Results are also presented with trends in areal density and as specific properties (divided by volumetric density) and are emphasized as the most accurate results.

An increase in areal density is observed with an increase in apparent thickness. This is shown in Figure 29 where the trend line is fit with an R^2 value of 0.81. This quantifies a level of confidence in trends we may see with apparent properties. It suggests that although apparent properties are not true indicators, there is a level of confidence on trends in their results. Trends found in specific properties and with areal density will be considered “true indicators”. Trends in specific properties that are consistent with apparent properties will also increase the overall confidence of both indicators.

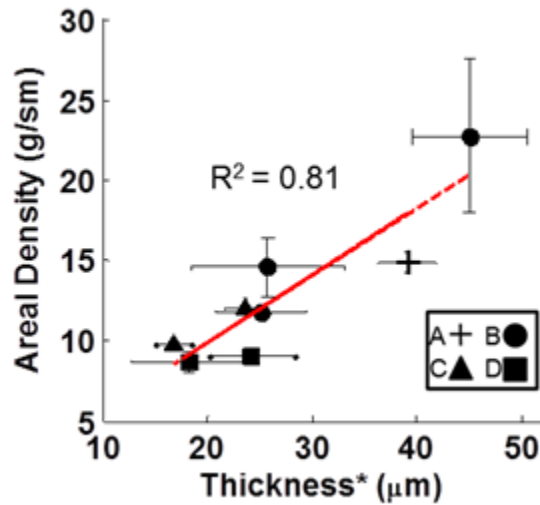


Figure 29. Areal density vs. thickness

**Apparent property*

4.1 CNT-Sheet Baseline Mechanical Properties

A plot of stress versus strain measured during the tensile test depicts the tensile behavior of the CNT-sheets and presents information about their mechanical properties discussed in detail in this section.

Stress is measured during the tensile test as the applied load divided by the cross sectional area ($A = tw$), as shown in the following:

$$\sigma_s = \frac{P}{A} = \frac{P}{tw} \quad (12)$$

Where:

σ_s = Stress under tension (MPa)

P = max load at failure (N)

A = cross sectional area of sheet (m^2)

t = apparent sheet thickness (m)

w = sheet width (m)

The apparent stress is measured against strain as a measurement of change in the dimensions of the sheet under tension shown in Equation 13.

$$\epsilon = \frac{\Delta L}{L_o} = \frac{L-L_o}{L_o} \quad (13)$$

Where:

ϵ = strain (mm/mm)

ΔL = change in length

L_o = mechanical gauge length or initial length

L = measured length

Example curves for tensile test data are shown in Figure 30a, and are representative from each type. Because measured properties can vary widely in each type, average strengths with error bars show values representative of each category in Figure 30b. For example, the extended lines on the second bar of Figure 30b represent the 95% confidence that any of the type B specimens would have strengths measured within the interval. These initial results demonstrate a large range in mechanical performance due to different manufacturing parameters.

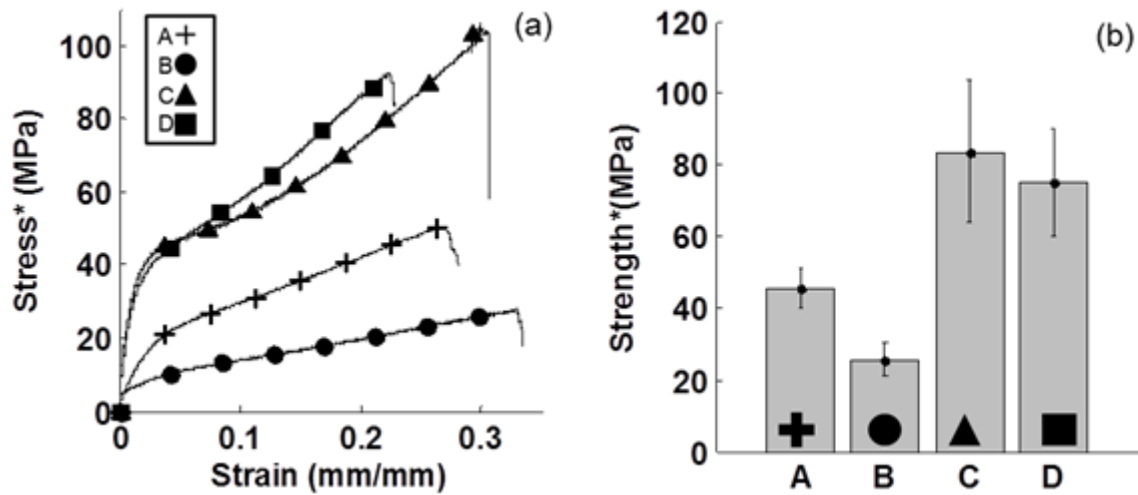


Figure 30. (a) Stress-strain curves for manufacturing parameters and (b) strength by specimen type
*Apparent property

The ultimate tensile strength is the stress at the time of failure and characterizes the mechanical strength property of the material. Average values for strength from each specimen type are shown in Figure 30b. The type A, specimen 1, achieved a strength of approximately 45 MPa. The type B, specimen 3, that is enhanced production has a reduced strength of roughly 50% from type A. Specimens 5 and 8 from type C and D respectively both show superior strengths with acid treatment. For standard production

rates, type C sheets are almost twice the strength achieved over the type A materials not treated with acid. Similarly, acid treated specimens for EP CNT materials in type D are approximately three times stronger than the untreated Type B. Untreated; EP CNT-sheets appear to be inferior in mechanical strength. In both production rate types, the acid treatment shows increased mechanical strength. This increase in strength appears to be more dramatic for the EP sheets.

Another property observed in the tensile, or stress-strain, behavior is the Young's modulus which is a property of material stiffness. It is measured by looking at the slope of the linear region found at the beginning of the stress-strain curve. Stiffness measurements are given in GPa as change in stress over a change in unitless (mm/mm) strain, shown in Equation 14.

$$E = \frac{\Delta\sigma_s}{\Delta\epsilon} \quad (14)$$

Where:

E = Apparent Young's modulus

$\Delta\epsilon$ = change in strain (mm/mm)

$\Delta\sigma_s$ = change in stress (MPa)

Modulus values were calculated by taking the change in stress over the change in strain from the data in Matlab from the linear region of the curves for each specimen type. Because calculated moduli varied for the specimens in each tensile test, they were averaged and presented in the following sections with one standard deviation. Because Young's modulus is affected by thickness in the calculation of stress, it is reported as

“apparent” modulus/stiffness. Modulus is shown averaged for each specimen type in Figure 31a. For untreated specimens, the enhanced production has lower stiffness shown in comparison of type A and B. For acid treated, enhanced production appears to increase with the spread of values in types C and D without statistical confidence. The level of strain at failure is shown in Figure 31b. Enhanced production shows no affect for the untreated specimens and a decrease in strain for those treated with acid. This reduction of strain in type D strengthens its related increase in modulus. The reduction in mechanical properties for enhanced production sheets are not reduced as with the non-acid treated case due to the synergistic effects of the included acid treatment.

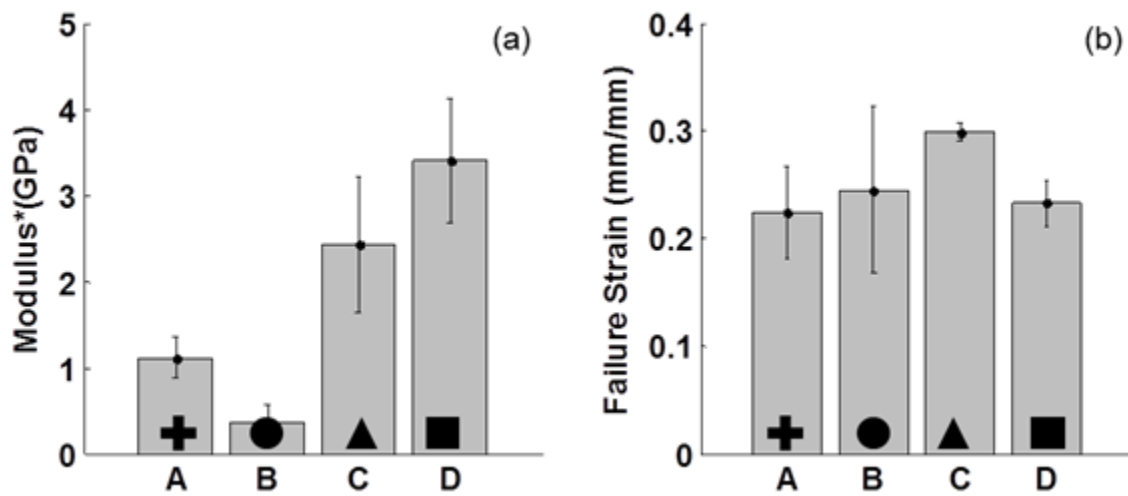


Figure 31. Bar charts showing (a) Young’s modulus and (b) failure strain by specimen type
*Apparent property

4.1.1 Specimen Failure and CNT Alignment

Under tensile load, straight samples underwent significant strain. Straight specimens changed into a dog bone shape as seen in Figure 33b due to necking. Samples did not fail at the center but at a location near, but away from the actual grips shown in

Figure 33c. Cheng et al. observed that simple mechanical stretching enhances alignment of the initially random dispersed CNTs in the sheet and increases the directional tensile strength [72]. Li et al. quantified alignment of CNT bundles in sheets under strain with x-ray and Raman scattering techniques [73]. A 40% elongated sheet showed an improvement in tensile strength of more than 200%. The process and change of properties was shown to be from alignment by the straightening of the long CNT bundles and the subsequent self-assembly and more dense packing shown in Figure 32 [73].

Similar results were observed in the CNT-sheets used in the present study and are shown in Figure 33d for a specimen after tensile failure. The observed failure location is expected to be due to the increased strength at the center at maximum strain location due to CNT alignment for each specimen. While greater mechanical properties are expected from tensile tests of highly aligned sheets, the values reported are representative of the presented CNT sheets with initially randomly oriented CNTs.

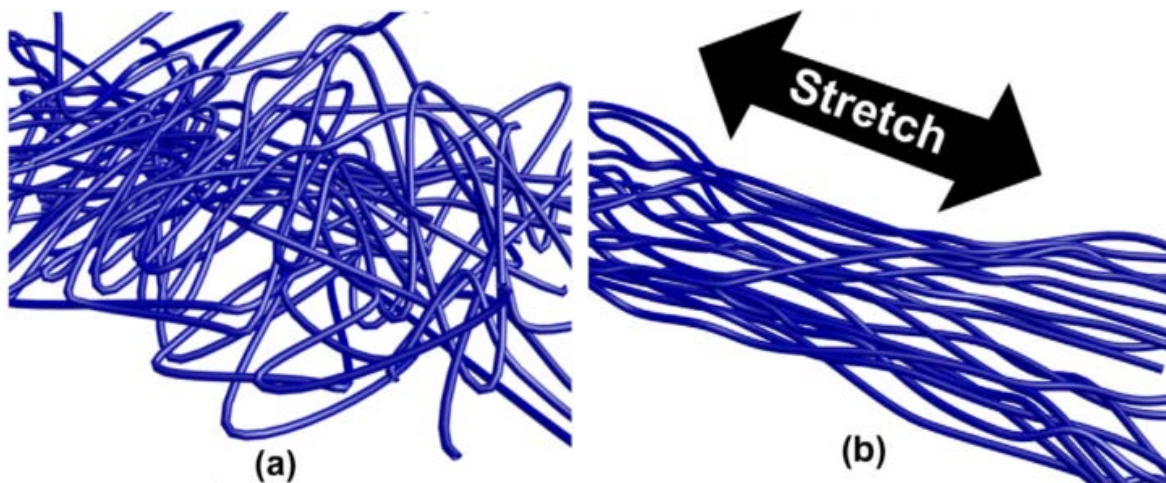


Figure 32. Illustration of CNT bundles in sheets after stretching. Randomly oriented and tangled CNT bundles before strain (a) and straightened, packed form after tensile strain

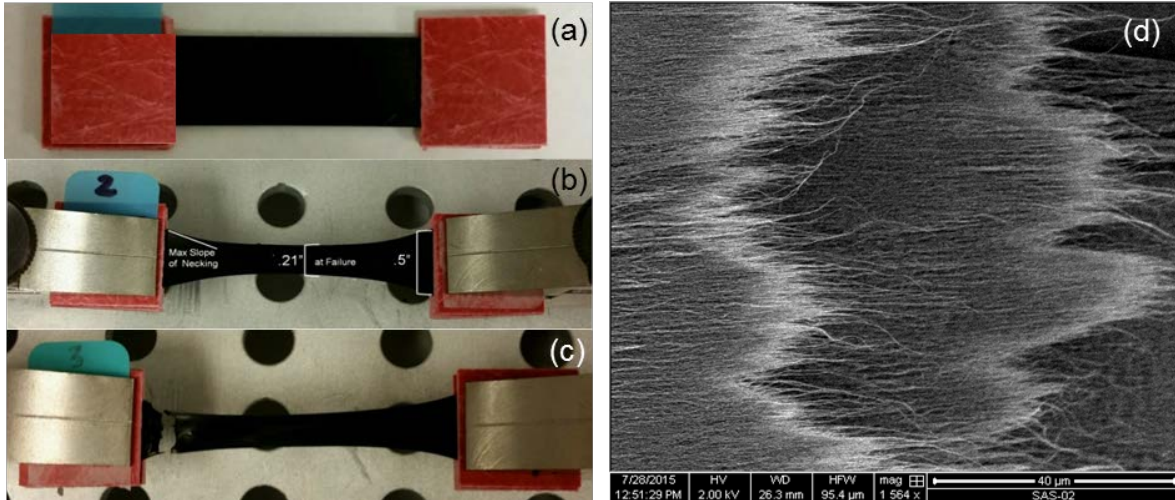


Figure 33. (a) Specimen, (b) Necking specimen before failure, (c) Specimen failure, and (d) acid treated EP CNT-sheet after tensile failure

The acid treated EP specimen shown in Figure 33d appears to have more directional fibers suggesting more alignment leading to increased strain during tensile loading. The acid treated EP specimens show a large increase in strength and stiffness. The strength is expected to increase in view of the load carrying fibers becoming more aligned. Nitric acid increases the bonding between CNTs, thus it is expected to increase the alignment by strain. This yields the morphology in Figure 33d in addition to the increase in mechanical performance.

An analysis of mechanical behavior from tensile tests would not be complete without some discussion on necking behavior. Observations made on the necking in tensile specimens suggest that the nature of the CNT-sheet microstructure influences how it necks. For metals, the stress-strain curve rises linearly until strain hardening begins at a yield point. From this point, stress rises to an ultimate tensile strength followed by a decrease in stress as necking occurs until failure. This necking is referred to as unstable, because it continues with decreasing applied stress until it fails. A different result occurs

for polymers. Unlike metals, the stress during necking reaches a local minimum and then begins to increase with stable necking until reaching failure at a larger stress value. This step is also referred to as a strain hardening process. This different behavior occurs when an amorphous polymer is stretched and causes molecules to become preferentially aligned along the stretching direction [74]. CNT-sheets are unique materials unlike metals or polymers. This is an important observation because similarities are seen in the stress-strain behavior of CNT-sheets and polymers. Supportive of the comparable tensile behavior, CNT-sheets have also been shown to have microscopic alignment of networks that, similar to polymers, become preferentially aligned with strain from a pristine amorphous state. Polymers vary in this stress-strain behavior from brittle to more ductile, rubber-like materials. The CNT-sheets also vary with behavior comparable to ductile to more rubber-like behavior. CNT-sheets that resulted in a form more like curve (a) in Figure 34a are acid treated. These materials have enhanced interactions due to the surface treatment. Figure 34b shows the resulting necking after failure for an acid treated specimen. Polystyrene (PSb) coated, specimen 10, which has a morphology showing enhanced load transfer also shows this curve behavior. The reference specimen along with other polymer coated samples is generally of the form illustrated in curve (b). The untreated, specimen 1, is shown after failure in Figure 34c. Finally, enhanced production specimens are found to have reduced necking and exhibit the behavior shown in the illustrated curve c of Figure 34a. Curve (c) demonstrates the least amount of strain hardening which process is expected to be discouraged by the presence of large amounts of impurities in addition to polymer. An example from this type is shown after failure in Figure 34d which shows a lot less necking at failure.

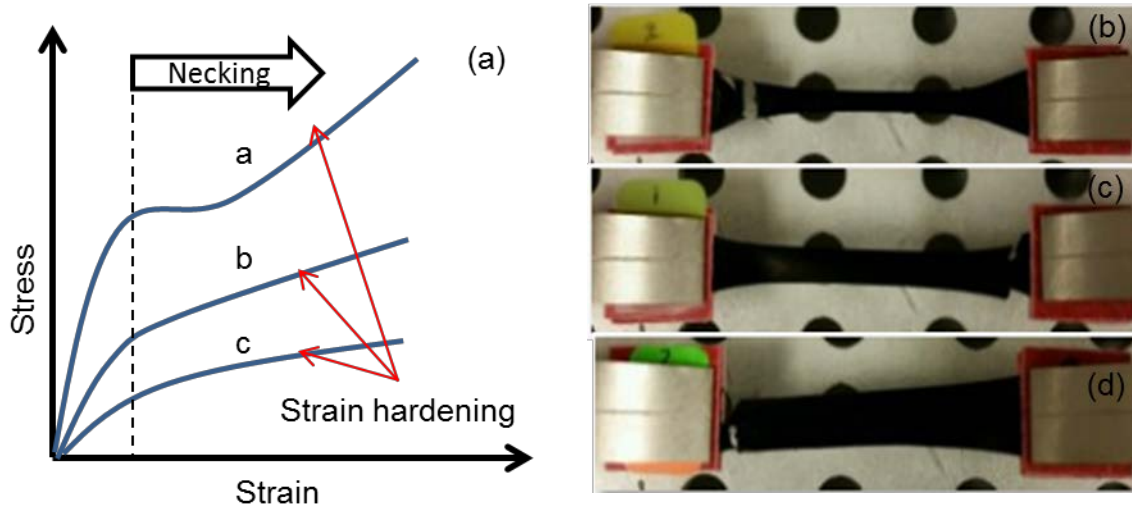


Figure 34. Illustration of typical stress-strain curves for CNT-sheets (a) and images of necking after failure for (b) acid treated specimen 5, (c) standard reference specimen 1, and (d) enhanced production polymer coated specimen 14

The alignment happening in the direction of strain during necking can be reviewed in more detail with image processing techniques in Matlab. Images acquired with scanning electron microscopy (SEM) can show the small bundles of CNTs in the sheets. These SEM images are processed into the Matlab software which uses a line extraction technique that quantified the peak orientations of lines with a Hough transform. The algorithm quantifies the distance of each observed line and the angle of its normal vector to a horizontal datum. It then plots the distance value versus the angle to produce a curve from the Hough transform. This is used to quantify the presence and alignment of CNTs in the sheet. The alignment is expected to affect the mechanical and electrical properties of the tested sheets. Figure 35 and Figure 36 show the Hough transform results before applying strain and Figure 37 and Figure 38 show the results after applying strain and the consequential alignment. The SEM image is displayed with vectors plotted that represent the peak orientations of the longest line segments. In the

parameter space matrix produced by Matlab, these peak values are the strongest lines. These points are also the brightest concentrations on the Hough transform curves. In Figure 35, the vectors show no alignment with peaks at approximately $\pm 45^\circ$. These peak values are also plotted on the Hough transform plot in Figure 36 from the parameter space matrix. To observe alignment in this analysis, these peak points would need to move from $\pm 45^\circ$ in the first case towards a constant angle value which would show alignment to one preferential orientation. Figure 37 shows another specimen after tensile failure which has seen approximately 30% strain. A clear visualization is seen with plotted vector segments being close to the same orientation. This is seen in the Hough transform in Figure 38 with peak orientations lying at approximately -45° . These results quantify the significant level of alignment happening within the network of CNTs inside CNT-sheets after tensile strain. This is evidence that supports the observed failure conditions and the level of necking and strain that occur. The alignment of CNTs during the process of stable necking shows the presence of strain hardening comparable to polymers. This is an important observation for future research because alignment in CNT-sheets is expected to have a tremendous impact on improved mechanical and electrical properties.

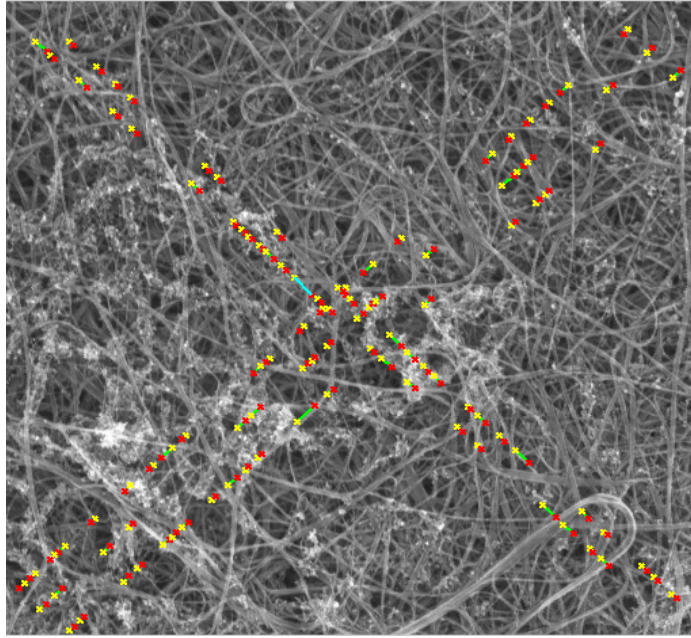


Figure 35. Matlab line extraction before strain with SEM morphology and line vectors

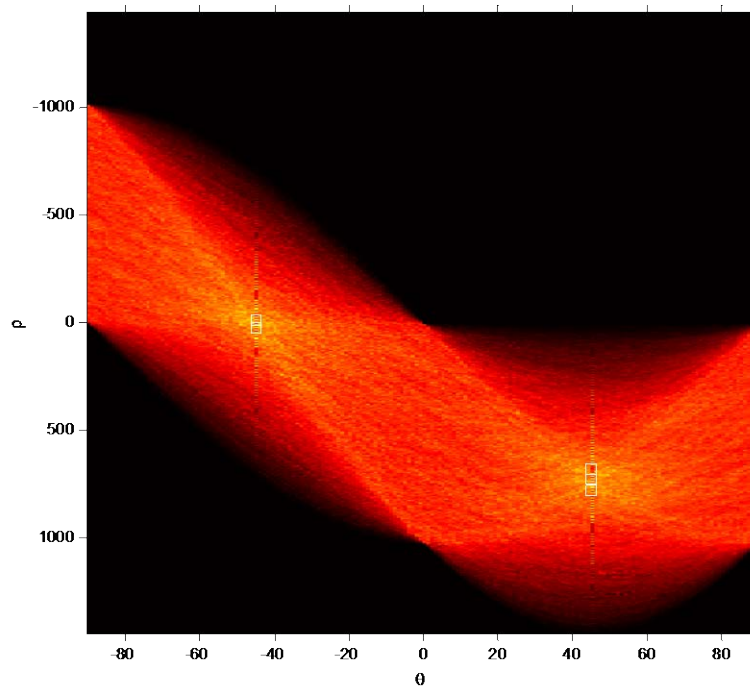


Figure 36. Hough line transform before strain

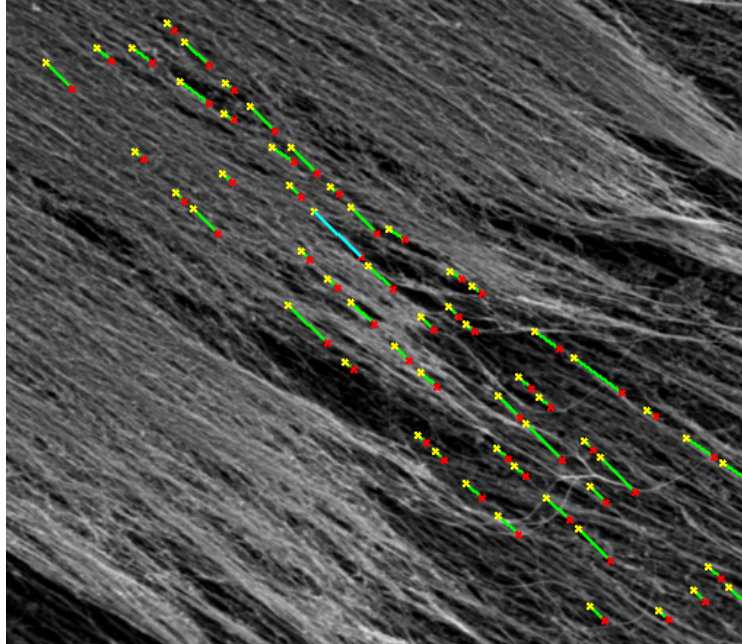


Figure 37. Matlab line extraction after strain with SEM morphology and line vectors

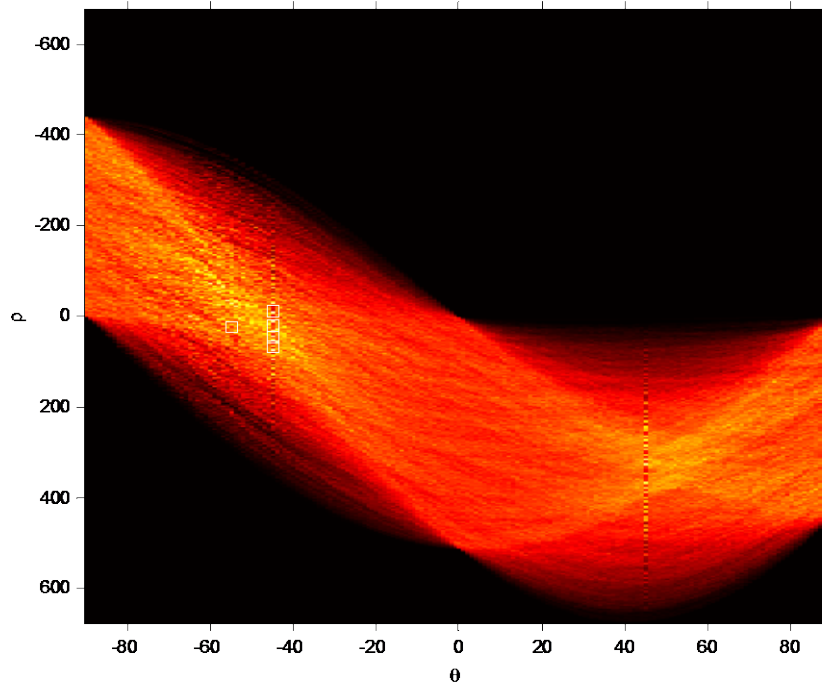


Figure 38. Hough line transform after strain

4.2.1 Volumetric Density

Volumetric density is a factor that could affect mechanical properties. Density is also affected by the apparent thickness as shown in Equation 15.

$$\rho = \frac{m}{V} = \frac{m}{twL} \quad (15)$$

Where:

ρ = apparent volumetric density (g/m³)

m = mass (g)

V = volume (m³)

Figure 39 shows the apparent strength and stiffness for each specimen versus volumetric density. Three groups appear in both charts that are separated by their different manufacturing parameters. Grouped together with the lowest strength and modulus values are the untreated enhanced production (EP) sheets from type B. Type A and C is seen above this group, represented by a cross marker and triangles. A trend appears showing standard production sheets that increase in strength with density. The acid treated EP specimens from type D stick out in a third group with superior strength and stiffness even over some non-EP specimens. The results are actually consistent inside of the following bounds: acid treated sheets show superior mechanical properties over their counterparts with the same production rate. The three acid treated standard production specimens show improved strength and stiffness over the other original non-EP specimens. Similarly, the two acid treated EP specimens are superior to the original three untreated EP specimens. For both EP and standard materials, using an acid

treatment is an effective manufacturing parameter in the improvement of mechanical strength and stiffness. Generally, EP specimens show decreased mechanical strength and stiffness from the standard specimen which is further exaggerated by its reduced performance at higher densities. Acid treated specimens show superior performance for both the case of standard and enhanced production sheets.

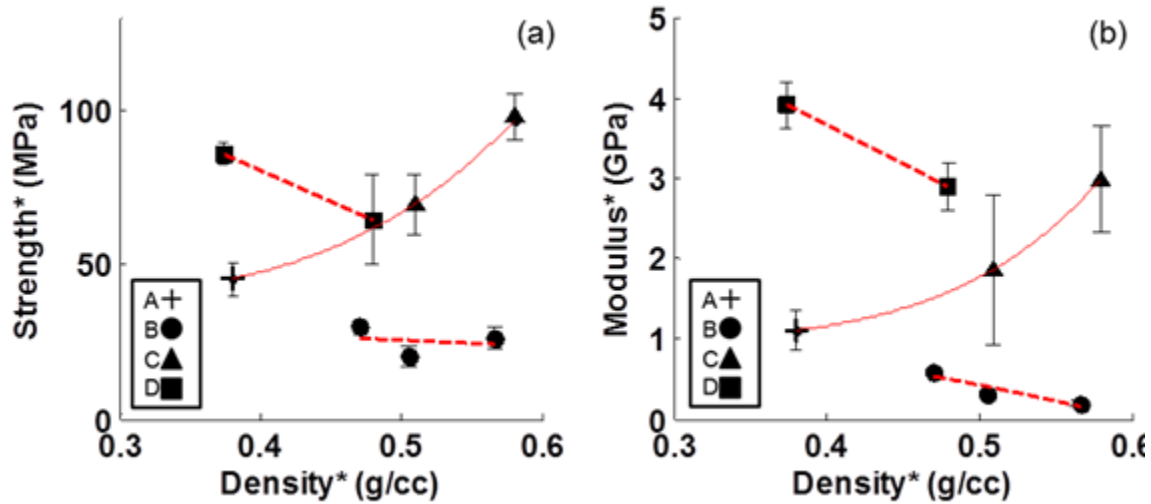


Figure 39. (a) Strength and (b) Young's modulus vs. volumetric density

*Apparent property

For standard production materials, strength and stiffness increase with volumetric density shown in Figure 39. This trend follows a model of power 2 with $f(x) = 744.7x^{4.65} + 36.98$ ($R^2=1$). A similar power model is fit with the measured modulus where $f(x) = 60.26x^{6.24} + 0.96$ ($R^2=1$). The enhanced production specimens separate into two different groups for both strength and modulus and show a general trend that increases as the apparent volumetric density goes down.

The amount of strain at failure also increases with volumetric density in Figure 40. This may be due to the increased CNT content that is being aligned under strain and factors expected from other manufacturing parameters.

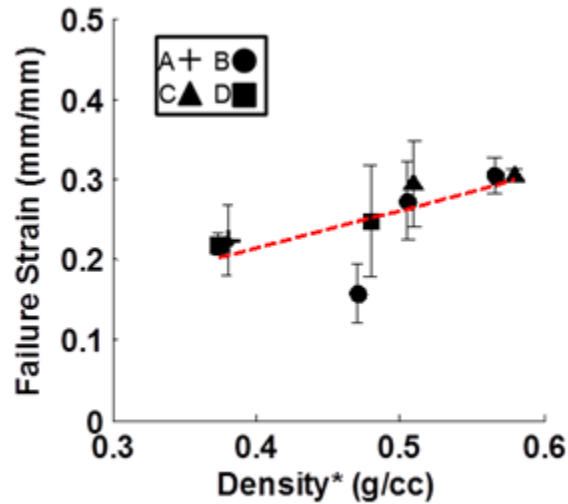


Figure 40. Strain to failure vs. volumetric density

**Apparent property*

The trends within each unique category (production rate and acid treatment) rely on density in the presented data. Looking at the larger picture between the three different groups may be more important in understanding how manufacturing parameters of production rate and acid treatments affect properties. For the standard production rate, the acid treated specimens are a part of the same trend with density. This suggests that density is a dominating manufacturing parameter for improved strength and stiffness. This review for the EP specimens yields more significant results. The acid treated EP specimens were observed in an approximate range from 117-322% larger strength than its other EP counterparts. The densities of these superior acid treated samples were less by values greater than 21%. The same observations of stiffness show moduli increasing by

397-1897% for the same range of density. For EP specimens, the acid treatment is concluded to be the dominating manufacturing parameter for improved mechanical performance over the observed trends in density.

4.2.2 Areal Density

These materials are produced with specifications in areal density being manufactured onto sheets with varying thickness along its planar dimension. The importance of considering areal density can be seen in the example of two specimens where areal density is defined as the mass per area defined by the sheet length and width below.

$$\text{Areal density} = \frac{m}{wL} \quad (16)$$

For the case of specimens 1 and 8 who respectively have comparable volumetric densities of 0.38 and 0.37 g/cc, they have large differences in thickness and areal density. With similar volumetric densities, the specimens differ by 15 microns in apparent thickness and specimen 1 has a greater areal density by more than 5 grams per square meter.

Areal density does not consider the thickness of the material which is considered in the strength calculation. Strength and modulus increase while areal density is reduced. This trend is seen general to all specimens and manufacturing parameters as seen in Figure 41.

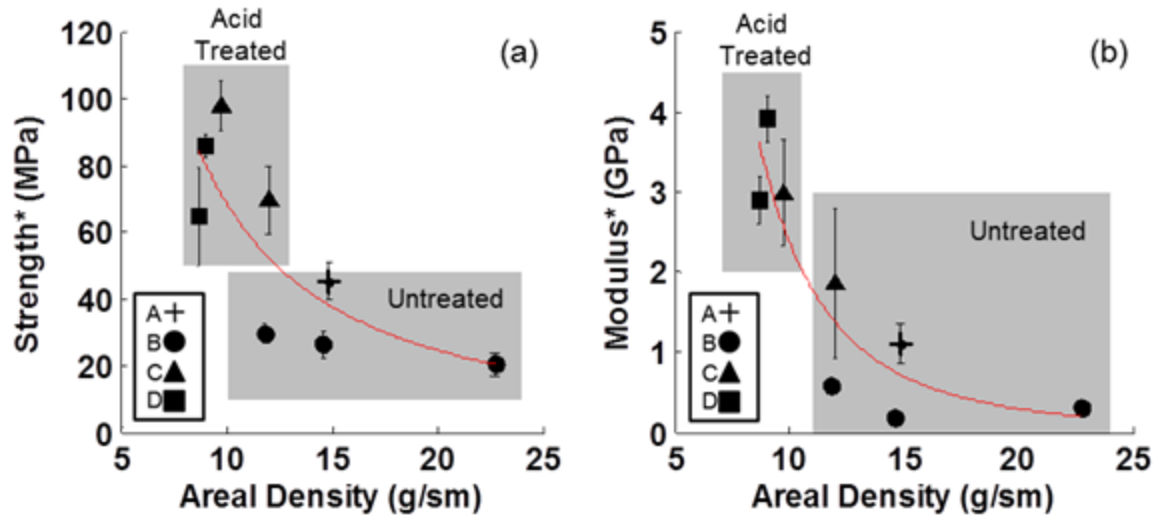


Figure 41. (a) Apparent strength and (b) apparent modulus vs areal density

*Apparent property

Types C and D which are treated with acid are found with smaller areal densities and hence larger strengths and moduli. Strain increases with areal density and data separates into two groups in Figure 42. The left group consists of acid treated type where the EP sheets have the smallest areal densities. Untreated sheets are found in the right trend that also increases in strain with areal density.

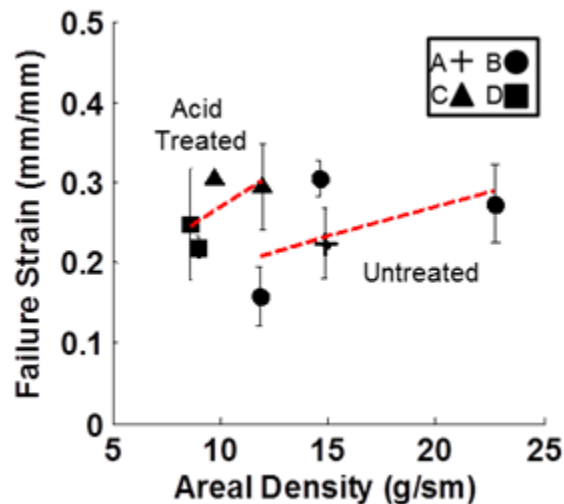


Figure 42. Failure strain vs. areal density

An areal density consideration supports the manufacturing parameter of nitric acid for improved strength and stiffness found in the previous conclusions. An important partnering trend is that the acid treated specimens with lower areal densities also have the smallest thickness.

4.2.3 Specific Properties

Because of the trends influenced by density shown previously, a review of specific properties will be instrumental in looking more acutely into the different manufacturing parameters of production rate and acid treatment. Specific properties refer to both strength and stiffness divided by volumetric density. Doing this allows the properties to be unbiased by density. This is beneficial in two ways: First the thickness is not considered in the calculation making the property no longer “apparent,” and second, specific properties are more useful in comparing the property and density of materials in one representation. Specific properties are often used for aerospace applications that are interested in materials with desirable properties and low density. A good example of this is with steel and aluminum with values shown in Table 5.

Table 5. Specific properties of steel and aluminum

	Strength (MPa)	Density (g/cm³)	Specific Strength MPa/(g/cm³)
Steel	450	8.05	55.9
Aluminum	300	2.7	111.1

Steel is stronger than aluminum by approximately 50% but it is also more than 100% more dense. By dividing strength by their respective densities in Equation 17, aluminum achieves a higher specific strength and is thus used in space structures rather than steel. Young’s modulus is likewise divided by density in Equation 18 to represent

specific stiffness. These specific properties are also important in electrical properties which are discussed later. One application of this principle is that while aluminum is less conductive than copper, it is used in power lines because it is significantly less dense. Its superior specific conductivity makes it a better candidate for long distance powerlines.

$$\textit{Specific Strength} = \frac{\sigma_s}{\rho} \quad (17)$$

$$\textit{Specific Modulus} = \frac{E}{\rho} \quad (18)$$

Strong trends can be seen when looking at the specific strength versus the specific modulus in Figure 43. Specific strength increases when specific modulus increases. Two linear trends are found and distinguished by the production rate. The EP specimens show consistent specific properties with an R^2 value of 0.992 fitted by the dashed line $f(x)=18.06x+35.58$. Above this group can be seen the standard production rate specimens with a similar linear trend yielding a strong R^2 value of 0.999 fitted by $f(x)=22.08x+55.19$ as shown by the solid line in Figure 43.

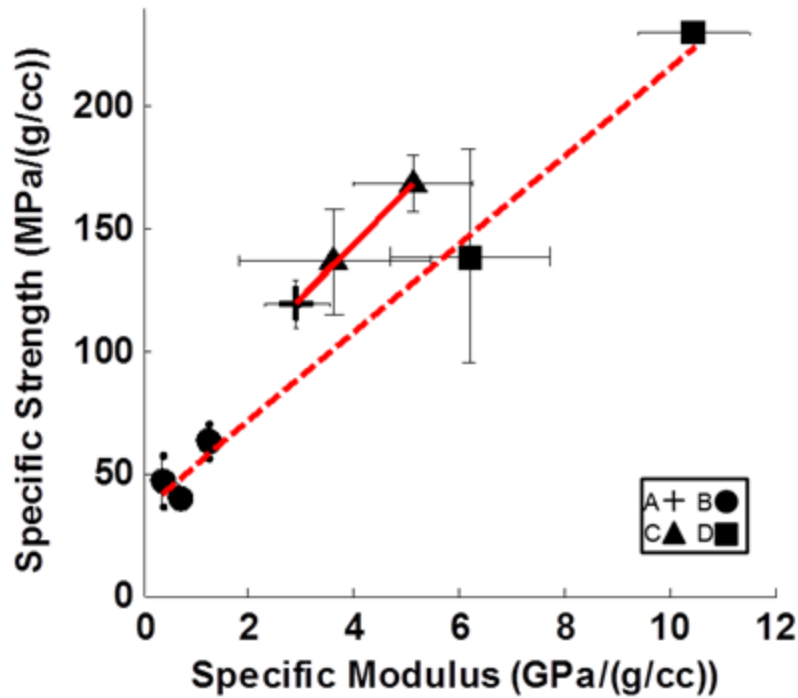


Figure 43. Specific strength vs. specific modulus

It can be seen from these results that EP specimens have reduced mechanical properties. This is specifically noted by the apparent strength and modulus unbiased by volumetric density. In both cases of different production rates, acid treated specimens show a significant increase in both strength and stiffness.

4.2.4 Overview of Manufacturing Parameters

The next objective is to identify the unique morphology identified by the different manufacturing parameters using scanning electron microscopy (SEM) with a field emission gun (FEG). Images showing the physical morphology and microstructure of different specimens are presented with their relation to the mechanical properties presented and the different manufacturing parameters of production rate and acid treatment.

Figure 44 and Figure 45 show the surface of a standard untreated and acid treated CNT-sheet before tensile loading. Specimen 1 from type A, which is not acid treated, presents a clear network of unaligned CNT bundles condensed into a sheet with planar isotropy. Specimen 6 from type B is observed in a similar form with regions of a smeared or matted appearance due to the acid treatment. One of these regions appears as a darker strip along the surface in Figure 45a. Comparing the greater magnification images in Figure 44b and Figure 45b shows an important difference in the microstructure. For the non-treated specimen in Figure 44, the CNT bundles appear to be more separated with more voids. Figure 45 shows the bundles have become more compact with increased interactions. Impurities are seen on the surface as light colored dross and is found more prominently on the surface of the untreated specimen. In addition to the purification and changes to surface morphology created by the nitric acid treatment, the compact nature of the resulting sheets is also expected to be a factor in the increased mechanical performance. This is a result of enhanced mechanical interlocking and load transfer between CNTs.

Figure 46a shows the surface of EP specimen 3 which has a drastically different surface morphology at the same magnification seen in Figure 44. The EP specimen at this magnification loses its clear appearance of networking bundles of CNTs. At a greater magnification shown in Figure 46b, the CNT networks can be seen again but saturated with catalyst and other carbonaceous impurities from production. Figure 46c shows the same saturation in an internal sheet layer concluding that this morphology is found though out all layers of the CNT-sheet.

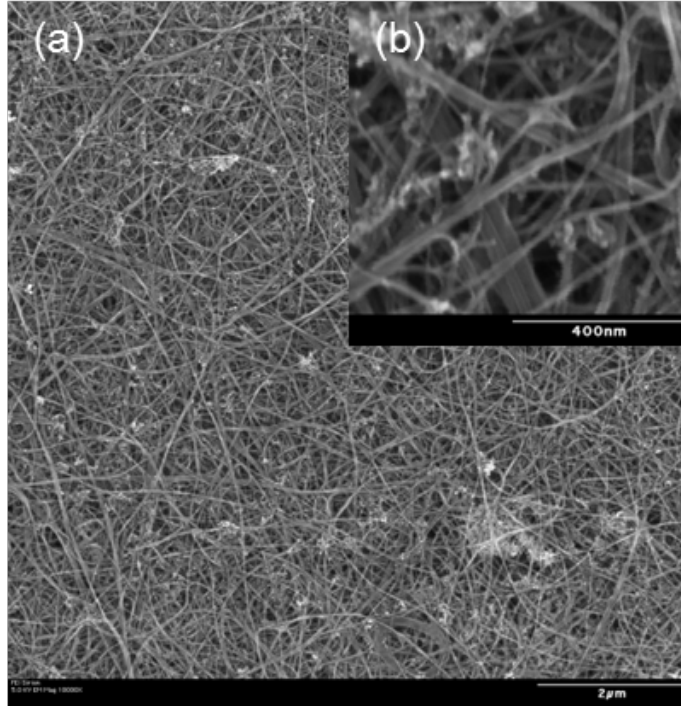


Figure 44. Surface morphology of untreated specimen 1 at (a) 10kx magnification and (b) 50kx

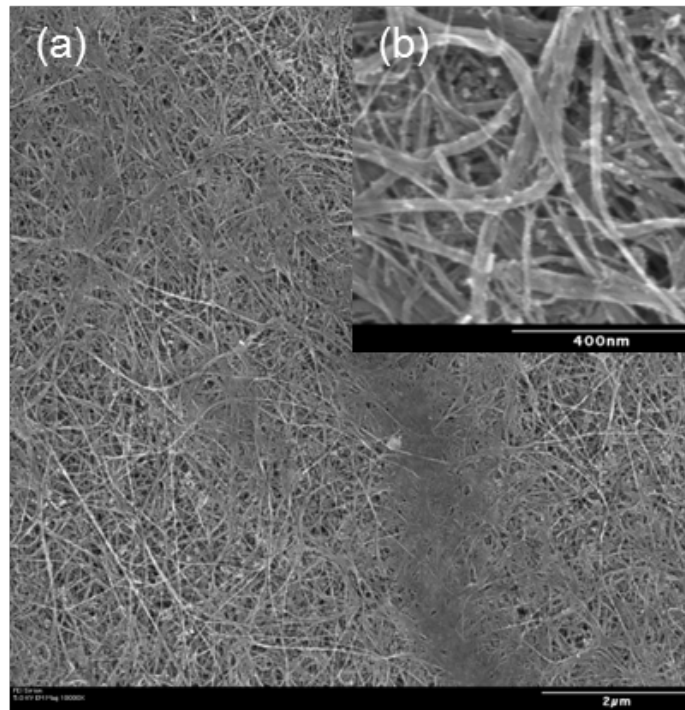


Figure 45. Surface morphology of acid treated specimen 6 at (a) 10k magnification and (b) 50kx

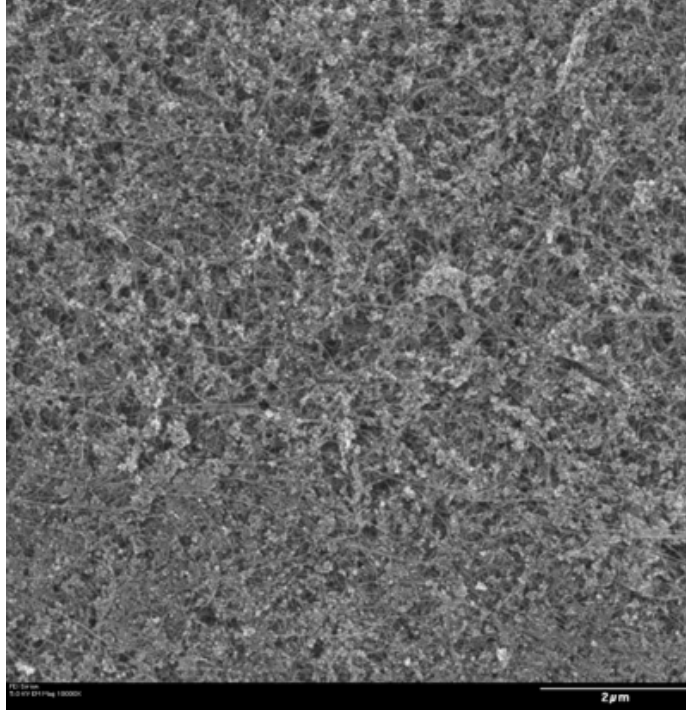


Figure 46. SEM images of enhanced production specimen 3 at 10kx magnification

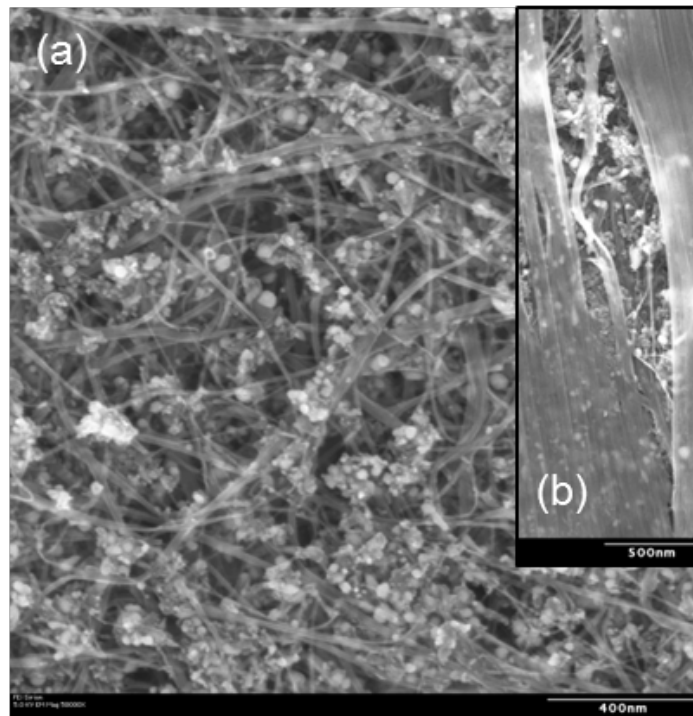


Figure 47. SEM image of EP CNT sheet at 50kx magnification and (b) internal layer at 25kx

The expected reduced count of thicker layers inside of the EP CNTs may be due to the saturated nature of the CNT aerogels that make layers in the sheets. The thicker layers have more encapsulated air pockets inside. These larger layers also appear to have more defined boundaries seen in Figure 48. To investigate this more closely CNT-sheets were cut and FEG-SEM was used to look into the sidewall profile. Figure 48a shows the larger more saturated layers with more prominent boundaries compared to the standard production sheet profile in Figure 48b. The highlighted layers in the EP CNT-sheet were approximately $5\mu\text{m}$ while the smaller, less defined, layers of specimen 1 were on the order of $1\mu\text{m}$. It's important to note that these softer boundary $1\mu\text{m}$ layers can be seen in the EP-specimen as well. The unique occurrence of the larger layers would dominate possible affects causing the reduction of mechanical properties demonstrated in the results presented.

This mechanism of failure is more exaggerated in the EP specimens over the standard growth specimens who fail through the thickness more like a homogenous, fiber dispersed sheet. The thicker layers have more encapsulated air pockets between thicker layers with more defined boundaries. The thinner layers accumulate more surface contact and thus increased mechanical interconnection and friction between layers. The improvement of mechanical properties by acid treatment was seen in tensile data to be most dramatic in EP materials. The dispersion and functionalization of CNTs may be assisted by the reduction of layers in the EP specimens. Boundaries treated with acid would coalesce into a more homogenous material through the thickness. This requires more attention in future studies with the SEM investigation of acid treated EP CNT-sheets.

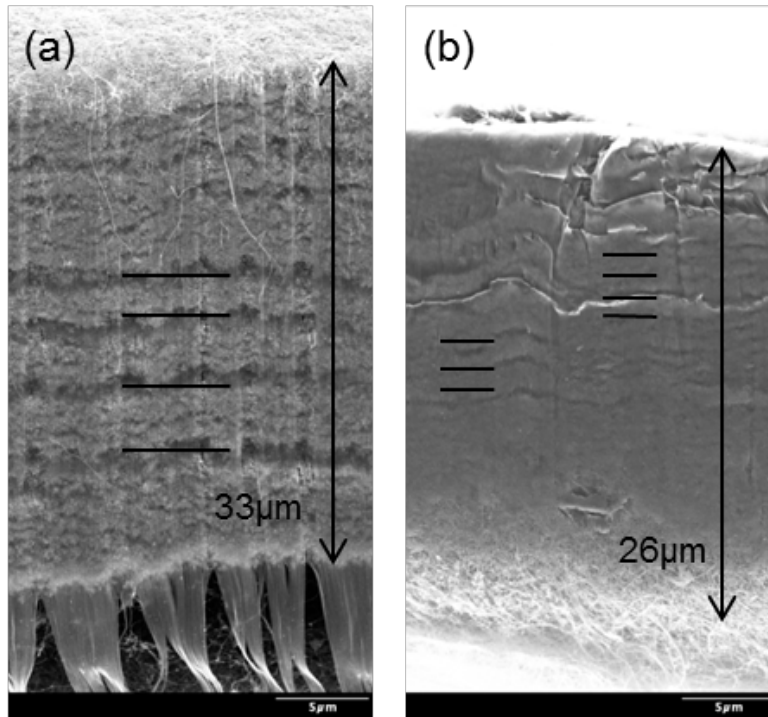


Figure 48. Internal layers in CNT thickness comparing (a) EP CNT-sheet and (b) Standard production specimen

The amount of impurities found saturated throughout the EP CNT-sheets is expected to be the dominating factor in the reduction of mechanical strength and stiffness as seen. This is also supported by the significant increase in performance in EP specimens that have been purified in a nitric acid treatment as the acid treatment would dissolve the impurities.

4.2.5 Polymer Coated Specimens

The review of mechanical properties for polymer coated sheets required a separate analysis because it introduced some unique behavior. Recalling from Figure 14, type E specimens are standard production while type F are enhanced production. Type E and F specimens contain both thermoplastic polyurethane (TPU) and polystyrene (PSb)

as polymers for coating. Table 6 presents a summary of polymer coated specimens along with their manufacturing details.

Table 6. Details of polymer coated CNT-sheets, types E-F

Sp ID	Thickness* (μm)	Density* (g/cm^3)	Areal density (g/m^2)	TPU	PSb
10 E	40.22 \pm 6.47	0.61 \pm 0.02	24.35 \pm 0.72		X
11 E	59.67 \pm 2.02	0.31 \pm 0.01	18.25 \pm 0.89	X	
12 F	50.33 \pm 4.36	0.50 \pm 0.01	25.40 \pm 0.32	X	
13 F	30.62 \pm 7.23	0.47 \pm 0.09	14.48 \pm 2.70		X
14 F	32.82 \pm 8.00	0.39 \pm 0.01	12.84 \pm 0.33	X	

**Apparent property; referring to the difficulty in measuring accurate thicknesses.*

Figure 49 shows five coated specimens referenced as type E and F with the standard reference specimen of type A. There is a distinct separation in properties dominated by the specimen production rate. Both the PSb and TPU coated specimens with standard production rates show an improvement in performance. Enhanced production sheets coated with PSb and TPU all have decreased strength with the PSb coated, specimen 13, being the lowest. The two TPU coated EP specimens from type F are consistent. Another separation is the level of strain at failure which can be distinguished by polymer type. TPU coated specimens have strain values between 15-25% with EP specimens being lower. PSb specimens have strain larger than 30% independent of production rate. The respective improvement and decrease of PSb coated specimens with different production rates is much more significant than the effects introduced by TPU. This demonstrates that polymer type is an important factor in addition to the production rate as manufacturing parameters.

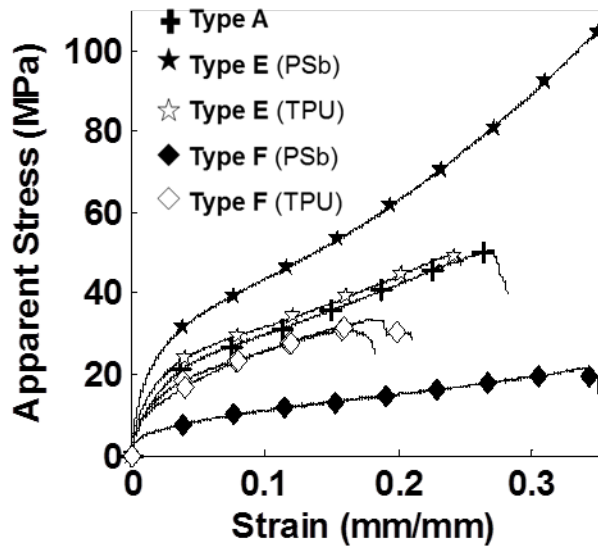


Figure 49. Tensile stress-strain curve for polymer coated CNT-sheet specimens.

One of the main reasons these coated sheets require a separate review in mechanical performance is because the amount of polymer present in the sheet is observed to vary considerably. Figure 50a shows the surface morphology of the PSb coated, specimen 10. A network of CNT bundles is seen comparable to uncoated sheets with less defined boundaries between CNTs. The significant increase in strength and stiffness for specimen 10 and the observed microstructure is supportive of the desired enhanced load transfer. Figure 50b shows a very different morphology where there is a lot more polymer present and the CNTs are dispersed throughout the matrix with less interactions. For this different morphology, polymer intercalation is not seen to support enhanced load transfer or in improving mechanical properties. Mechanical properties in this case would be more representative of the TPU polymer with CNTs as a filler and would not exploit their full advantages.

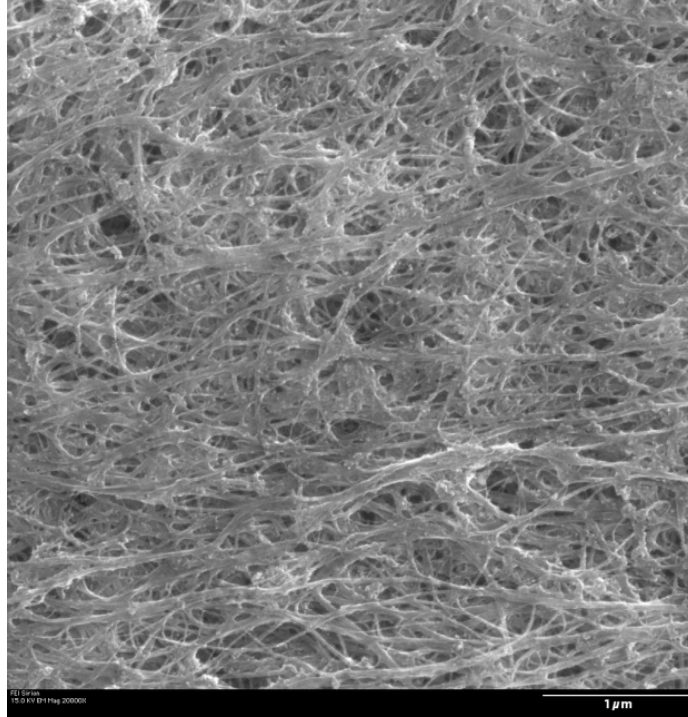


Figure 50. Surface morphology of PSb coated specimen 10 at 20kx magnification

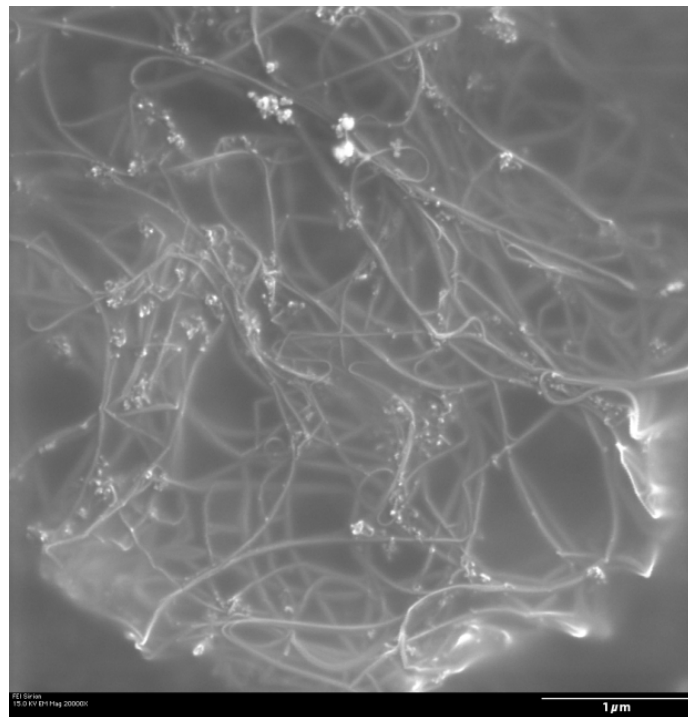


Figure 51. Surface morphology of TPU coated specimen 11 at 20kx magnification

4.2 CNT-Sheet Baseline Electrical Properties

Electrical conductivity is a measurement that represents how well a material is able to transport electricity. This is directly related to and calculated from the level of resistance measured in the material. Resistivity in Equation 19 takes the resistance (ohms) multiplied by the cross-sectional area of the current's path and divides it by gauge length. This is an intrinsic property that represents how well a material opposes the flow of electrons.

$$\text{Resistivity} = \rho_r = \frac{R A}{L} = \frac{R t w}{L} \quad (19)$$

Where:

ρ_r = apparent electrical resistivity (Ωm)

R = resistance (Ω)

A = cross-sectional area of sheet (m^2)

t = apparent sheet thickness (m)

w = sheet width (m)

Conductivity is the inverse of the relationship in Equation 20 representing the ability of a material to allow current flow. Conductivity is measured in Siemens ($1/\Omega$) per meter.

$$\text{Conductivity} = \sigma_e = \frac{1}{\rho_r} = \frac{L}{R t w} \quad (20)$$

Where:

σ_e = electrical conductivity (S/m)

Because the conductivity calculation is affected by thickness it is reported as “apparent conductivity.” Reviewing results for all 6 specimen types in Figure 52 immediately present some important trends. Starting with the baseline properties of specimen 1, types B through F distinguish themselves with varied electrical conductivity performance. The best performance is found in the acid treated materials from types C and D. Reduced conductivity is seen for polymer coated specimens in groups E and F. For standard growth rate, acid treated, and polymer coated specimens conductivity is reduced with enhanced production. This is also true for EMI shielding effectiveness seen in Figure 52b. EMI shielding capabilities. This means that enhanced production diminishes all electrical properties. The varying dimensions and mass of each specimen make it necessary to review the results with respect to thickness, as well as both volumetric and areal density. Understanding these trends will help clarify the impact of each groups’ unique manufacturing parameters.

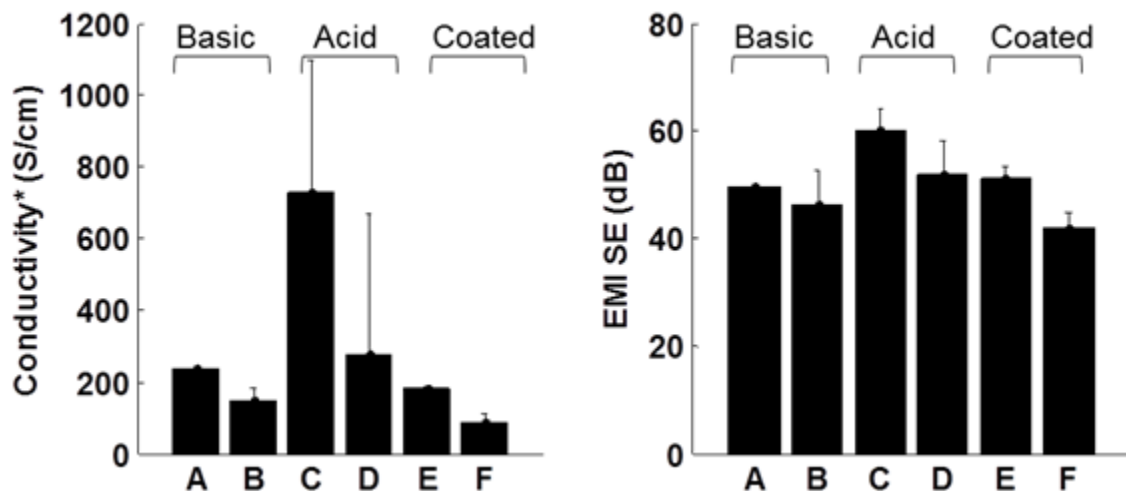


Figure 52. Conductivity and EMI shielding by manufacturing parameter type

**Apparent property*

4.2.1 Volumetric Density

Overall trends in conductivity and EMI shielding do not appear to be effected by density for the data presented in Figure 53. Polymer coated, type F, show low performance in both data sets with large volumetric density ranges. Acid treated specimens in types C and D both increase and decrease with density. One important observation is separating performance into two groups. The conductivity of acid treated specimens is higher (shaded region) than the other types in Figure 53a. Both manufacturing parameters of enhanced production and polymer coatings fall below the baseline properties of type A in the non-shaded region. For EMI shielding, this observation is conflicted as specimens from EP and polymer coated types rise in performance to the regions dominated by the acid treated groups.

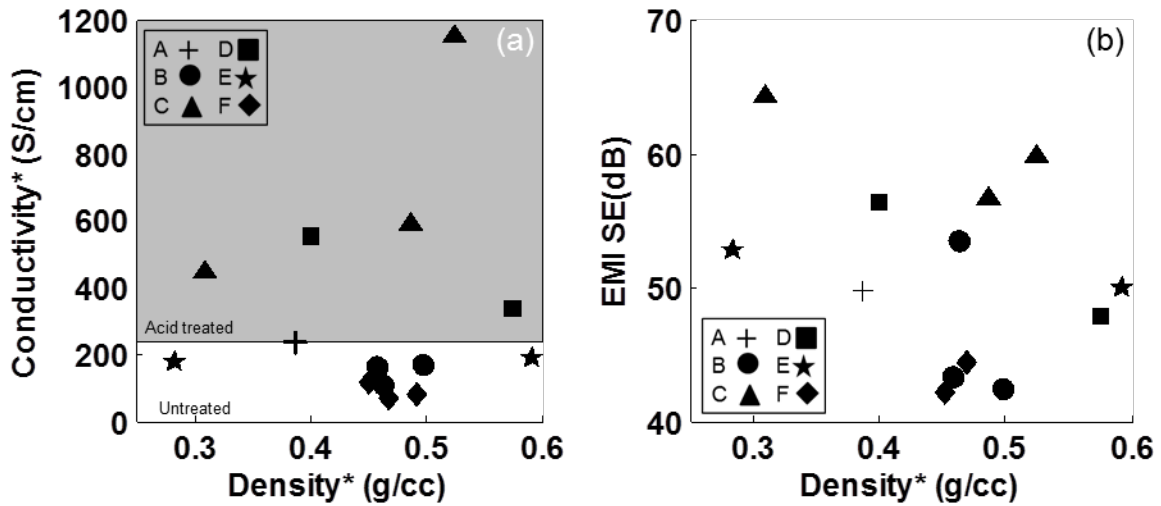


Figure 53. Electrical properties vs. density: (a) conductivity and (b) EMI SE

*Apparent property

Volumetric density is not an apparent factor in either conductivity or EMI shielding properties. Acid treatment is the dominating factor for improved electrical properties, and both enhanced production and polymer coatings reduce performance. These factors appear to follow a principle of linear superposition where the acid treatment improves the initially degraded performance caused by EP. This is also seen where type F has the worst properties and are both EP and polymer coated.

4.2.2 Areal Density

Areal density does not consider the thickness of the material which is used in the conductivity calculation. An interesting trend shows that apparent conductivity grows with reduced areal density in Figure 54. This is true for the acid treated types C and D. Conductivity remains constant over a wide range of areal densities for untreated. This apparent trend is not found for EMI shielding. Areal density does not take into account thickness, thus investigating thickness as a factor will be an important next step to exploit EMI shielding behavior as well as further analyzing trends in conductivity

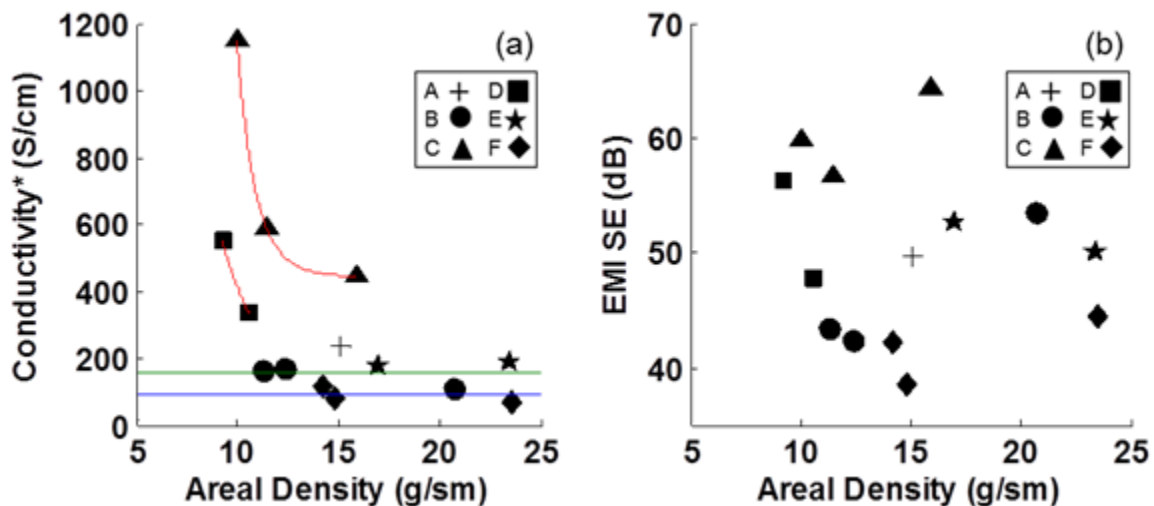


Figure 54. Electrical properties vs. areal density: (a) conductivity and (b) EMI SE

*Apparent property

4.2.3 Apparent Thickness

The increase of apparent conductivity follows previously noted trends in areal density as seen in Figure 55. The trend is more general to all groups and is exaggerated for acid treated specimens who in large part are observed to be thinner and have lower areal densities. The first observable trend in EMI shielding is three levels of performance. The first group (identified by 2) seen in Figure 55b is the middle of the scatter at approximately 52 dB. Specimens from type D and E are primarily found here with the standard reference specimen type A. Types B and F are found with a scatter around 42 dB (identified by 1). Finally the acid treated, type C, have the best shielding capabilities around 64 dB (identified by 3).

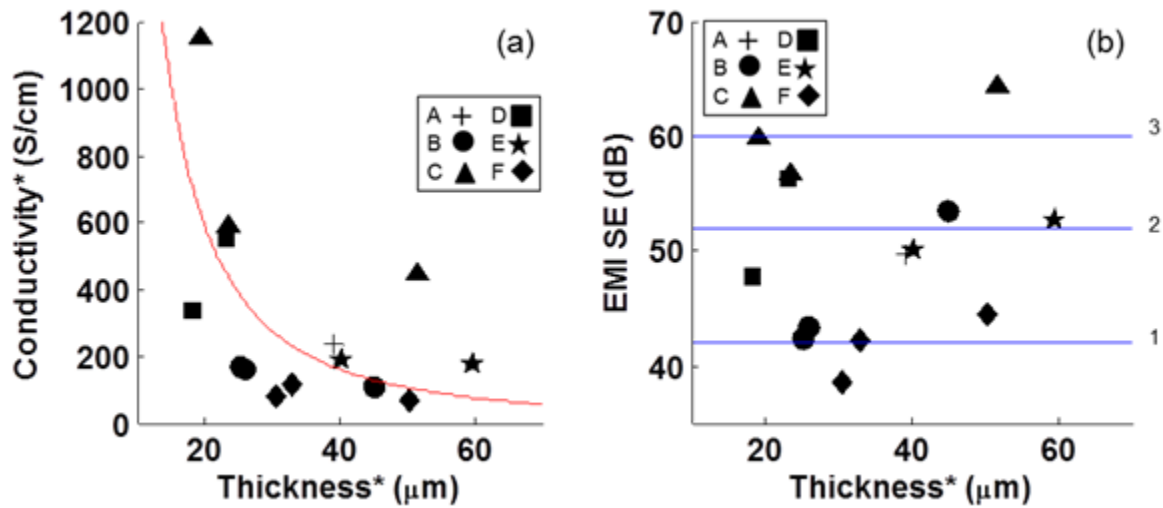


Figure 55. Electrical properties vs. thickness: (a) conductivity and (b) EMI SE

*Apparent property

Groups are found in EMI shielding scattered about performance lines that differ by approximately 10 dB. Enhanced production and polymer coatings decrease EMI shielding. Acid treatment and thickness increase performance. Similar to conductivity,

the results of these factors in electrical properties follow a principle of linear superposition with thickness joining these manufacturing parameters. From the performance of specimen 1 in type A, EP and polymer coated types B and F drop to the lower performing group of around 42 dB. Specimens that are expected to have reduced shielding properties from these affects can be improved with acid treatment and thickness. This can be seen for the acid treatment in group D which is EP but have EMI SE in the middle performance group. For the case of thickness, all type B specimens which are EP are in the bottom group except for specimen 3. This EMI SE for specimen 3 of greater than 50dB is from its larger thickness.

Specimen B seems to be the only outlier in EMI shielding in Figure 55b who is observed above the higher level performance group. This helps exploit the importance of thickness in EMI SE. For each manufacturing parameter type, EMI shielding increases with apparent thickness. By dividing properties by apparent thickness, the results of conductivity and EMI shielding present stronger trends. The scatter of data points are drawn closer to the trend in conductivity per unit thickness in Figure 56a. This presents conclusive trends for EMI shielding seen in Figure 56b. EMI shielding properties per unit thickness increase with thickness for all specimen variable types.

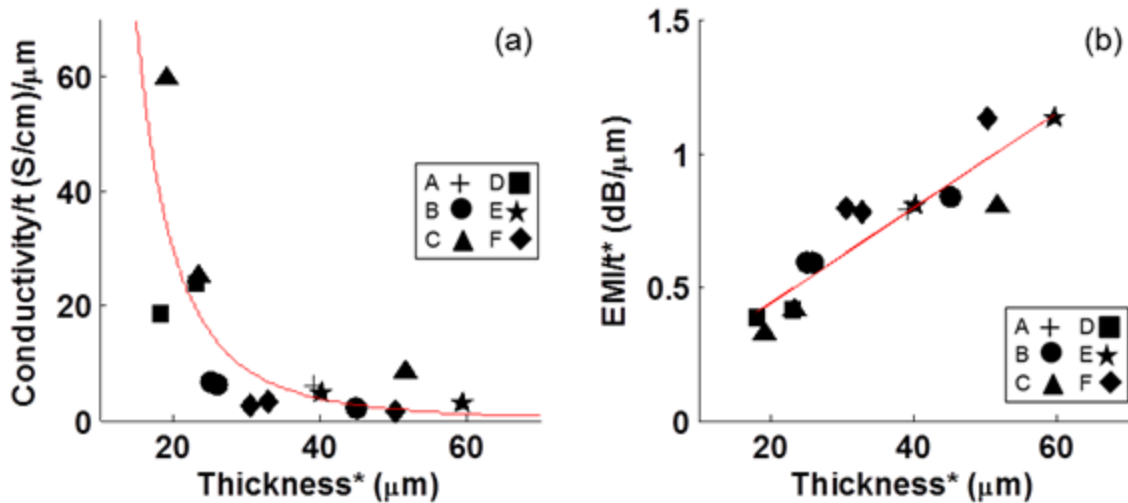


Figure 56. Electrical properties per unit thickness: (a) Conductivity and (b) EMI SE

**Apparent property*

4.2.4 Overview of Manufacturing Parameters

Using a FEG-SEM, high resolution images were taken of the surface morphology of different manufacturing parameters in the CNT-sheets. Figure 57 shows a clear network of randomly dispersed bundles of CNTs for type A. For the acid treated specimen of type B in Figure 58, a similar structure is seen with a matted compact appearance due to treatment in a nitric acid bath. Acid treatments facilitate the functionalization of CNTs and the dispersion of the fibril network which may assist in the more dense appearance and the reduced thicknesses in types C and D. The result is a changed surface morphology and becoming more compact. This acid treatment is seen to be a large factor in both electrical properties. Misak et al. reported that the compact nature of the acid functionalized CNTs in yarns contributed to the increase in conductivity [17] and the addition of function groups increased the mobility of electrons [20]. This offers clarification to why the acid treated CNT types are thinner and the

growing trend with reduced thicknesses is a product of the more compact nature of the acid treatment. Fabrication methods that decrease boundary defects and voids within bulk CNT materials are expected to greatly increase physical properties [47]. This is a part of the underlying effects seen from acid treatment as well as the lower properties of EP CNT-sheets supported by this SEM investigation of microstructure.

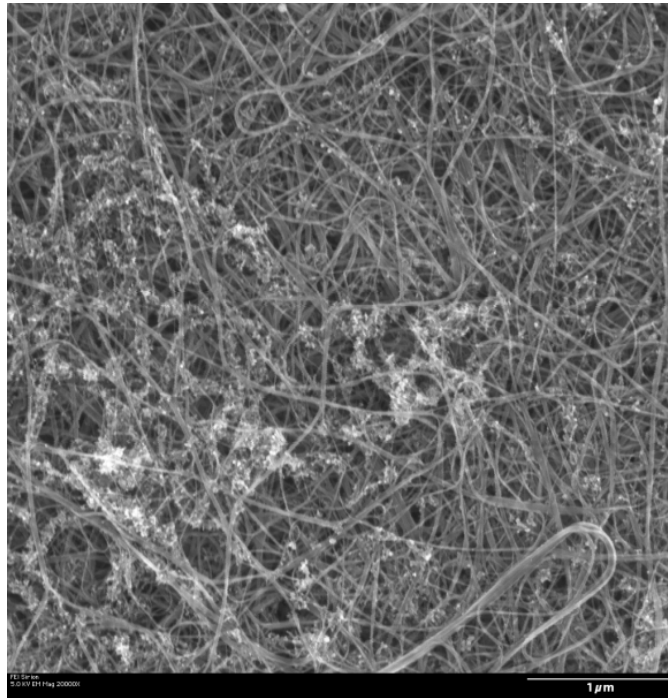


Figure 57. Surface morphology at 20kx magnification for untreated specimen 1

EP-CNTs are seen in Figure 59 to have a different morphology. The less distinguishable CNT networks are saturated with impurities that can include different forms of carbon and residual catalysts. This microstructure is even less compact, filled with more voids and non-conductive fillers interfering with electron transport through the interlocking CNTs.

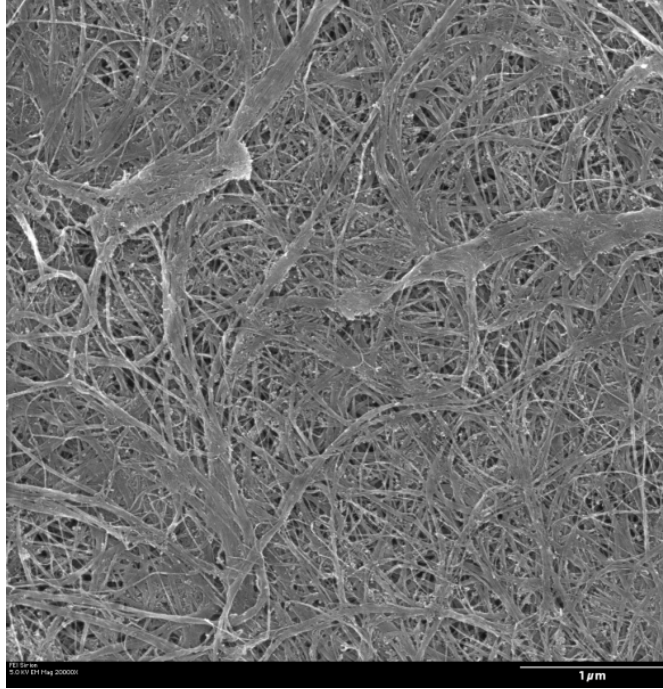


Figure 58. Surface morphology for at 20kx magnification for acid treated specimen 6

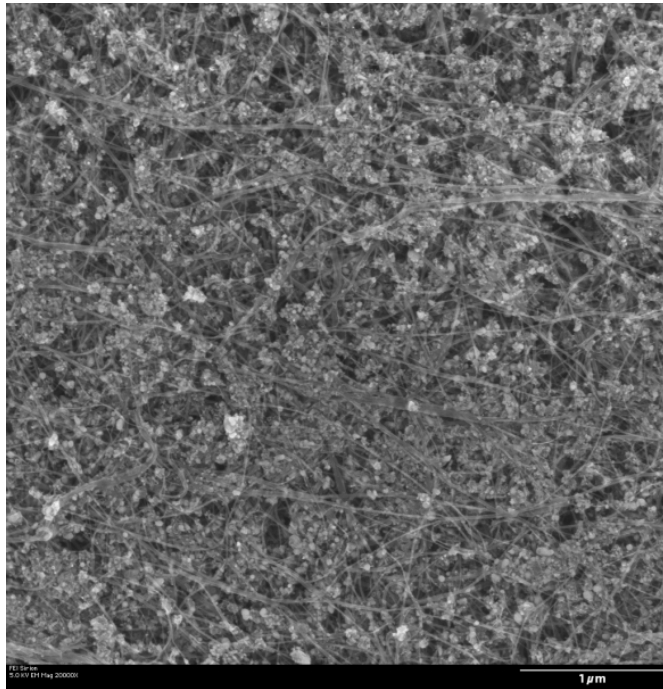


Figure 59. Surface morphology for at 20kx magnification for enhanced production specimen 4

Magnifying a little closer on a specimen coated with Polystyrene in Figure 60 a clear difference is seen with the polymer introduced into the CNT bundles. While the motivation to introduce polymers for enhanced load transfer between CNT networks, it does not appear to be a manufacturing parameter encouraging electron transport or EMI shielding.

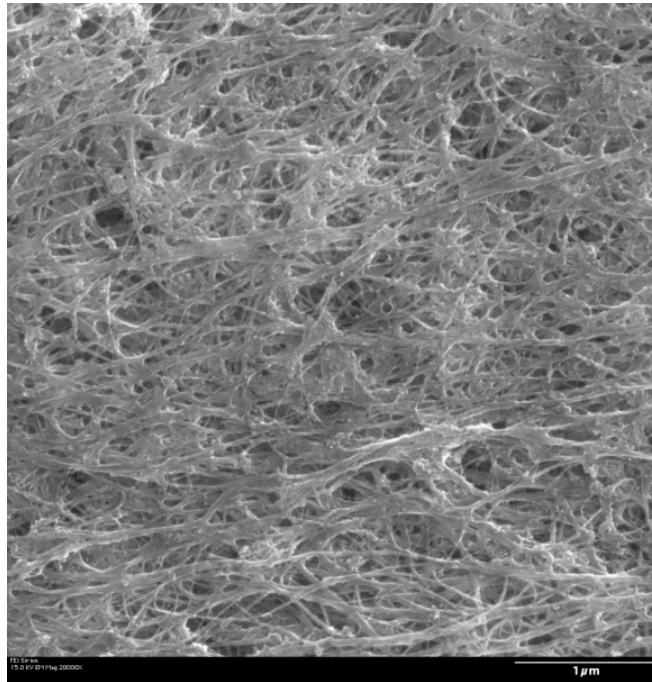


Figure 60. Surface morphology for at 20kx magnification for PSb coated specimen 10

Important observations have been reported from this study that compliment current research being evaluated for the exploitation of manufacturing parameters to improve the electrical properties of CNT-sheets.

4.3 Effects from Space Environments

CNT-sheets, while still under their potential for mechanical and physical properties, display impressive qualities created through a variety of different manufacturing parameters. Before introducing them into space; studies must address how stable these properties and underlying manufacturing parameters are under transient and destructive orbit conditions. Consider a material less dense than other space materials and only 30 μm in thickness. Now expose this sheet of material that is thinner than the average human hair to the bombardment of erosive atomic oxygen or cycle it over 1400 times between -60 and 120°C. What would happen to it? This is the nature of conditions a spacecraft might see in LEO for 3 months and is what will be answered in this next portion of research. Mechanical and electrical properties are compared for specimen 1 and 6 for before and after ATOX exposure and thermal fatigue to determine the stability of properties over time in the harsh space environment. Specimen 6 from type B was selected with particular interest in how durable the improved properties from the acid treatments are. Changes in morphology and microstructure are reviewed for better understanding of the environment effects.

Because the specimen size for ATOX and thermal fatigue exposure was limited, 0.5 (12.7mm) inch wide specimens were shortened to lengths of approximately 1.5 in (38.1mm) which required reduced gauge lengths for the tensile tests. Widths were the same as the first baseline tensile tests and it could not be immediately concluded that changes in width to gauge length ratios would not affect the tensile behavior. In order to confidently compare post exposure mechanical performance to the pre-exposed specimens, another set of baseline tensile tests were performed with reduced gauge

lengths. These new baseline results were taken for specimens 1 and 6 and are identified in Table 7 and Table 8 with the identifier “B” for baseline. Also reported are the results after atomic oxygen identified by “A”, and for thermal fatigue with “T”. For electrical conductivity tests, ATOX exposed samples were measured for electrical resistance on both sides and averaged to make sure data wasn’t biased by the changed surface morphology on only the exposed side of the specimen. The comparisons presented in this section’s charts are accurate comparisons with all test conditions and procedures remaining the same. The new variable introduced is the environments of atomic oxygen and thermal loading.

Error bars were plotted for test specimens from each type. These were used as confidence intervals to help make conclusions on whether or not properties actually changed from the space environments affects. For example, an average value may appear to change slightly but if the error bars are large than a conclusion might not be made to say there was any definitive change.

Table 7. Details of CNT sheets for space environment exposure

Identifier	Thickness* (μm)	Density* (g/cm^3)	Areal Density (g/m^2)	Acid Treated	ATOX	Thermal Fatigue
1 - B	36.00 \pm 0.82	0.42 \pm 0.01	15.16 \pm 0.29			
1 - A	39.11 \pm 2.77	0.42 \pm 0.03	16.58 \pm 1.05		X	
1 - T	39.62 \pm 1.65	0.42 \pm 0.02	16.43 \pm 0.15			X
6 - B	29.33 \pm 5.03	0.44 \pm 0.08	12.62 \pm 0.11	X		
6 - A	23.52 \pm 1.83	0.52 \pm 0.01	12.28 \pm 0.35	X	X	
6 - T	26.83 \pm 2.32	0.52 \pm 0.02	13.85 \pm 0.70	X		X

**Apparent property; referring to the difficulty in measuring accurate thicknesses.*

The amount of exposed specimens available for testing limited EMI tests to a single specimen. The results assume the same standard deviation for EMI as the pre-

exposed sample set for each specimen type. This is an assumption presented later when using a statistical t-test to determine if properties changed after the space environments. Only one specimen was available for conductivity tests as well but several measurements were taken across its surface to create the distribution of confidence.

Table 8. Specific strength and stiffness, strain, apparent conductivity and EMI SE for space environment exposure

Id	Areal Density (g/m ²)	Specific Strength MPa/(g/cm ³)	Specific Stiffness GPa/(g/cm ³)	Failure Strain (mm/mm)	Conductivity* (S/cm)	EMI Shielding (dB)
1-B	15.16 ±0.29	126.9 ±14.02	3.02 ±0.27	0.22 ±0.05	236.4 ±25.02	49.70 ±0.60
1-A	16.43 ±0.15	114.76 ±8.20	5.27 ±1.46	0.13 ±0.04	160.6 ±11.86	49.49 ±0.60 ⁺
1-T	16.58 ±1.05	137.58 ±8.63	4.70 ±1.36	0.24 ±0.05	217.4 ±14.17	51.39 ±0.60 ⁺
6-B	12.62 ±0.11	130.4 ±11.92	4.44 ±0.86	0.27 ±0.04	589.5 ±88.73	56.63 ±3.87
6-A	12.28 ±0.35	130.62 ±3.45	7.62 ±0.14	0.17 ±0.03	382.3 ±21.66	55.20 ±3.87 ⁺
6-T	13.85 ±0.70	140.79 ±8.88	7.94 ±0.93	0.18 ±0.05	460.2 ±7.03	56.21 ±3.87 ⁺

*Apparent property; referring to the difficulty in measuring accurate thicknesses.

⁺ Standard deviation assuming same spread as unexposed data.

4.3.1 Atomic Oxygen Results

No change in specific strength is observed for both groups seen in Figure 61a. Specific stiffness shows an increase for both in Figure 61b by 74% and 71% respectively for specimen 1 and 6. There is also a consistent reduction in the amount of strain at failure by 40% and 39% for the same specimens shown in Figure 62a. Figure 62b shows that areal density increases by 9% for type A and drops more slightly by 3% for type B.

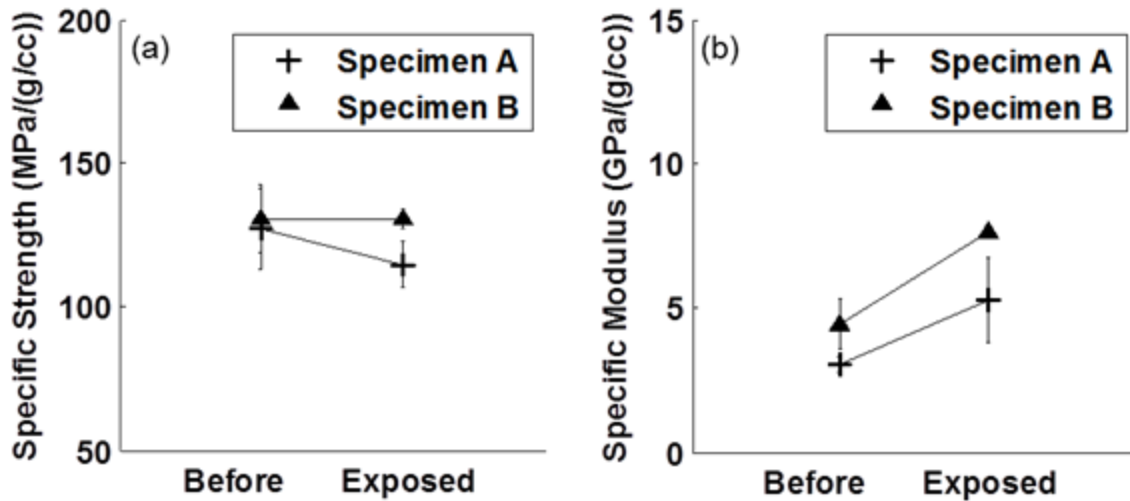


Figure 61. Effects of atomic oxygen on (a) specific strength, and (b) specific stiffness

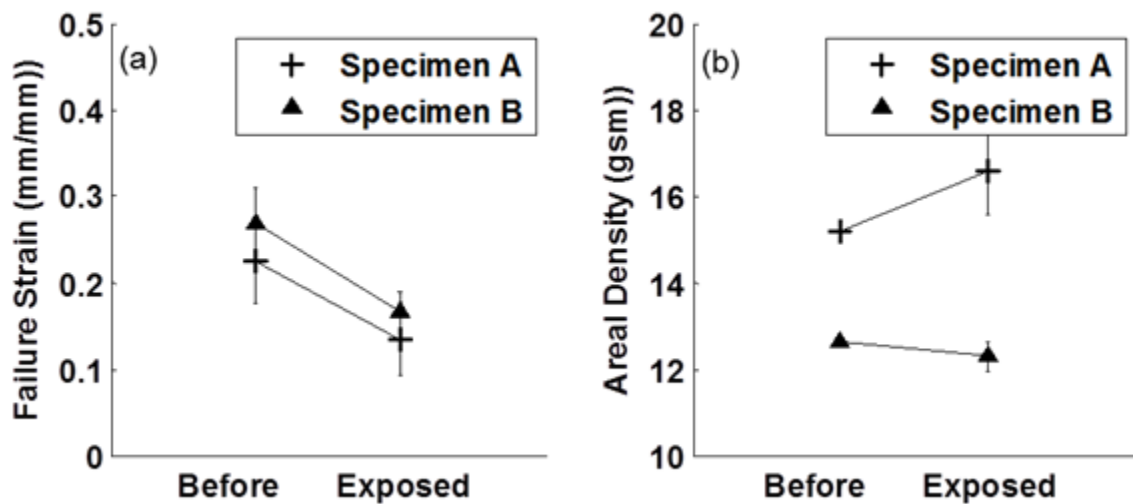


Figure 62. Effects of atomic oxygen on (a) failure strain, and (b) areal density

An important note to consider is that equal variances in the compared data cannot be directly verified, thus it must be assumed that the data set has unequal variance. This difference observed in the spread of measured data will be an important assumption when performing the t-tests for statistical analysis. This analysis is presented with the

conclusions in chapter 5 for determining the most probable changes in properties as a result of the space environment.

A reduction is seen in Figure 63a where the apparent conductivity for both groups drops by 32% and 35% for the respective specimens 1 and 6. EMI shielding drops by less than 1% in specimen 1 and 2% for specimen 6 as seen in Figure 63b.

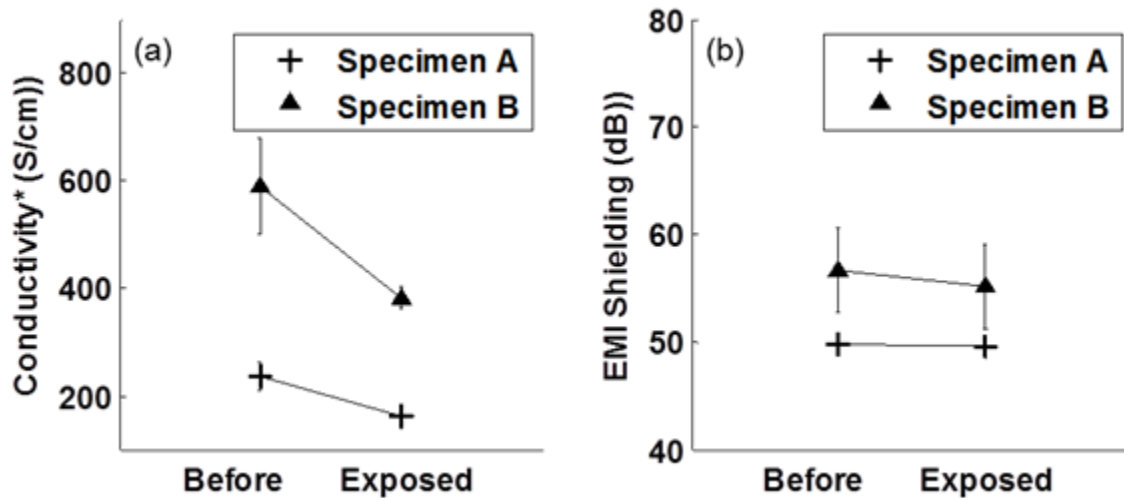


Figure 63. Effects of atomic oxygen on (a) conductivity and (b) EMI shielding

*Apparent property

SEM performed on materials in the STS-5 mission observing the effects of ATOX on surface morphology and observed an erosion pattern with valleys and troughs of approximately 1 micron size that gave them an appearance described as “carpet like” [36]. A similar morphology is observed in Figure 65 and Figure 67. In contrast to the clear CNT networks seen in Figure 64 and Figure 66, erosion from ATOX has shown to break down the fibril network, traded for the pitted, “carpet like” appearance in both specimens.

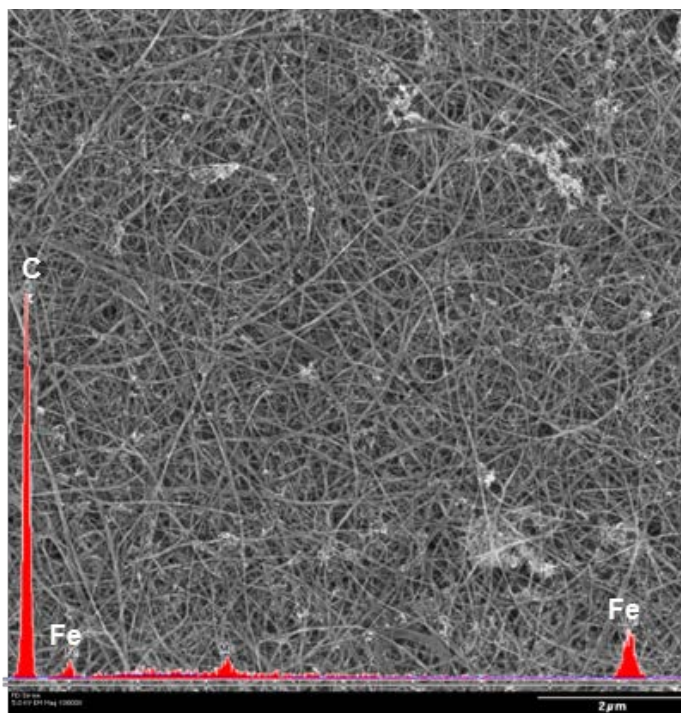


Figure 64. Surface morphology and EDX of CNT-sheets for specimen 1 before exposure

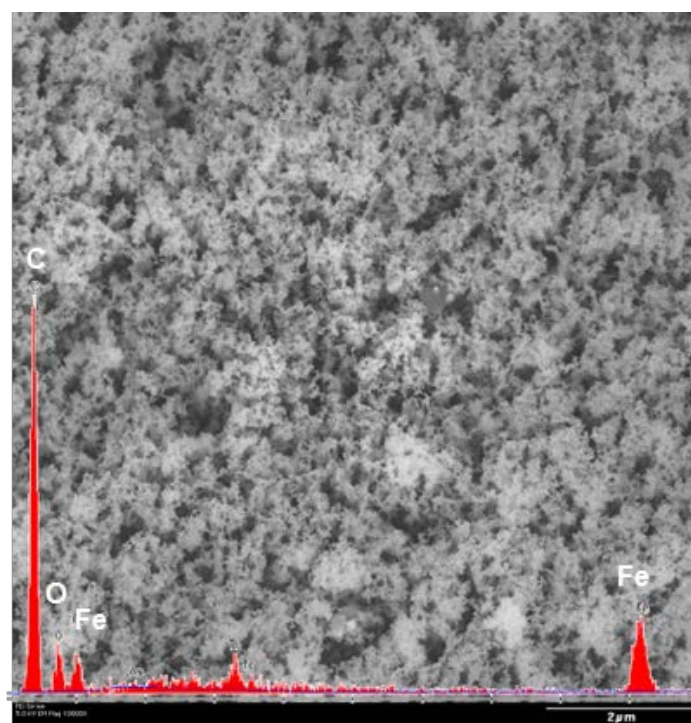


Figure 65. Surface morphology and EDX of CNT-sheets for specimen 1 after ATOX

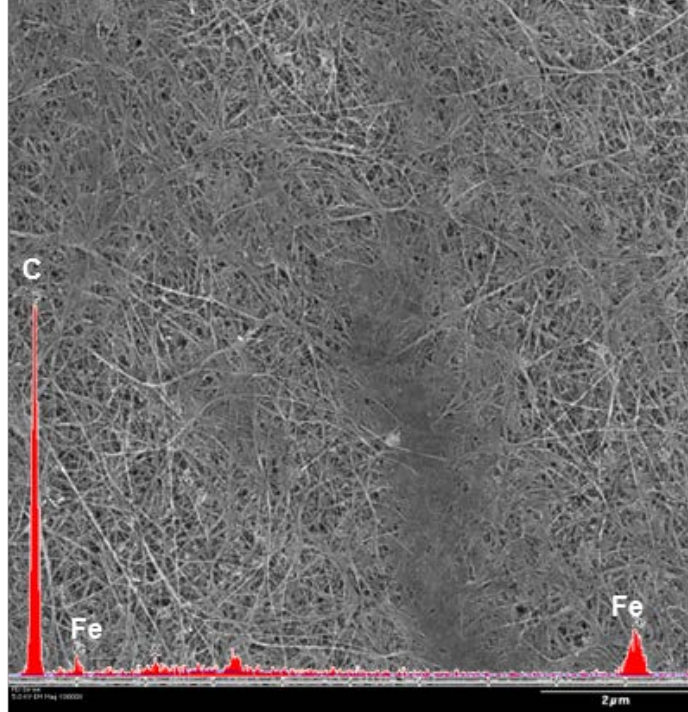


Figure 66. Surface morphology and EDX of CNT-sheets for specimen 6 before exposure

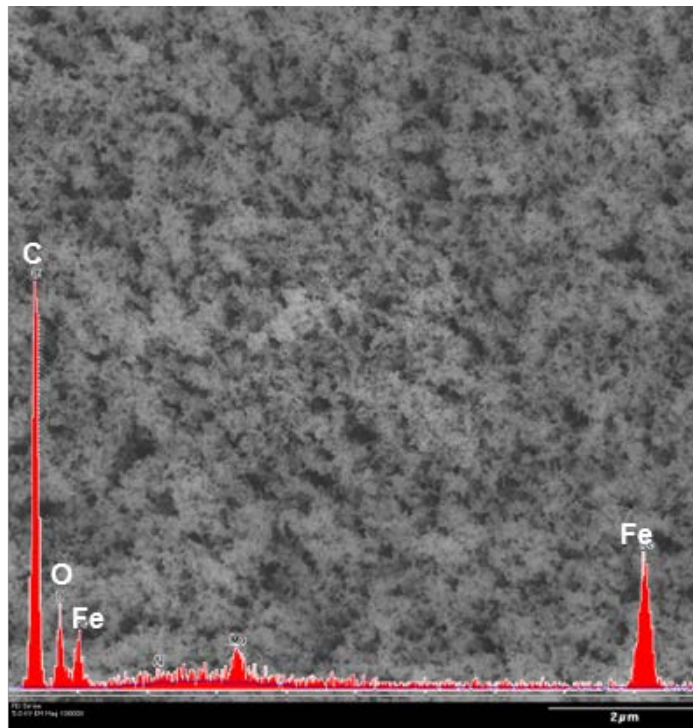


Figure 67. Surface morphology and EDX of CNT-sheets for specimen 6 after ATOX

Energy dispersive x-ray (EDX) spectroscopy analysis showed erosion of the surface layer with a loss of carbon and increase in oxygen. Table 9 shows data for before and after ATOX from the EDX analysis. The results show chemical composition by atomic percent. All elements reported within less than 1% composition are considered negligible and less accurate. These are neglected in the “other” category. After making this assumption, the only composition of interest is carbon and the iron catalyst. For the ATOX specimens, oxygen becomes a new major component of the composition.

EDX was performed before and after ATOX exposure. The biggest change that occurs in both specimens is the arrival and significant increase of oxygen becoming approximately 8 atomic weight percent of the final composition. In addition, the carbon decreases by about 10 atomic weight percent in both cases. Finally, there is an increase in the presence of iron after ATOX in both specimens. A study done on Teflon (comprised mainly of carbon, fluorine, and oxygen) showed similar results where fluorine and oxygen content was reported to slightly increase after ATOX [39].

Table 9. Atomic weight composition of CNT-sheets before and after atomic oxygen

Element	1 Before (At %)	1 After (At %)	6 Before (At %)	6 After (At %)
Carbon (C)	96.91	86.72	96.07	87.3
Iron (Fe)	2.67	3.65	3.11	4.07
Oxygen (O)	0	8.64	0	7.28
Total Other (Ti,Mo,Pd)	.42	.99	.82	1.35

The increase in oxygen content and changes to surface morphology shown demonstrate that oxidation is occurring and is a factor causing surface erosion which is the main concern for materials in low earth orbit. The small increase in the atomic percent of iron observed after ATOX can also be attributed to the depletion of carbon

while iron is unaffected by the oxidation process. The erosion of the surface layer also has been seen to expose residual catalyst materials and impurities as shown in Figure 68 that have been encapsulated beneath layers in the production process.

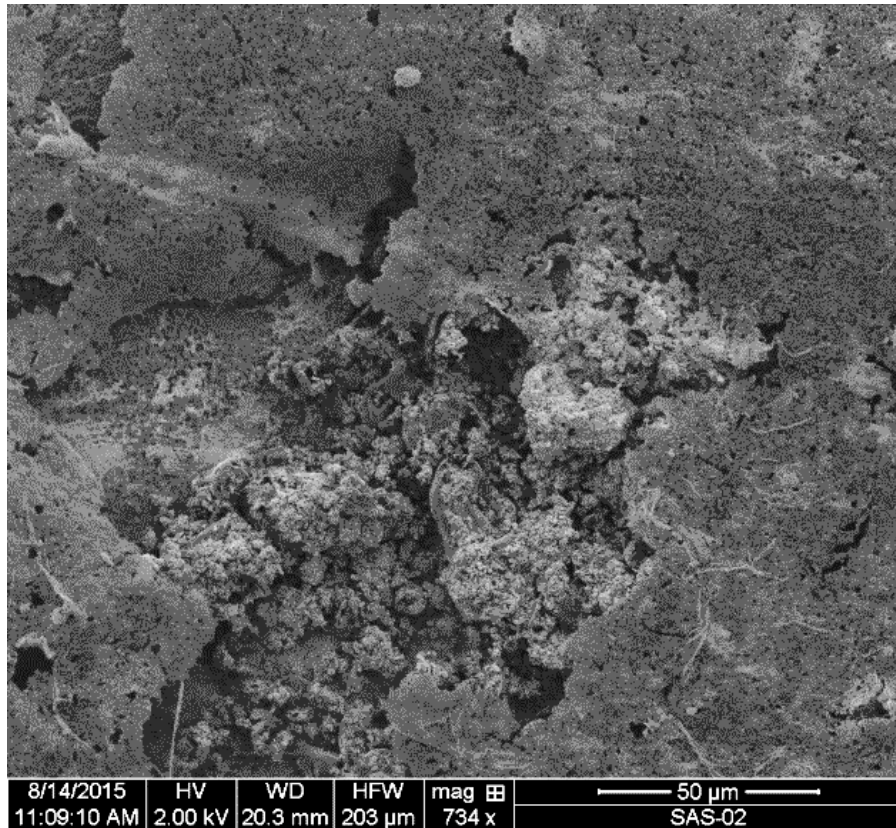


Figure 68. Exposed catalyst material after ATOX

Differences seen in areal density are related to either a depletion or addition of mass to the materials; the addition being from oxygen and the depletion from the erosion of carbon. Detailed investigation in the processes that attribute to changes in mass is not presented and is needed to clearly quantify the erosion rate and penetration depth for ATOX effects in CNT-sheets. More extensive research in how deep the sheets were

penetrated would be valuable in better determining stability and possible differences between the 2 specimens.

While surface erosion is observed in the surface morphology the mechanical properties do not appear to be negatively affected due to ATOX in either the standard or acid treated specimens. The erosion rate on CNT-yarns from ATOX was calculated by Misak et al. to be $2.64 \times 10^{-25} \text{ cm}^3/\text{atom}$, comparable to carbon vitreous [75]. This resistance to atomic oxygen is better than graphite/epoxy composite [T300/5208] ($29 \times 10^{-25} \text{ cm}^3/\text{atom}$) [37] and much less resistant than copper ($0.087 \times 10^{-25} \text{ cm}^3/\text{atom}$) [75]. Electrical properties do however show a substantial reduction in conductivity for both types. EMI SE remains unaffected after atomic oxygen. Although EMI SE is affected by an electrical property, the reduction in conductivity does not equally impact shielding effectiveness for CNT-sheets.

4.3.2 Thermal Fatigue Results

There is no observed change in the specific strength of either specimen type after thermal fatigue shown in Figure 69a. Specific stiffness is increased for both types. The specific stiffness of the acid treated group increases by 79% in Figure 69b and there is a softer increase for the untreated specimen by 55%. Figure 70a shows a reduction of strain at failure by 40% for specimen 1, and a small 6% for specimen 6. Changes in mass are shown in Figure 70b where areal density appears to increase for both specimens with a softer level of confidence.

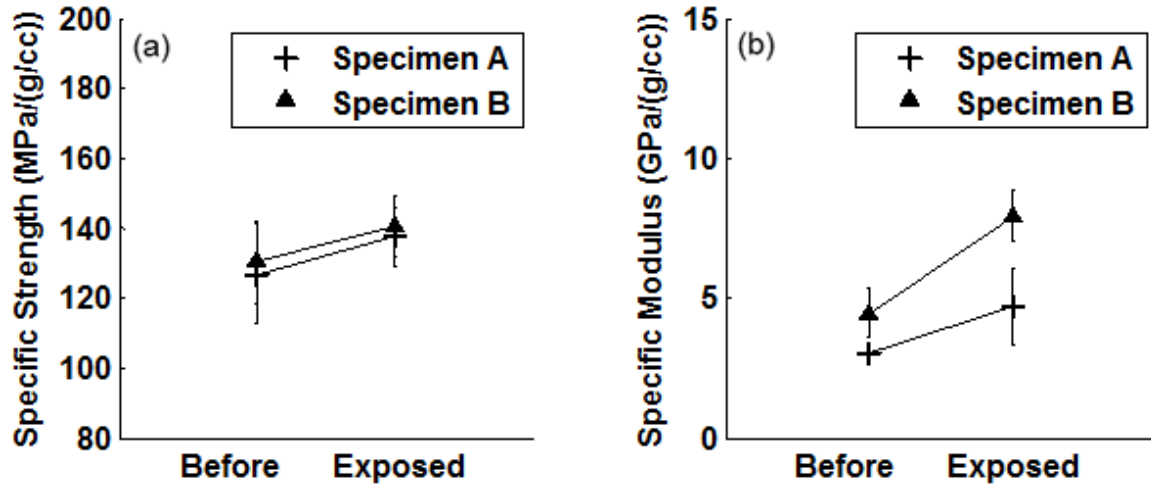


Figure 69. Effects of thermal fatigue on (a) specific strength, and (b) specific stiffness

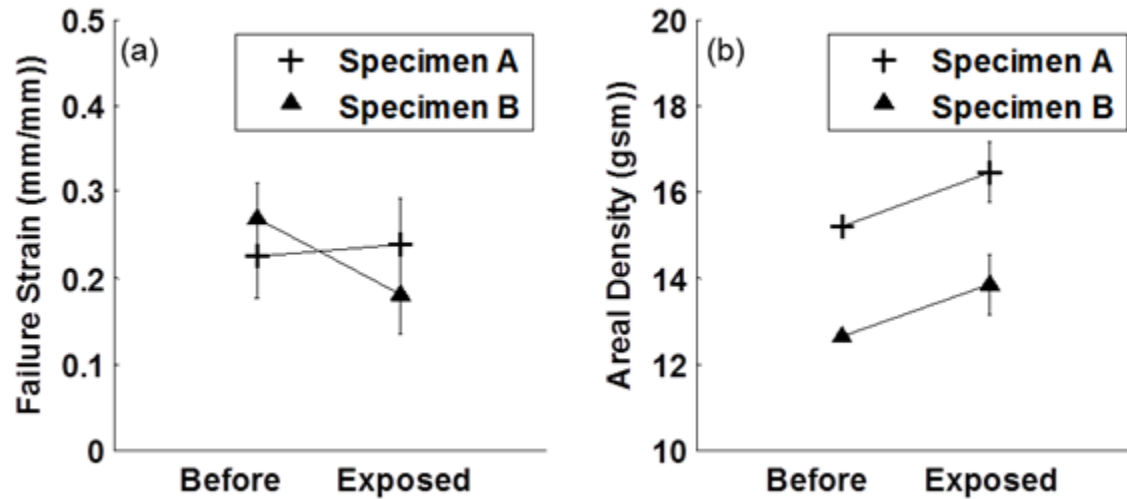


Figure 70. Effects of thermal fatigue on (a) failure strain, and (b) areal density

In review of electrical properties in Figure 71, the untreated sheet is not affected in either electrical conductivity or EMI shielding properties due to thermal fatigue. For the acid treated specimen, apparent conductivity is reduced by 26%. For CNT yarns, thermal fatigue presented no effect on tensile strength but caused a comparable decrease in conductivity by 18% [70].

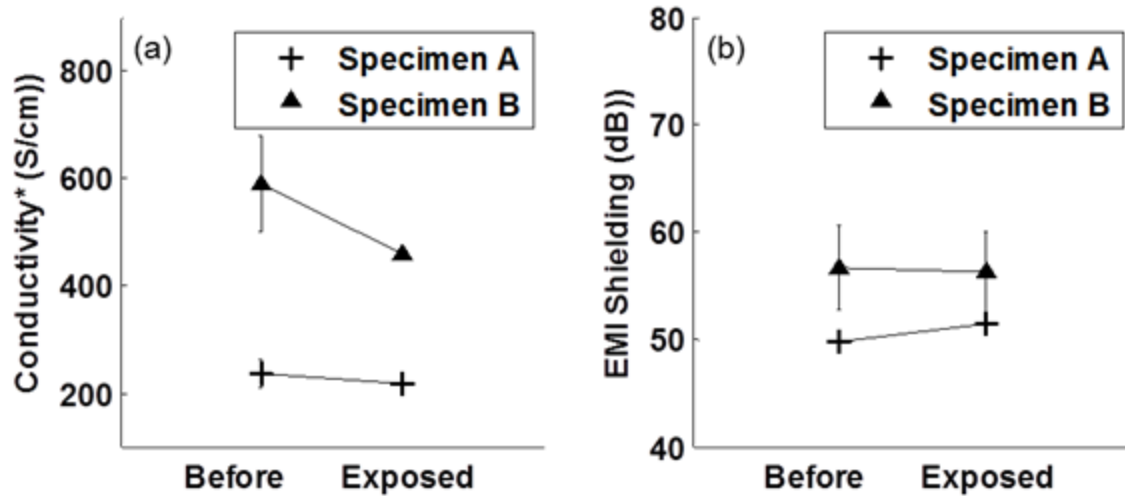


Figure 71. Effects of thermal fatigue on (a) conductivity and (b) EMI shielding

**Apparent property*

SEM images present no apparent change in surface morphology. In Figure 72, specimen 1 can be seen again with its characteristic fiber network and presence of carbonaceous and catalyst impurities. Specimen 6 in Figure 73 also presents to have the expected compact and matted appearance after thermal fatigue.

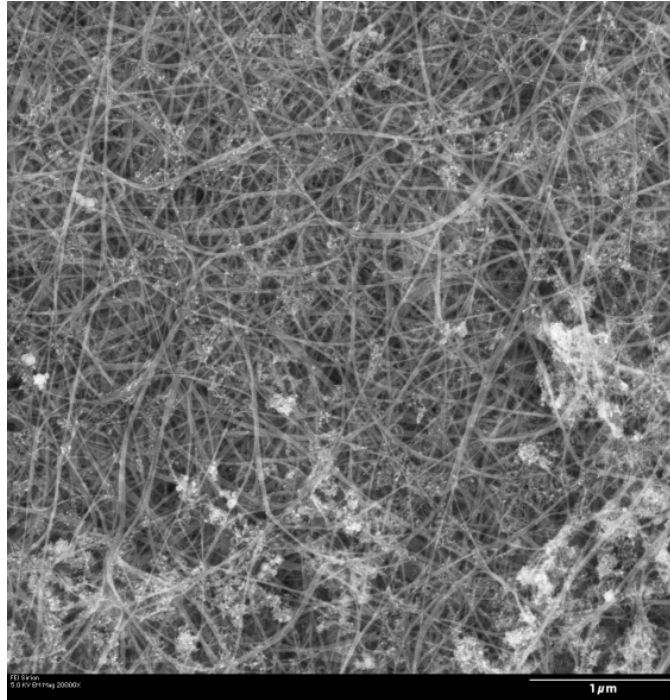


Figure 72. Surface morphology of CNT-sheets after thermal fatigue for specimen 1

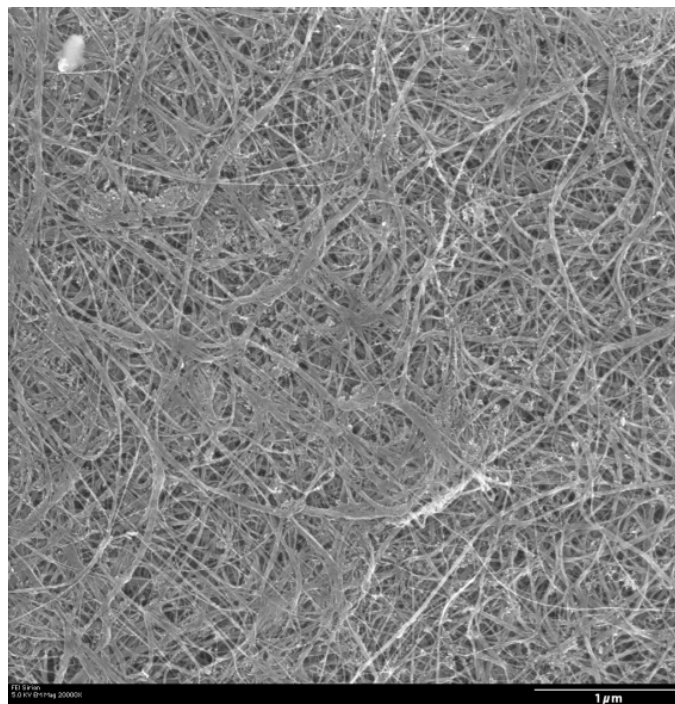


Figure 73. Surface morphology of CNT-sheets after thermal fatigue for specimen 6

This microscopic investigation is supportive of the data which has demonstrated no statistically significant changes in strength. Changes are found for both specimens where conductivity decreases after atomic oxygen. Because measurements were taken on both sides of the specimen, the changes are expected to be from a loss in conductive area and not due to surface conditions. More significant reductions in conductivity occur in the acid treated specimen. Misak et al. explained that CNTs need room to expand and contract under thermal cycling and will eventually buckle [70]. The compacted morphology of the acid treated sheets restricts movement with increased CNT interaction which results in more crack formations and buckling. Discontinuities caused by thermal fatigue in this manner are less able to carry electricity as seen in fatigued CNT-yarns. While the reductions due to thermal fatigue were not strong in statistical change and micro cracks were not observed, this is only a possible conjecture for the observed properties. It is important to note in the same study on CNT-yarns that the strength was also not affected by thermal fatigue due to inter-boundary frictions with other continuous yarns limiting the effect of the microscopic crack formations. In similar principle, CNT-sheets are composed of micron thick layers that interact and create the effect of continuous sheets even with the presence of micron size cracks. Therefore the changes in microstructure from acid treatment facilitate the destructive nature of thermal fatigue for in the more compact sheets. This is the case for conductivity only where EMI shielding effectiveness was unchanged by neither atomic oxygen nor thermal fatigue.

V. Conclusions and Recommendations

5.1 Chapter Overview

Each of the investigative questions from chapter 1 is directly answered with summarized data and conclusions found throughout the research analysis. Discussion is also included on the significance of the research for CNT-sheets as promising materials for use in the space environment. Finally, recommendations are made for next steps in future research for CNT-sheets in their evolving preparation for space.

5.2 Conclusions of Research

The 14 different types of CNT-sheets were evaluated and compared in terms of tensile and electrical behavior, including manufacturing parameters of enhanced production, acid treatment, and polymer coatings. Further investigation reviewed inter-group variables including thickness and both volumetric and areal density. Relationships and property dependence on the morphology and microstructure were also studied and were supportive in the holistic conclusions presented in this section. The following conclusions are presented in the context of answering the investigative questions presented in Table 2 from chapter 1:

1. What are the baseline mechanical properties of CNT-sheets and what are the manufacturing parameters that create those properties?

Table 10 and Table 11 show the baseline mechanical properties of CNT-sheets from all 6 specimen types. Following these properties are conclusion statements about the manufacturing parameters that affect the measured properties.

Table 10. Apparent tensile strength, modulus and failure strain of CNT-sheets baseline properties

Sp ID	Thickness* (µm)	Density* (g/cm ³)	Areal density (g/m ²)	Strength* (MPa)	Modulus* (GPa)	Strain to Failure
1 A	39.11 ±2.77	0.38 ±0.02	14.88 ±0.60	45.32 ±5.62	1.11 ±0.24	0.22 ±0.04
2 B	25.77 ±7.31	0.50 ±0.09	12.81 ±2.36	25.26 ±2.54	0.20 ±0.05	0.21 ±0.10
3 B	45.00 ±5.54	0.51 ±0.11	22.76 ±4.82	20.36 ±3.12	0.32 ±0.03	0.27 ±0.05
4 B	25.11 ±4.34	0.47 ±0.02	11.82 ±0.45	29.80 ±2.52	0.58 ±0.02	0.16 ±0.04
5 C	16.78 ±1.65	0.58 ±0.01	9.74 ±0.12	97.76 ±7.35	2.98 ±0.67	0.30 ±0.01
6 C	23.44 ±1.83	0.48 ±0.06	11.29 ±1.46	63.88 ±2.55	1.20 ±0.81	0.32 ±0.00
7 D	19.42 ±5.59	0.44 ±0.03	8.46 ±0.58	72.24 ±8.29	3.16 ±0.22	0.21 ±0.00
8 D	24.21 ±4.12	0.37 ±0.02	9.05 ±0.45	85.84 ±3.51	3.91 ±0.30	0.22 ±0.01

*Apparent property

Table 11. Apparent tensile strength, modulus, and failure strain for polymer coated CNT-sheets

Sp ID	Thickness* (µm)	Density* (g/cm ³)	Areal density (g/m ²)	Strength* (MPa)	Modulus* (GPa)	Strain to Failure
10 E	40.22 ±6.47	0.61 ±0.02	24.35 ±0.72	116.5 ±9.48	2.28 ±0.27	0.38 ±0.04
11 E	59.67 ±2.02	0.31 ±0.01	18.25 ±0.89	43.59 ±5.36	0.95 ±0.04	0.20 ±0.03
12 F	50.33 ±4.36	0.50 ±0.01	25.40 ±0.32	32.74 ±2.29	0.77 ±0.03	0.17 ±0.01
13 F	30.62 ±7.23	0.47 ±0.09	14.48 ±2.70	17.10 ±3.91	0.31 ±0.07	0.21 ±0.03
14 F	32.82 ±8.00	0.39 ±0.01	12.84 ±0.33	30.84 ±1.30	0.89 ±0.09	0.16 ±0.01

*Apparent property

Conclusions:

- For standard production CNT-sheets, volumetric density was the dominating parameter that affected apparent strength and stiffness.
- Enhanced production CNT-sheets have reduced mechanical performance and are found with a large presence of impurities throughout the CNT network
- The acid treatment parameter increases mechanical strength and stiffness for both production rates. The effects of this manufacturing parameter are exaggerated in EP CNT-sheets which demonstrated the highest performance among the studied specimens. For EP CNT-sheets, acid-treatment is the

dominating factor for improved mechanical properties due to the process of purification and increased bonding.

- Evidence is found that strain at failure is dominated by the amount of alignment found under tensile behavior in the sheets formed by initially randomly oriented and wavy CNTs.

2. What are the baseline electrical properties of CNT-sheets and what are the manufacturing parameters that create those properties?

Table 12 shows the baseline electrical properties of CNTs from all 6 types.

Following these properties are conclusion statements about the manufacturing parameters that affect the measured electrical properties.

Table 12. Apparent conductivity and EMI shielding effectiveness of CNT-sheets

Id	Thickness* (μm)	Density* (g/cm^3)	Areal density (g/m^2)	Conductivity* (S/cm)	EMI (dB)
A 1	39.11 \pm 2.77	0.38 \pm 0.02	15.08 \pm 0.10	236.37 \pm 25.02	50.15 \pm 0.66
B 2	25.77 \pm 7.31	0.46 \pm 0.11	11.28 \pm 0.31	162.65 \pm 43.74	40.92 \pm 0.76
B 3	45.00 \pm 5.54	0.46 \pm 0.03	20.74 \pm 1.32	108.62 \pm 1.74	55.98 \pm 0.30
B 4	25.11 \pm 4.34	0.50 \pm 0.05	12.35 \pm 0.84	171.36 \pm 29.06	42.01 \pm 0.74
C 5	19.20 \pm 1.65	0.52 \pm 0.06	9.98 \pm 0.11	1146.7 \pm 126.3	61.70 \pm 0.94
C 6	23.44 \pm 1.83	0.49 \pm 0.04	11.43 \pm 1.50	589.48 \pm 88.73	60.90 \pm 0.37
C 9	51.67 \pm 4.67	0.31 \pm 0.02	15.92 \pm 1.32	444.78 \pm 67.02	68.29 \pm 0.22
D 7	18.23 \pm 0.52	0.58 \pm 0.12	10.53 \pm 2.51	337.68 \pm 16.73	48.80 \pm 0.75
D 8	23.11 \pm 0.77	0.40 \pm 0.04	9.24 \pm 0.74	552.20 \pm 81.64	53.17 \pm 0.70
E 10	40.22 \pm 6.47	0.59 \pm 0.10	23.45 \pm 1.14	185.21 \pm 25.30	49.55 \pm 2.97
E 11	59.67 \pm 2.03	0.28 \pm 0.00	16.96 \pm 0.50	174.09 \pm 3.60	52.80 \pm 0.67
E 12	50.33 \pm 4.36	0.47 \pm 0.03	23.53 \pm 1.30	71.37 \pm 6.12	43.60 \pm 0.73
E 13	30.62 \pm 7.23	0.49 \pm 0.06	14.80 \pm 1.63	78.20 \pm 19.60	41.24 \pm 0.84
E 14	32.82 \pm 8.00	0.45 \pm 0.12	14.21 \pm 1.19	114.28 \pm 26.85	43.59 \pm 0.75

*Apparent property

Conclusions:

- The dominant factor in improved electrical conductivity is acid treatment. A small reduction in conductivity is found due to polymer intercalation and

enhanced production. The lowest performing specimens were polymer coated EP-CNT sheets. This combined effect of both manufacturing parameters follows a principle of linear superposition of additivity.

- Improved conductivity in acid treated specimens is affected by the compactness of the CNT structure from the treatment. This is seen with increased conductivity with reduced thicknesses. Enhanced production CNTs appear to be affected in a similar manner but negatively as the network of CNTs are separated with the saturation of impurities from production.
- EMI shielding effectiveness is reduced with enhanced production and polymer coatings. Increases in EMI shielding are attributed to material thickness and acid treatment. EMI shielding per unit thickness increased linearly with thickness for all specimen types. Both factors for improved or reduced properties, to include thickness; follow a linear principle of superposition for final holistic EMI SE properties.

3. What are the resulting effects of thermal fatigue and atomic oxygen exposure on electro-mechanical properties?

The manufacturing parameter examined was the treatment with nitric acid to determine the stability of improved properties through exposure to atomic oxygen and thermal cycling. A summary of changes to baseline properties in CNT-sheets are reported in Table 13. All percent changes from the baseline specimen are shown from the average of three specimens. A T-test was performed assuming unequal variances to determine with confidence which properties were affected. A p-value of less than .05 established 95% confidence that the exposure caused a change in property and is

highlighted in the darkest shade. Changes with less confidence of 90 and 85% are highlighted in lighter shades. Finally, T-test results show that reported P-values of greater than 0.15 are represented by white for no affect or change in property.

Table 13. T-test results assuming unequal variances for property changes in CNT-sheets

Property	Specimen 1		Specimen 6 (Treated)	
	ATOX	Thermal	ATOX	Thermal
Specific Strength	-10%	+8%	<+1%	+8%
Specific Modulus	+74%	+55%	+71%	+79%
Failure Strain	-40%	-6%	-39%	-33%
Areal Density	+9%	+8%	-3%	+10%
Apparent Conductivity	-32%	-8%	-35%	-26%
EMI Shielding	<-1%	+3%	-2%	-1%

LEGEND

Change	Change	Change	No Change
P < 0.05 (95%)	P < 0.10 (90%)	P < 0.15 (85%)	P > 0.15
Definitive	Probable	Unlikely	No Change

In material science, changes are often only significant if they are greater than 10%. With this consideration, values in Table 13 are most significant when they are larger and associated with a smaller P-value. Taking the T-test and the percent value of change into account, results are shown in Table 14 as a summary of changes from the space environment. The darkest shade represents most probably change with small P-values (95% confidence) and large percent value changes in the property. The lighter shade for thermal effects on failure strain for specimen 1 show a small percent change but with a 90% confidence associated with its P-value. All other values in white show no change as a result of a large P-value from the T-test or an insignificant change in value.

Table 14. Summary of space environment effects on CNT-sheets

Property	Specimen 1		Specimen 6 (Treated)	
	ATOX	Thermal	ATOX	Thermal
Specific Strength	-10%	+8%	<+1%	+8%
Specific Modulus	+74%	+55%	+71%	+79%
Failure Strain	-40%	-6%	-39%	-33%
Areal Density	+9%	+8%	-3%	+10%
Apparent Conductivity	-32%	-8%	-35%	-26%
EMI Shielding	<-1%	+3%	-2%	-1%

LEGEND

Change	Change	Change	No Change
Most Probable	Probable	Unlikely	No Change

The significant changes are seen in both specimens with an increase in stiffness partnered with an associated reduction in strain at failure. This suggests results of enhanced bonding within CNT interactions in the sheets. The significance here is that for space materials this is not a negative result. Stiffness is a desirable property for structures. The other change is in electrical conductivity, where significant reductions were found for both specimens after atomic oxygen and for the acid treated specimen from thermal fatigue.

Following are conclusion statements regarding the effects of atomic oxygen exposure and thermal fatigue on both electrical and mechanical properties.

- Atomic oxygen causes the erosion of surface layers in CNT-sheets where EDX analysis showed the depletion of carbon by approximately 10 atomic percent and the addition of oxygen by approximately 8 atomic percent.

This was reported for both the acid treated and untreated sheets.

- After atomic oxygen, changes in mechanical properties were found in both sheets and are as follows: strength was unchanged; stiffness increased by 55-79%, and failure strain was reduced by 6-40%. Changes in electrical properties were consistent for conductivity where both sheets decreased by 32-35% after atomic oxygen. For EMI shielding, the specimens remained unchanged.
- After thermal fatigue, both specimens had no change in specific strength while seeing a 55-79% increase in stiffness. Both specimens also decreased in the level of strain at failure with the reduction being larger for the acid treated type. Electrical conductivity had a significant decrease by 26% for the acid treated type while the conductivity was unchanged for the untreated type.
- The stability of acid treatment in specimen 6 appears to be consistent with the untreated CNT-sheet with exception to thermal fatigue. Previous work performed on CNT-yarns attributes this to micro fractures due to kink bands and buckling caused from cyclic contractions and expansions of CNTs in the acid treated morphology more restrictive of their individual movement. The observed instability of conductivity is expected to come from structural defects introduced by thermal fatigue and facilitated by the compact morphology introduced by functionalization with nitric acid.

These conclusions offer valuable insight for the current state of mechanical and electrical properties of CNT-sheets. The results are important in understanding the manufacturing parameters being investigated by researchers for improving macroscopic properties of CNT-sheets.

5.3 Significance of Research

This is the first set of research to comprehensively review the electrical and mechanical properties of CNT-sheets and the manufacturing parameters that create the observed properties in its bulk material form. Space environments testing were performed on CNT-sheets which demonstrate stability and where they can be used to reduce weight on current space systems.

While these materials are still evolving in a reach toward their potential properties, they currently have properties unlike other materials and are exceptional candidates for space applications. One of these is their low density. The present CNT-sheets used in this study have densities that reach as low as 0.38 g/cm^3 which is smaller than current higher performance fibers and composites used in space. Secondly these densities are found in sheets that have thicknesses as small as $17\mu\text{m}$ that exhibit unique planar isotropy. This means that its current mechanical and electrical properties are independent of direction inside of a plane thinner than a human hair. This is different than the impressive properties of high performance fibers that are layered in different orientations to try and provide properties in the required directions. The uniqueness of this planar isotropy is particularly valuable for membranes in inflatable structures and airlocks on space systems that hold stresses from internal pressures. The systems need to

be lightweight, thin, and resilient to space environments which make CNT-sheets a best solution. This research presents a unique material that can be directly applied to current spacecraft systems impacting weight reductions and new technologies.

5.4 Recommendations for Action

The results demonstrate that the stability of acid treated CNT-sheets are consistent with untreated sheets with exception to the effects of thermal fatigue on electrical conductivity. Both are mechanically resilient to atomic oxygen with a significant decrease to conductivity. The untreated CNT-sheet appears to be the better choice for applications in space with motivation to find manufacturing parameters for improved conductivity different than treatment with acid. It is recommended for use in EMI shielding where its mechanical properties and EMI shielding effectiveness is unaffected by both atomic oxygen and thermal fatigue. It is also recommended for use in structural membranes that require flexible (low modulus) membranes with planar isotropic properties. This is because specific strength is unaffected by both environments. Furthermore their extremely low densities are capable of reducing mass on spacecraft with their application.

Recommendations for action would be to continue applications of CNT-sheets used for EMI shielding aboard spacecraft. Flight demonstrations are also recommended for the use of structural membranes resilient to harsh orbit conditions.

5.5 Recommendations for Future Research

Since this is the first set of research to characterize the performance of CNT-sheets in the space environment, there are several paths forward to development a

comprehensive analysis of their performance in space. Three are recommended which include characterizing additional properties of CNT-sheets, expanding the space environments effects more broadly, and looking more in depth at the manufacturing parameters investigated in this research.

Another impressive property found in CNT materials is its thermal conductivity which creates an interest for efficient, multipurpose, and lightweight thermal management systems in spacecraft. A comprehensive characterization should be performed for the same 14 specimens looking at each of the variables and manufacturing parameters and their effects on thermal properties. Radiation shielding properties are also an interesting application to space vehicles that carry people and lightweight shielding materials in astronaut suits.

Another area of recommended research is to look more broadly at other space environment conditions. One of these which are of great interest is the effect of UV radiation on CNT-sheet properties. UV radiation in the vacuum conditions of low earth orbit can reach spacecraft components at short wavelengths of less than 200nm with enough energy to break C-C bonds and functional groups [30]. This can strongly affect material properties. In addition to UV radiation, the synergistic effects of thermal fatigue, atomic oxygen, and UV exposure would more accurately represent how the space environment would impact CNT-sheets.







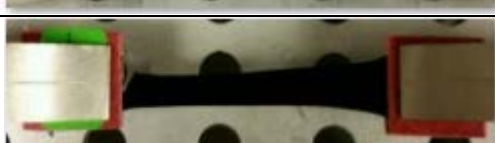

The final recommendation into future work includes looking more in depth at the manufacturing parameters presented in this research to understand how scientists can improve the properties and stability of CNT-sheets and other bulk/macro products. One method of interest is to use Raman spectroscopy to look more closely at the amount of





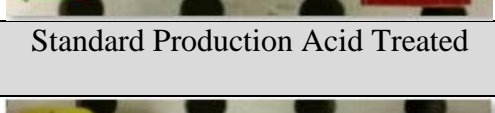






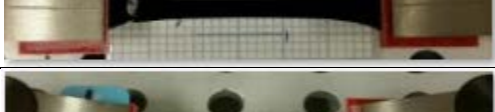
defects in the CNTs that impact mechanical and electrical properties. This would be particularly valuable in acid treated sheets which are known to yield more defects and function groups linked to the CNT structure. Another recommendation is more in-depth investigation of the polymer coated CNT-sheets. Specifically additional research could look more closely at the differences between the two different polymers and how to best leverage their content to maximize sheet properties. The final recommendation is to further investigate the synergistic effects of acid treatment with the enhanced production sheets. While enhanced production diminished all mechanical and physical properties, the acid treated EP CNT-sheets had the highest specific strength and stiffness.





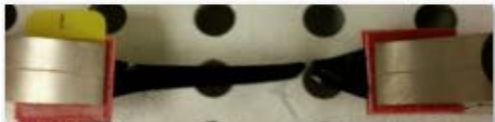






These recommendations are only a few examples of additional research that needs to be done to more fully exploit the current state of CNT-sheets. Continued work in this field will help scientists and engineers present the most advanced material known in a product that will revolutionize the way the Department of Defense is able to operate in space.



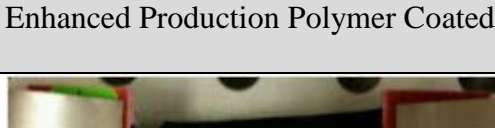
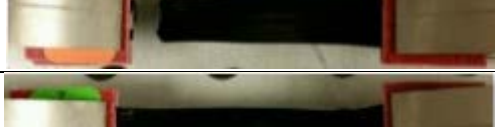







Appendix A. Images of CNT-sheet Specimen Failure

Images of CNT-sheet specimens from 6 categories after tensile tests are included. Demonstrated here is the unique necking condition that varies between manufacturing parameters and the associated failure conditions that occur after strain induced alignment.

Type A	Standard Production Untreated
Specimen 1.1 Lot 70676	
Specimen 1.2 Lot 70676	
Specimen 1.3 Lot 70676	
Type B	Enhanced Production Untreated
Specimen 2.1 Lot 80109	
Specimen 2.4 Lot 80109	
Specimen 2.5 Lot 80109	
Specimen 3.1 Lot 80140	
Specimen 3.2 Lot 80140	

Specimen 3.3 Lot 80140	
Specimen 4.1 Lot 80010	
Specimen 4.2 Lot 80010	
Specimen 4.3 Lot 80010	
Type C	Standard Production Acid Treated
Specimen 5.1 Lot 70440	
Specimen 5.2 Lot 70440	
Specimen 5.3 Lot 70440	
Specimen 6.1 Lot 70682	
Specimen 6.2 Lot 70682	
Specimen 6.3 Lot 70682	
Specimen 9.1 Lot 71125	
Specimen 9.2 Lot 71125	

Specimen 9.3 Lot 71125	
Type D	Enhanced Production Acid Treated
Specimen 7.1 Lot 326_08	
Specimen 7.2 Lot 326_08	
Specimen 7.3 Lot 326_08	
Specimen 8.1 Lot 326_10	
Specimen 8.2 Lot 326_10	
Specimen 8.3 Lot 326_10	
Type E	Standard Production Polymer Coated
Specimen 10.1 Lot 71234 (PSb)	
Specimen 10.2 Lot 71234 (PSb)	
Specimen 10.3 Lot 71234 (PSb)	
Specimen 11.1 Lot 71126 (TPU)	

Specimen 11.2 Lot 71126 (TPU)	
Specimen 11.3 Lot 71126 (TPU)	
Type F	Enhanced Production Polymer Coated
Specimen 12.1 Lot 80147 (TPU)	
Specimen 12.2 Lot 80147 (TPU)	
Specimen 12.3 Lot 80147 (TPU)	
Specimen 13.1 Lot 80121 (PSb)	
Specimen 13.2 Lot 80121 (PSb)	
Specimen 13.3 Lot 80121 (PSb)	
Specimen 14.1 Lot 80120 (TPU)	
Specimen 14.2 Lot 80120 (TPU)	
Specimen 14.3 Lot 80120 (TPU)	

Appendix B. Matlab Script for Line Extraction and Hough Transform

Hough Line Transform for Image processing and Line Extraction

```
close all; , clear all; , clc

I = imread('2-7076B 20kx.tif'); imshow(I, []); %Read and display SEM image
I2 = imcrop(I, [0 0 1024 1020]); % Remove Data bar from SEM
rotI = imrotate(I2, 0, 'crop'); %Rotate image if needed
figure, imshow(rotI, []); % Display cropped and rotated image
BW = edge(rotI, 'canny'); %extract edges
[H, T, R] = hough(BW); %H, theta , rho hough transform of the binary image
%The hough function is designed to detect lines. The function uses the
%parametric representation of a line: rho = x*cos(theta) + y*sin(theta).
%The function returns rho, the distance from the origin to the line along
%a vector perpendicular to the line, and theta, the angle in degrees
%between the x-axis and this vector. The function also returns the Standard
%Hough Transform, H, which is a parameter space matrix whose rows & columns
%correspond to rho and theta values respectively
imshow(H, [], 'XData', T, 'YData', R, ...
        'InitialMagnification', 'fit'); %Display Hough Transform
xlabel('\theta'), ylabel('\rho');
axis on, axis normal, hold on;
colormap(hot)
%find peaks in hough transform
P = houghpeaks(H, 5, 'threshold', ceil(0.3*max(H(:))));
x = T(P(:, 2)); y = R(P(:, 1));
plot(x, y, 's', 'color', 'white'); %Plot peaks represening most probably lines

% Find lines and plot them
lines = houghlines(BW, T, R, P, 'FillGap', 5, 'MinLength', 7);
figure, imshow(rotI), hold on
max_len = 0;
for k = 1:length(lines)
    xy = [lines(k).point1; lines(k).point2];
    plot(xy(:, 1), xy(:, 2), 'LineWidth', 2, 'Color', 'green');
    % Plot beginnings and ends of lines
    plot(xy(1, 1), xy(1, 2), 'x', 'LineWidth', 2, 'Color', 'yellow');
    plot(xy(2, 1), xy(2, 2), 'x', 'LineWidth', 2, 'Color', 'red');
    % Determine the endpoints of the longest line segment
    len = norm(lines(k).point1 - lines(k).point2);
    if ( len > max_len)
        max_len = len;
        xy_long = xy;
    end
end
plot(xy_long(:, 1), xy_long(:, 2), 'LineWidth', 2, 'Color', 'cyan');
```

Appendix C. Other Applications of Carbon Nanotube Materials

Other properties of carbon nanotubes are shown that are reported in literature and demonstrate their unique and expansive applications.

Properties	Applications
Mechanical	Structures [76]
Electromagnetic properties	Artificial muscle [42]
Electroacoustic properties	Speakers [42]
Chemical Properties	Air and Water Filtration [42] [76]
Thermal	Thermal conductivity and insulation [76]
Electrical	Field Emission transistors [42] [43] Diodes [43] Ballistic electrical connectors [42] Photovoltaic Cells [42] Logic-gate based on SWNT [43]
Size	Biomedicine cell penetration and Drug Delivery [42]
Fluorescent Properties	In vitro and in vivo imaging [42]
Sorbent Properties	Contaminant removal in water pollution

Bibliography

- [1] “LeMay Center for Doctrine ‘Volume 1 - Basic Doctrine,’” *Air Force Doctrine*, 2015. [Online]. Available: <https://doctrine.af.mil/dnv1vol1.htm>.
- [2] “LeMay Center for Doctrine ‘Volume 3 - Command,’” *Air Force Doctrine*, 2015. [Online]. Available: <https://doctrine.af.mil/dnv1vol3.htm>.
- [3] “Space Operations Joint Publication 3-14,” Washington D.C., 2013.
- [4] S. Rawal, J. Brantley, and N. Karabudak, “Development of Carbon Nanotube-based Composite for Spacecraft Components,” *6th Int. Conf. Recent Adv. Sp. Technol.*, pp. 13–19, 2013.
- [5] I. (National S. G. Bekey, “The Effect of Carbon Nanotubes on the Weight and Likely Cost of Space Systems and Launch Vehicles, Both Near and Far Terms: The Coming of ‘Carbon Spacecraft’ and ‘Carbon Launch Vehicles,’” *El Segundo*, 2011.
- [6] Y. K. Yap, Ed., *B-C-N Nanotubes and Related Nanostructures*. New York: Springer, 2009.
- [7] P. Wagner, “Carbon Nanotubes: Small Structures with Big Promise,” *Def. Syst. Inf. Anal. Cent.*, 2015.
- [8] M.-S. Ha, O.-Y. Kwon, and H.-S. Choi, “Improved Electrical Conductivity of CFRP by Conductive Nano-Particles Coating for lightning Strike Protection,” *J. Korean Soc. Compos. Mater.*, vol. 23, pp. 31–36, 2010.
- [9] B. Q. Han, F. a. Mohamed, and E. J. Lavernia, “Mechanical properties of iron processed by severe plastic deformation,” *Metall. Mater. Trans. A*, vol. 34, no. 1, pp. 71–83, 2003.
- [10] “Properties table of Stainless steel, Metals and other conductive materials.” [Online]. Available: <http://www.tibtech.com/conductivity.php>. [Accessed: 18-Dec-2015].
- [11] “Conductivity of Metals Sorted By Resistivity.” [Online]. Available: <http://eddy-current.com/conductivity-of-metals-sorted-by-resistivity/>.
- [12] “Application Data Sheet: Mechanical Properties of Copper and Copper Alloys at Low Temperatures.” [Online]. Available: http://www.copper.org/applications/industrial/DesignGuide/props/tensile_strength.html.
- [13] M. Yu, B. Files, S. Arepalli, and R. Ruoff, “Tensile loading of ropes of single wall carbon nanotubes and their mechanical properties,” *Phys. Rev. Lett.*, vol. 84, no. 24, pp. 5552–5, 2000.
- [14] A. Ghemes, Y. Minami, J. Muramatsu, M. Okada, H. Mimura, and Y. Inoue, “Fabrication and mechanical properties of carbon nanotube yarns spun from ultra-long multi-walled carbon nanotube arrays,” *Carbon N. Y.*, vol. 50, no. 12, pp.

4579–4587, 2012.

- [15] M. Foygel, R. D. Morris, D. Anez, S. French, and V. L. Sobolev, “Theoretical and computational studies of carbon nanotube composites and suspensions: Electrical and thermal conductivity,” *Phys. Rev. B - Condens. Matter Mater. Phys.*, vol. 71, no. 10, pp. 1–8, 2005.
- [16] M. S. Arnold, S. I. Stupp, and M. C. Hersam, “Enrichment of Single-Walled Carbon Nanotubes by Diameter in Density Gradients,” *Nano Lett.*, vol. 5, no. 4, pp. 713–718, 2005.
- [17] H. E. Misak and S. Mall, “Electrical conductivity, strength and microstructure of carbon nanotube multi-yarns,” *Mater. Des.*, vol. 75, pp. 76–84, 2015.
- [18] P. A. (Air F. I. of T. Hunt, “Electromagnetic Interference Behavior of Multiwall Carbon Nanotubes and Carbon Nanofibers Composites Under Fatigue,” Air Force Institute of Technology, 2012.
- [19] K. Y. Chong and L. Commander, “Evaluation of Nanocomposites for use in Satellite Structures,” Air Force Institute of Technology, 2011.
- [20] H. E. Misak, R. Asmatulu, M. O’Malley, E. Jurak, and S. Mall, “Functionalization of carbon nanotube yarn by acid treatment,” *Int. J. Smart Nano Mater.*, vol. 5, no. 1, pp. 34–43, 2014.
- [21] J. N. Coleman, W. J. Blau, A. B. Dalton, E. Muñoz, S. Collins, B. G. Kim, J. Razal, M. Selvidge, G. Vieiro, and R. H. Baughman, “Improving the mechanical properties of single-walled carbon nanotube sheets by intercalation of polymeric adhesives,” *Appl. Phys. Lett.*, vol. 82, no. 11, pp. 1682–1684, 2003.
- [22] F. H. Gojny, J. Nastalczyk, Z. Roslaniec, and K. Schulte, “Surface modified multi-walled carbon nanotubes in CNT/epoxy-composites,” *Chem. Phys. Lett.*, vol. 370, no. 5–6, pp. 820–824, 2003.
- [23] B. D. Dunn, *Metallurgical Assessment of Spacecraft Parts, Materials, and Processes*. Chichester: John Wiley & Sons in Association with Praxis Publishing, 1997.
- [24] A. J. Butrica, *Single Stage to Orbit: Politics, Space Technology, and the Quest for Reuseable Rocketry*. Baltimore: The John Hopkins University Press, 2003.
- [25] D. Jacob, G. Sachs, and S. Wagner, Eds., “Basic Research and Technologies for Two-Stage-to-Orbit Vehicles,” Wiley-VCH Verlag GmbH & Co., Bonn, 2005.
- [26] H. Kuczera and P. W. Sacher, *Reusable Space Transportation Systems*. Heidelberg: Springer-Verlag Berlin Heidelberg, 2011.
- [27] “X-33 EC96-43631-2: VentureStar by Lockheed Martin in Orbit - Computer Graphic,” 1996. [Online]. Available: <http://www.dfrc.nasa.gov/Gallery/Photo/X-33/HTML/EC96-43631-2.html>. [Accessed: 12-Nov-2015].
- [28] W. F. (The A. C. Tosney, B. L. (The A. C. Arnheim, and J. B. (The A. C. Clark,

- “The influence of Development and Test on Mission Success,” *Fourth Int. Symp. Environ. Test. Sp. Program.*, 2001.
- [29] “Department of Defense Standard Practice Product Verification Requirements for Launch , Upper Stage , and Space.” 1999.
- [30] E. Grossman and I. Gouzman, “Space environment effects on polymers in low earth orbit,” *Nucl. Instruments Methods Phys. Res. Sect. B Beam Interact. with Mater. Atoms*, vol. 208, no. 1–4, pp. 48–57, 2003.
- [31] J. R. (University of S. C. Wertz, D. F. (NASA G. S. F. C. Everett, and J. J. (Raytheon) Puschell, Eds., *Space Mission Engineering: The New SMAD*. Hawthorne: Microsm Press, 2011.
- [32] V. L. Pisacance, *The Space Environment and its Effects on Space Systems*. Reston: American Institute of Aeronautics and Astronautics, Inc, 2008.
- [33] T. F. Tascione, *Introduction to the Space Environment*, Second. Malabar: Krieger Publishing Company, 1994.
- [34] K. B. Shin, C. G. Kim, C. S. Hong, and H. H. Lee, “Prediction of failure thermal cycles in graphite/epoxy composite materials under simulated low earth orbit environments,” *Compos. Part B Eng.*, vol. 31, no. 3, pp. 223–235, 2000.
- [35] J. T. Visentine, “Atomic oxygen effects measurements for shuttle missions STS-8 and 41-G,” Sep. 1988.
- [36] L. J. Leger, J. T. Visentine, and J. F. Kuminecz, “AI AA-84-0548 Low Earth Orbit Atomic Oxygen Effects on Surfaces NASA,” in *Lyndon B . Johnson Space Center AIAA 22nd Aerospace Sciences*, 1984.
- [37] Z. A. Iskanderova, J. I. Kleiman, Y. Gudimenko, and R. C. Tennyson, “Protection of Space Materials from the Space Environment,” in *Generalization of the Predictive Model of Erosion of Carbon-Based Materials by Atomic Oxygen*, 1998.
- [38] R. L. Kiefer, R. a. Anderson, M. H. Y. Kim, and S. a. Thibeault, “Modified polymeric materials for durability in the atomic oxygen space environment,” *Nucl. Instruments Methods Phys. Res. Sect. B Beam Interact. with Mater. Atoms*, vol. 208, no. 1–4, pp. 300–302, 2003.
- [39] X.-H. Zhao, Z.-G. Shen, Y.-S. Xing, and S.-L. Ma, “An experimental study of low earth orbit atomic oxygen and ultraviolet radiation effects on a spacecraft material – polytetrafluoroethylene,” *Polym. Degrad. Stab.*, vol. 88, no. 2, pp. 275–285, 2005.
- [40] J. Burrell, “Disruptive Effects of Electromagnetic Interference on Communication and Electronic Systems,” no. April, pp. 1–34, 2003.
- [41] S. Iijima, “Helical microtubules of graphitic carbon,” *Letters to Nature*, vol. 354. pp. 56–58, 1991.
- [42] N. Guldi, Dirk M., Martin, Ed., *Carbon Nanotubes and Related Structures*

Synthesis, Characterization, Functionalization, and Applications. Weinheim: Wiley-VCH Verlag GmbH & Co., 2010.

- [43] P. J. F. Harris, *Carbon Nanotube Science Synthesis, properties, and applications*. New York: Cambridge University Press, 2009.
- [44] R. Rafiee and R. Pourazizi, "Evaluating the Influence of Defects on the Young's Modulus of Carbon Nanotubes Using Stochastic Modeling 2. CNT Morphology and Defect Types," *Sci. York*, vol. 17, no. 3, pp. 758–766, 2014.
- [45] R. K. Johnson and A. Kohlmeyer, "Carbon / Boron Nitride Nanostructure Builder Plugin, Version 1.5." [Online]. Available: <http://www.ks.uiuc.edu/Research/vmd/plugins/nanotube/>. [Accessed: 09-Nov-2015].
- [46] P. Nikolaev, "Gas-Phase Production of Single-Walled Carbon Nanotubes from Carbon Monoxide: A Review of the HiPco Process," *J. Nanosci. Nanotechnol.*, vol. 4, no. 4, pp. 307–316, Apr. 2004.
- [47] H. E. Misak and S. Mall, "Investigation into microstructure of carbon nanotube multi-yarn," *Carbon N. Y.*, vol. 72, pp. 321–327, 2014.
- [48] M. Zhang, S. Fang, A. a Zakhidov, S. B. Lee, A. E. Aliev, C. D. Williams, K. R. Atkinson, and R. H. Baughman, "Strong, transparent, multifunctional, carbon nanotube sheets.," *Science*, vol. 309, no. 5738, pp. 1215–1219, 2005.
- [49] M. Endo, H. Muramatsu, T. Hayashi, Y. A. Kim, M. Terrones, and M. S. Dresselhaus, "Nanotechnology: 'buckypaper' from coaxial nanotubes.," *Nature*, vol. 433, no. 7025, p. 476, Feb. 2005.
- [50] L. Berhan, Y. B. Yi, a. M. Sastry, E. Munoz, M. Selvidge, and R. Baughman, "Mechanical properties of nanotube sheets: Alterations in joint morphology and achievable moduli in manufacturable materials," *J. Appl. Phys.*, vol. 95, no. 8, pp. 4335–4345, 2004.
- [51] J.-F. Colomer, C. Stephan, S. Lefrant, G. Van Tendeloo, I. Willems, Z. Kónya, a Fonseca, C. Laurent, and J. . Nagy, "Large-scale synthesis of single-wall carbon nanotubes by catalytic chemical vapor deposition (CCVD) method," *Chem. Phys. Lett.*, vol. 317, no. 1–2, pp. 83–89, 2000.
- [52] J. Kong and A. M. Cassell, "Chemical vapor deposition of methane for single-walled carbon nanotubes," *Chem. Phys. Lett.*, no. August, pp. 567–574, 1998.
- [53] X. Zhang, K. Jiang, C. Feng, P. Liu, L. Zhang, J. Kong, T. Zhang, Q. Li, and S. Fan, "Spinning and processing continuous yarns from 4-inch wafer scale super-aligned carbon nanotube arrays," *Adv. Mater.*, vol. 18, no. 12, pp. 1505–1510, 2006.
- [54] C. D. Tran, W. Humphries, S. M. Smith, C. Huynh, and S. Lucas, "Improving the tensile strength of carbon nanotube spun yarns using a modified spinning process," *Carbon N. Y.*, vol. 47, no. 11, pp. 2662–2670, 2009.

- [55] T. Dürkop, B. M. Kim, and M. S. Fuhrer, “Properties and applications of high-mobility semiconducting nanotubes,” *J. Phys. Condens. Matter*, vol. 16, no. 18, pp. R553–R580, 2004.
- [56] P. X. Hou, C. Liu, and H. M. Cheng, “Purification of carbon nanotubes,” *Carbon N. Y.*, vol. 46, no. 15, pp. 2003–2025, 2008.
- [57] J.-M. Moon, K. H. An, Y. H. Lee, Y. S. Park, D. J. Bae, and G.-S. Park, “High-Yield Purification Process of Singlewalled Carbon Nanotubes,” *J. Phys. Chem. B*, vol. 105, no. 24, pp. 5677–5681, Jun. 2001.
- [58] B. Q. Wei, R. Vajtai, and P. M. Ajayan, “Reliability and current carrying capacity of carbon nanotubes,” *Appl. Phys. Lett.*, vol. 79, no. 8, pp. 1172–1174, 2001.
- [59] B. Xu, J. Yin, and Z. Liu, “Phonon Scattering and Electron Transport in Single Wall Carbon Nanotube,” pp. 215–43, 2013.
- [60] T. H. Niu C, Sichel E, Hoch R, Moy D, “High power electrochemical capacitors based on carbon nanotube electrodes,” *Appl Phys Lett*, vol. 70, no. 1480–1482, p. 1997, 1997.
- [61] Y. S. Song and J. R. Youn, “Influence of dispersion states of carbon nanotubes on physical properties of epoxy nanocomposites,” *Carbon N. Y.*, vol. 43, no. 7, pp. 1378–1385, 2005.
- [62] M. Nadler, J. Werner, T. Mahrholz, U. Riedel, and W. Hufenbach, “Effect of CNT surface functionalisation on the mechanical properties of multi-walled carbon nanotube/epoxy-composites,” *Compos. Part A Appl. Sci. Manuf.*, vol. 40, no. 6–7, pp. 932–937, 2009.
- [63] S. J. V. Frankland, A. Caglar, D. W. Brenner, and M. Griebel, “Molecular Simulation of the Influence of Chemical Cross-Links on the Shear Strength of Carbon Nanotube–Polymer Interfaces,” *J. Phys. Chem. B*, vol. 106, no. 12, pp. 3046–3048, Mar. 2002.
- [64] F. Avilés, J. V. Cauich-Rodríguez, L. Moo-Tah, a. May-Pat, and R. Vargas-Coronado, “Evaluation of mild acid oxidation treatments for MWCNT functionalization,” *Carbon N. Y.*, vol. 47, no. 13, pp. 2970–2975, 2009.
- [65] X. Wang, Q. Jiang, W. Xu, W. Cai, Y. Inoue, and Y. Zhu, “Effect of carbon nanotube length on thermal, electrical and mechanical properties of CNT/bismaleimide composites,” *Carbon N. Y.*, vol. 53, pp. 145–152, 2013.
- [66] J. N. Coleman, U. Khan, W. J. Blau, and Y. K. Gun’ko, “Small but strong: A review of the mechanical properties of carbon nanotube-polymer composites,” *Carbon N. Y.*, vol. 44, no. 9, pp. 1624–1652, 2006.
- [67] Z. Spitalsky, D. Tasis, K. Papagelis, and C. Galiotis, “Carbon nanotube–polymer composites: Chemistry, processing, mechanical and electrical properties,” *Prog. Polym. Sci.*, vol. 35, no. 3, pp. 357–401, 2010.
- [68] J. B. Moon, M. G. Kim, C. G. Kim, and S. Bhowmik, “Improvement of tensile

- properties of CFRP composites under LEO space environment by applying MWNTs and thin-ply,” *Compos. Part A Appl. Sci. Manuf.*, vol. 42, no. 6, pp. 694–701, 2011.
- [69] J.-H. Han and C.-G. Kim, “Low earth orbit space environment simulation and its effects on graphite/epoxy composites,” *Compos. Struct.*, vol. 72, no. 2, pp. 218–226, 2006.
- [70] H. E. Misak, V. Sabelkin, S. Mall, and P. E. Kladitis, “Thermal fatigue and hypothermal atomic oxygen exposure behavior of carbon nanotube wire,” *Carbon N. Y.*, vol. 57, pp. 42–49, 2013.
- [71] “Nanocomp Technologies, Inc.” [Online]. Available: <http://www.nanocomptech.com/sheets-mats>. [Accessed: 23-Oct-2015].
- [72] Q. Cheng, J. Bao, J. Park, Z. Liang, C. Zhang, and B. Wang, “High mechanical performance composite conductor: Multi-walled carbon nanotube sheet/bismaleimide nanocomposites,” *Adv. Funct. Mater.*, vol. 19, no. 20, pp. 3219–3225, 2009.
- [73] S. Li, J. G. Park, Z. Liang, T. Siegrist, T. Liu, M. Zhang, Q. Cheng, B. Wang, and C. Zhang, “In situ characterization of structural changes and the fraction of aligned carbon nanotube networks produced by stretching,” *Carbon N. Y.*, vol. 50, no. 10, pp. 3859–3867, 2012.
- [74] I. M. Ward and J. Sweeny, *Mechanical Properties of Solid Polymers*, Third. John Wiley & Sons, Ltd., 2013.
- [75] M. R. Reddy, “Review effect of low earth orbit atomic oxygen on spacecraft materials,” *J. Mater. Sci.*, vol. 30, no. 2, pp. 281–307, 1995.
- [76] M. Meyyappan, Ed., *Carbon Nanotubes Science and Applications*. Boca Raton: CRC Press, 2005.

Vita

Lieutenant Jacob W. Singleton graduated from Davis High School in Kaysville, Utah (UT) in June 2007. In August 2007, he started undergraduate work at Utah State University in Logan, UT. There he worked at the Space Dynamics Laboratory as a research assistant working on attitude determination and control system design for small satellites. He participated in additional research underneath the Rocky Mountain NASA Space Grant Consortium and was awarded the Air Force Research Award for the AFROTC cadet category. He graduated Cum Laude with a Bachelor of Science degree in Mechanical Engineering in May 2014. After graduation, he received his commission into the United States Air Force and soon after entered active duty in August of 2014.

His first assignment was at the Air Force Institute of Technology in a graduate program for astronautical engineering. He earned a membership to Tau Beta Pi in December 2015. Upon graduation, he will be assigned to the Air Force Research Laboratory at the Space Vehicles Directorate located at Kirtland AFB, New Mexico.

REPORT DOCUMENTATION PAGE

Form Approved
OMB No. 074-0188

The public reporting burden for this collection of information is estimated to average 1 hour per response, including the time for reviewing instructions, searching existing data sources, gathering and maintaining the data needed, and completing and reviewing the collection of information. Send comments regarding this burden estimate or any other aspect of the collection of information, including suggestions for reducing this burden to Department of Defense, Washington Headquarters Services, Directorate for Information Operations and Reports (0704-0188), 1215 Jefferson Davis Highway, Suite 1204, Arlington, VA 22202-4302. Respondents should be aware that notwithstanding any other provision of law, no person shall be subject to any penalty for failing to comply with a collection of information if it does not display a currently valid OMB control number.

PLEASE DO NOT RETURN YOUR FORM TO THE ABOVE ADDRESS.

1. REPORT DATE (DD-MM-YYYY) 24 Mar 2016			2. REPORT TYPE Master's Thesis			3. DATES COVERED (From - To) Aug 2014 - Mar 2016		
4. TITLE AND SUBTITLE Electro-Mechanical Characterization of Carbon Nanotube Sheets in Simulated Space Environments: The Dawn of "Carbon Spacecraft"					5a. CONTRACT NUMBER			
					5b. GRANT NUMBER			
					5c. PROGRAM ELEMENT NUMBER			
6. AUTHOR(S) Singleton, Jacob W., Second Lieutenant, USAF					5d. PROJECT NUMBER			
					5e. TASK NUMBER			
					5f. WORK UNIT NUMBER			
7. PERFORMING ORGANIZATION NAMES(S) AND ADDRESS(S) Air Force Institute of Technology Graduate School of Engineering and Management (AFIT/ENV) 2950 Hobson Way, Building 640 WPAFB OH 45433-8865					8. PERFORMING ORGANIZATION REPORT NUMBER AFIT-ENY-MS-16-M-240			
9. SPONSORING/MONITORING AGENCY NAME(S) AND ADDRESS(ES) Intentionally left blank					10. SPONSOR/MONITOR'S ACRONYM(S)			
					11. SPONSOR/MONITOR'S REPORT NUMBER(S)			
12. DISTRIBUTION/AVAILABILITY STATEMENT DISTRIBUTION STATEMENT A: APPROVED FOR PUBLIC RELEASE; DISTRIBUTION UNLIMITED.								
13. SUPPLEMENTARY NOTES This material is declared a work of the U.S. Government and is not subject to copyright protection in the United States.								
14. ABSTRACT Carbon nanotube (CNT) materials are exciting candidates for spacecraft by virtue of their unprecedented specific mechanical and electrical properties. Analysis in this thesis identifies 14 types of CNT-sheets with distinct variables, and discovers the mechanisms controlling macroscopic properties. Specimen variables include acid treatment, polymer coatings, production method, and combinations. Mechanical testing includes tensile-tests and investigation with scanning electron microscopy and energy-dispersive x-ray spectroscopy. Physical properties testing include electromagnetic interference (EMI) shielding effectiveness (SE) and electrical conductivity. This research also highlights the resilience of CNT-sheets to atomic oxygen and thermal fatigue qualifying them for performance in space. EP CNT-sheets have decreased mechanical and electrical properties from a large composition of impurities. Acid treatment increases both mechanical and electrical properties. The acid treated sheets are better consolidated and have reduced impurities which lead to superior properties. This investigation found that strength and EMI SE are unaffected by atomic oxygen and thermal fatigue. Young's modulus increases in both environments while strain decreases. Electrical conductivity decreases from atomic oxygen for both specimens as a result of reduced conductive area. Thermal fatigue only diminishes electrical conductivity in the more compact acid treated sheets.								
15. SUBJECT TERMS Carbon nanotubes, CNT sheet, space environment, atomic oxygen, thermal fatigue, tensile test, electrical conductivity, electromagnetic shielding effectiveness, spacecraft								
16. SECURITY CLASSIFICATION OF:			17. LIMITATION OF ABSTRACT	18. NUMBER OF PAGES	19a. NAME OF RESPONSIBLE PERSON			
a. REPORT	b. ABSTRACT	c. THIS PAGE			Shankar Mall, Ph.D (ENY)			
U	U	U	UU	154	19b. TELEPHONE NUMBER (Include area code) (937) 255-6565, x 4587 (shankar.mall@afit.edu)			